Multimessenger Astroparticle Physics: A Selective Review

1. Ultra-high energy cosmic rays: Observations
2. Ultra-high energy cosmic rays: theoretical challenges, multi-messenger aspects
3. High Energy Neutrinos and Multimessenger Aspects
4. Axions and axion-like particles as dark matter
5. Astrophysical and experimental signatures

DFG Deutsche Forschungsgemeinschaft

PROJEKTTRÄGER FÜR DAS Bundesministerium für Bildung und Forschung

Universität Hamburg
DER FORSCHUNG | DER LEHRE | DER BILDUNG

Günter Sigl
II. Institut theoretische Physik, Universität Hamburg

XLVIII International Meeting on Fundamental Physics, Benasque, Spain, 7.9-10.9.2021

The All Particle Cosmic Ray Spectrum

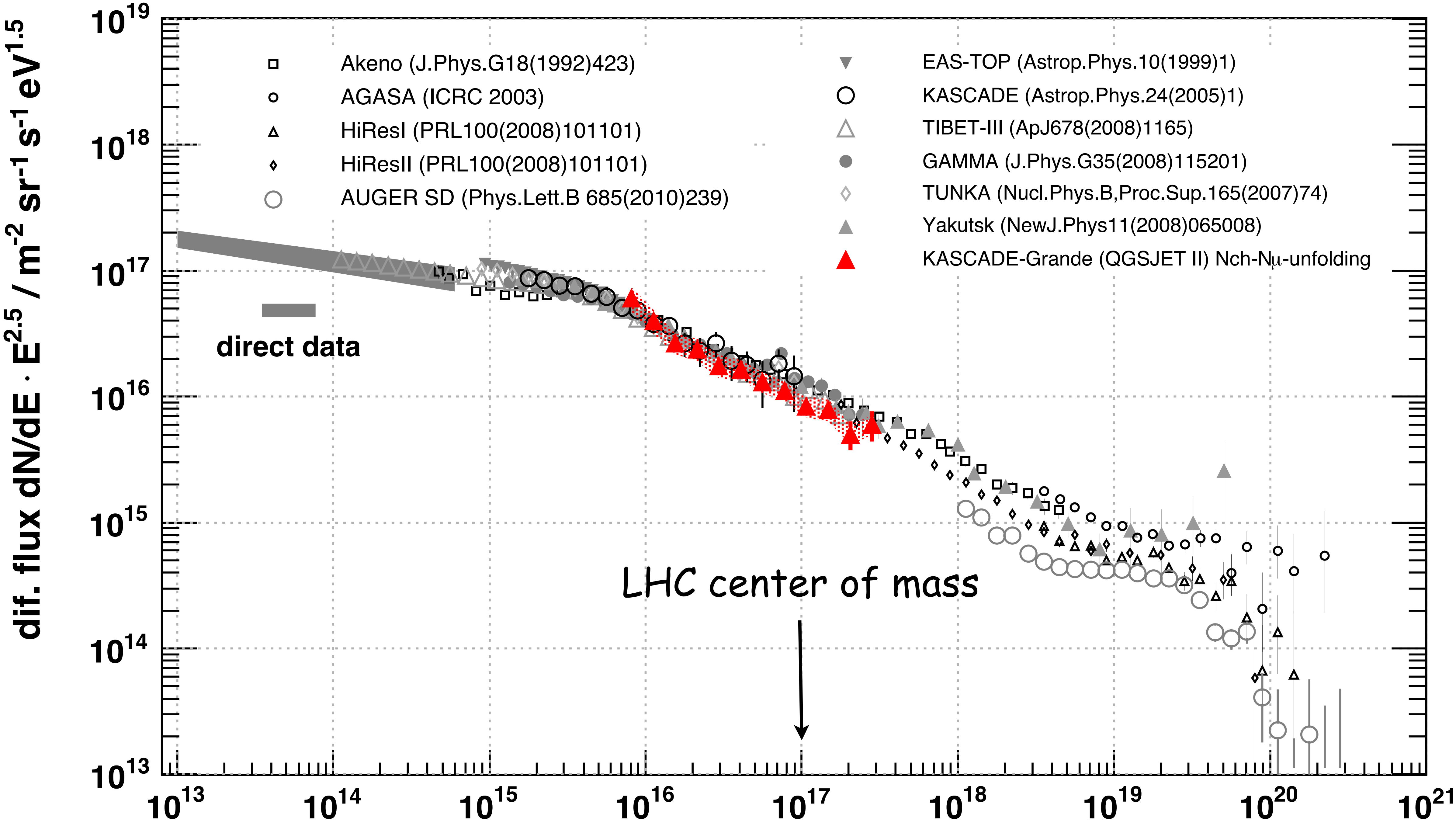

KASCADE-Grande collaboration, arXiv:1111.5436

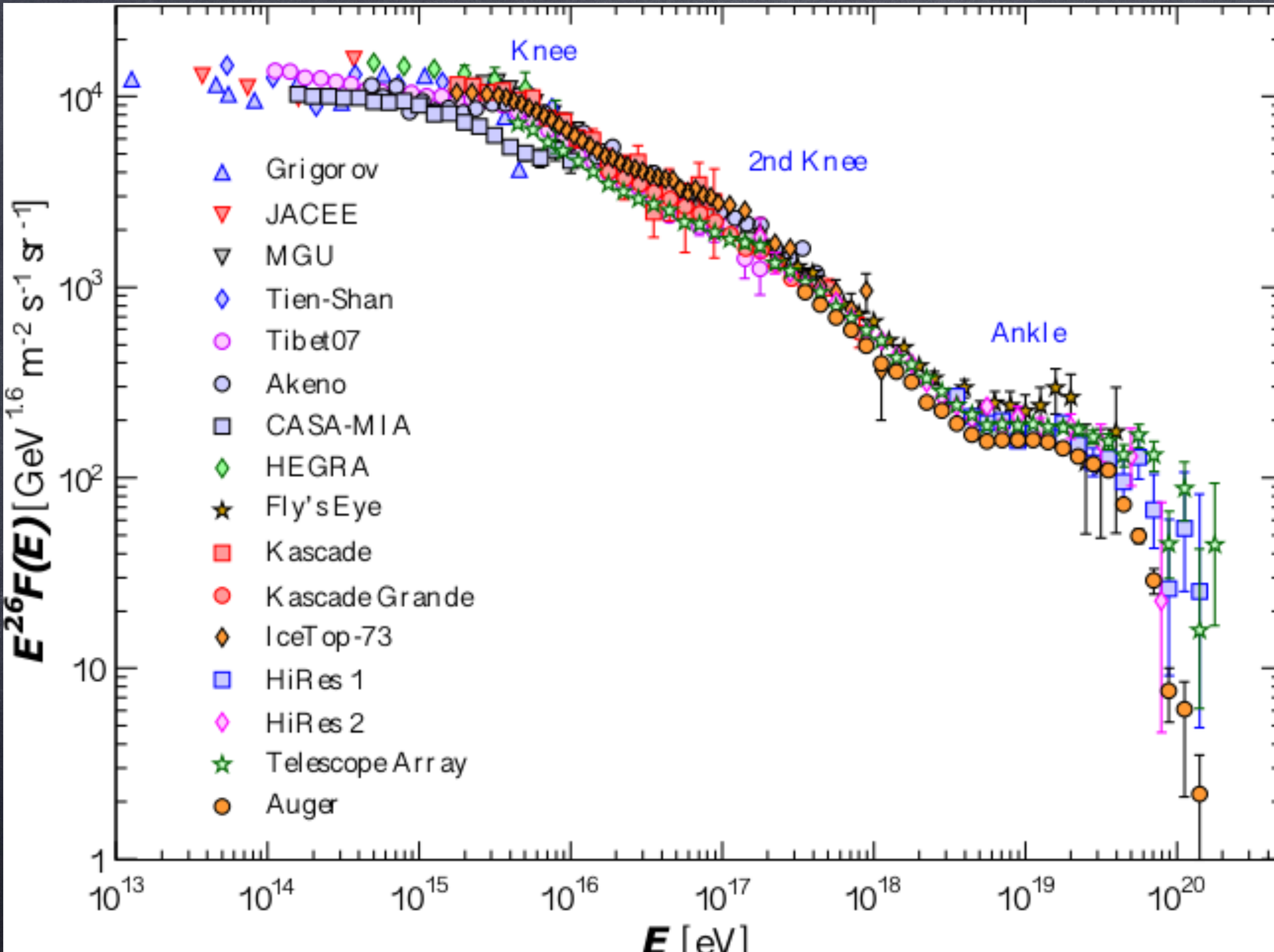

Knee
2nd Knee
Ankle
Grigorov
JACEE
MGU
Tien-Shan
Tibet07
Akeno
CASA-MIA
HEGRA
Fly's Eye
Kascade
Kascade Grande
IceTop-73
HiRes 1
HiRes 2
Telescope Array
Auger
$E^{2.6}F(E)$ [GeV$^{1.6}$ m^{-2} s^{-1} sr^{-1}]
E [eV]

Pierre Auger Spectra

Auger exposure = 120,000 km² sr yr as of end 2020

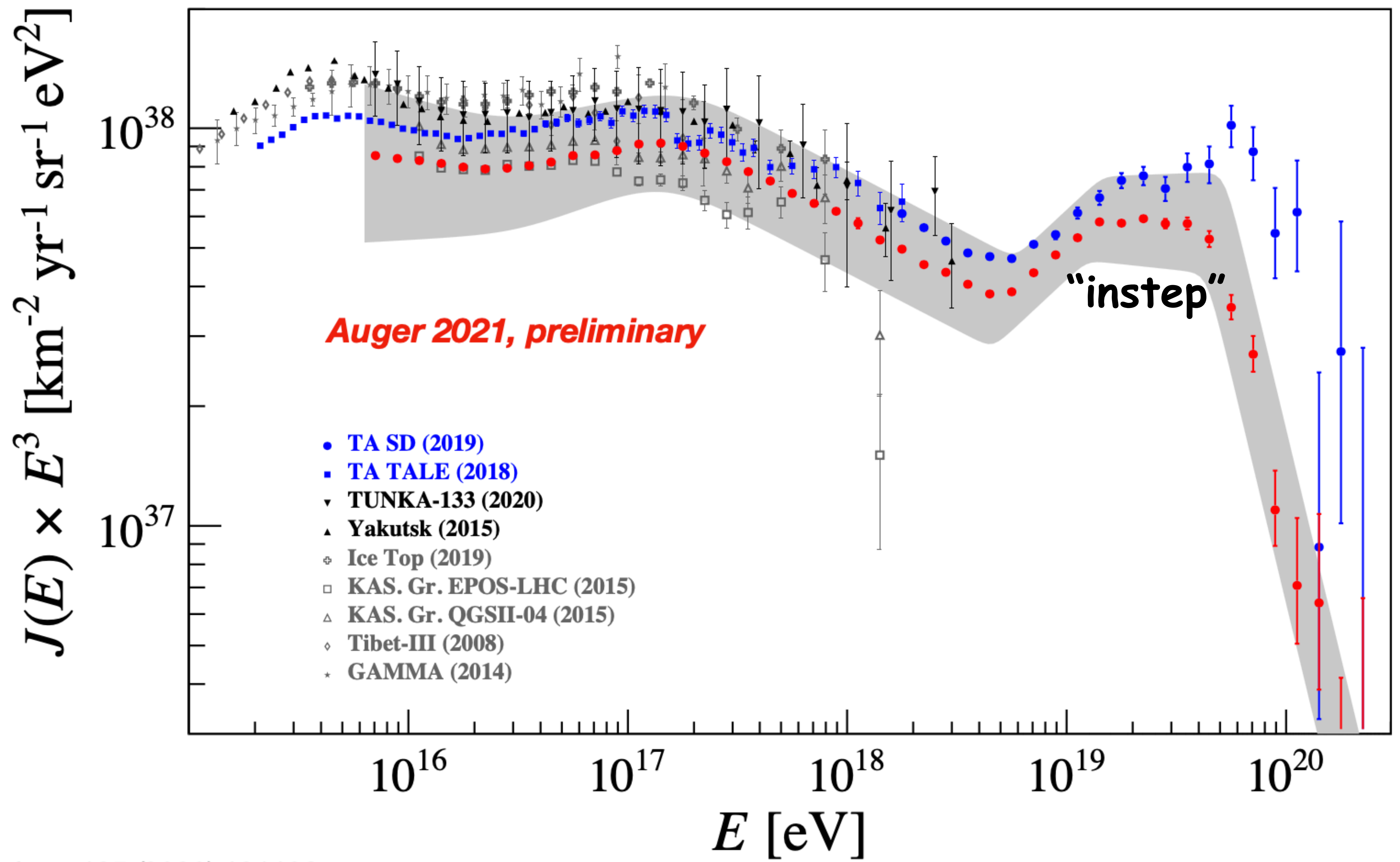

Phys. Rev. Lett. 125 (2020) 121106
Phys. Rev. D102 (2020) 062005
submitted to Eur. Phys. J. C (2021)

taken from R. Engel, Pierre Auger highlights, ICRC 2021

(Vladimir Novotny)

Atmospheric Showers and their Detection

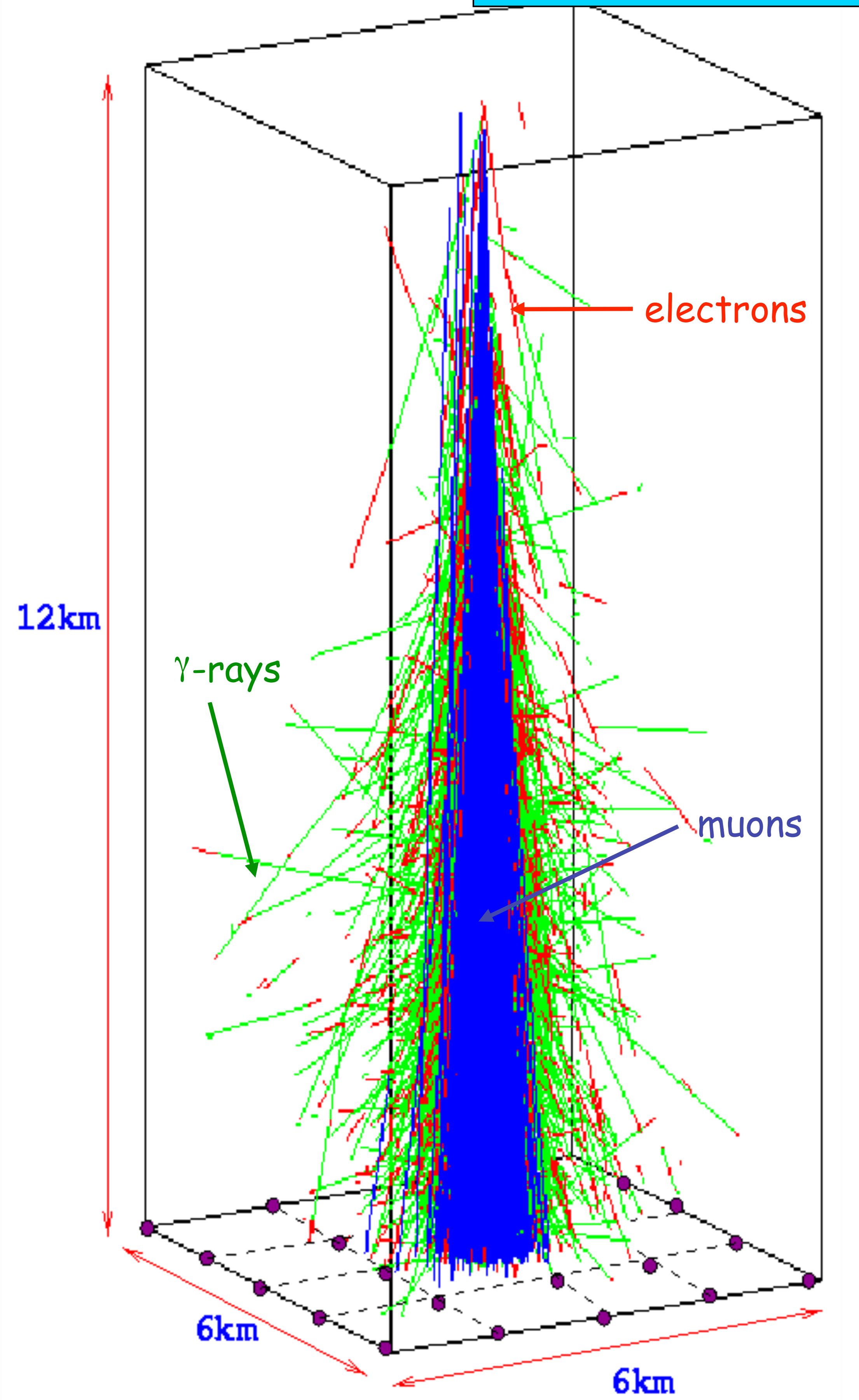

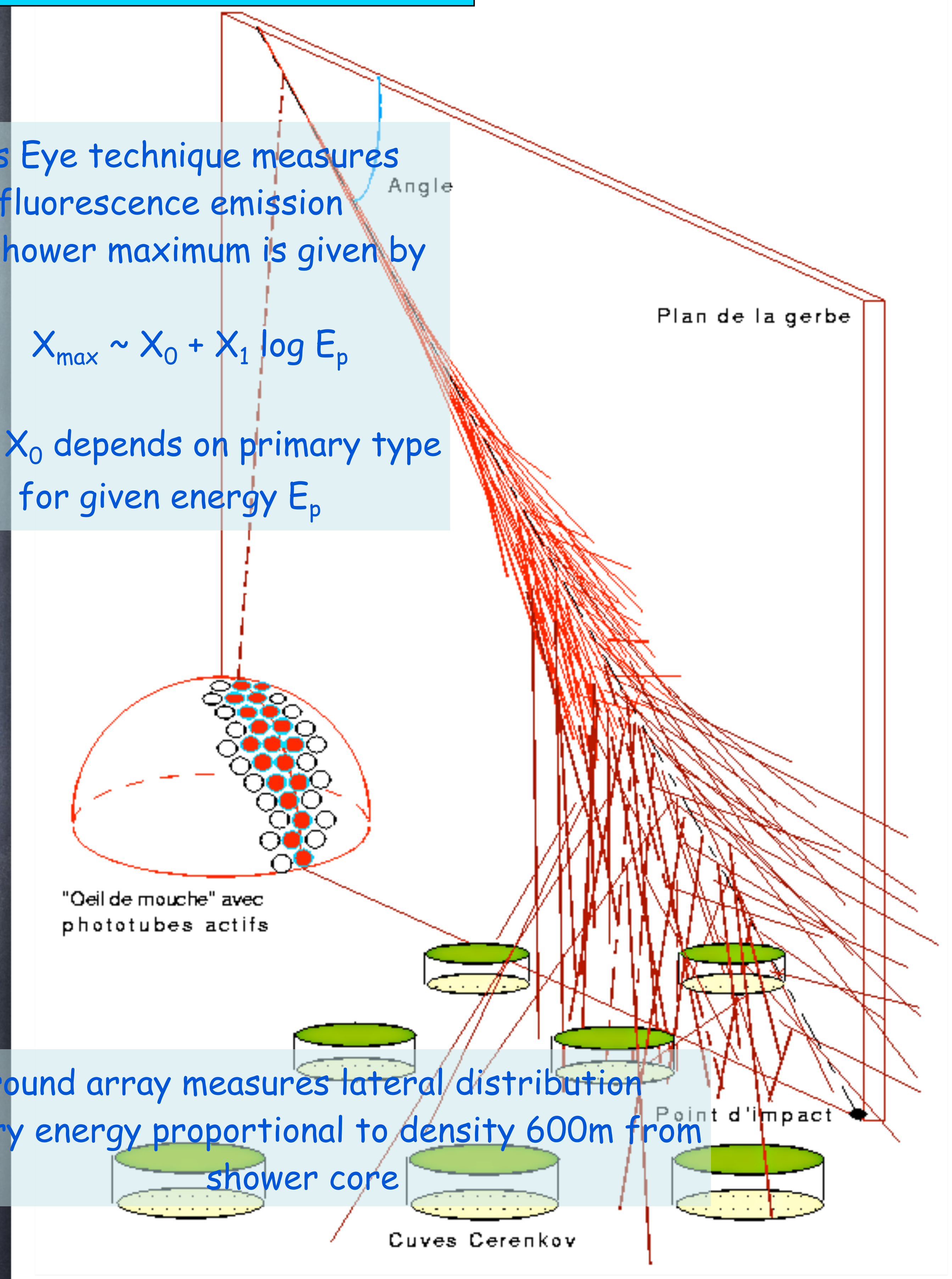

Fly's Eye technique measures fluorescence emission
The shower maximum is given by

$$X_{max} \sim X_0 + X_1 \log E_p$$

where X_0 depends on primary type for given energy E_p

Ground array measures lateral distribution
Primary energy proportional to density 600m from shower core

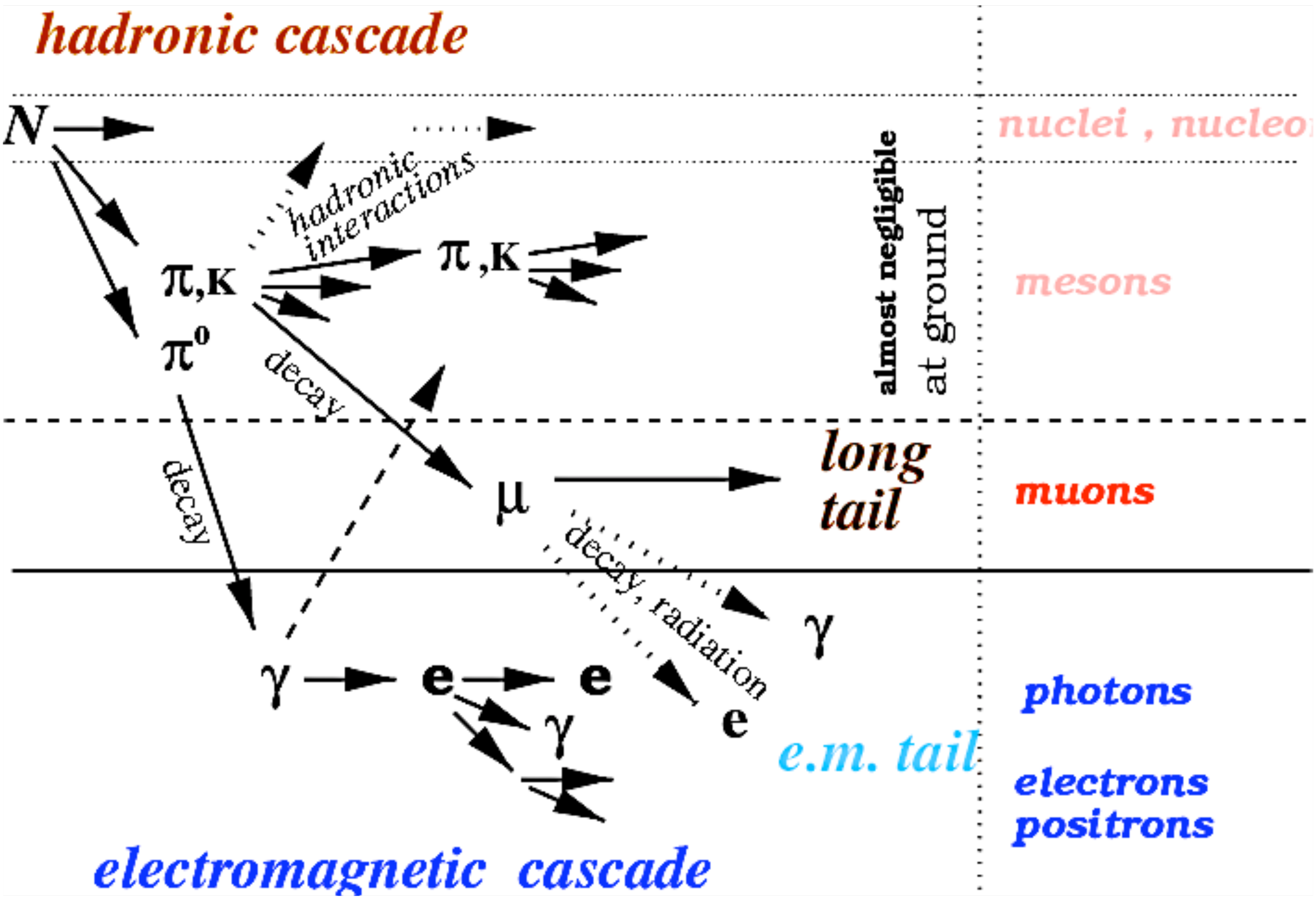
hadronic cascade
N
hadronic interactions
π,K
π,K
π0
decay
decay
almost negligible
at ground
nuclei , nucleo
mesons
μ
long tail
muons
decay, radiation
γ
γ
e
e
γ
e
e.m. tail
photons
electrons
positrons
electromagnetic cascade

Some Air Shower Physics

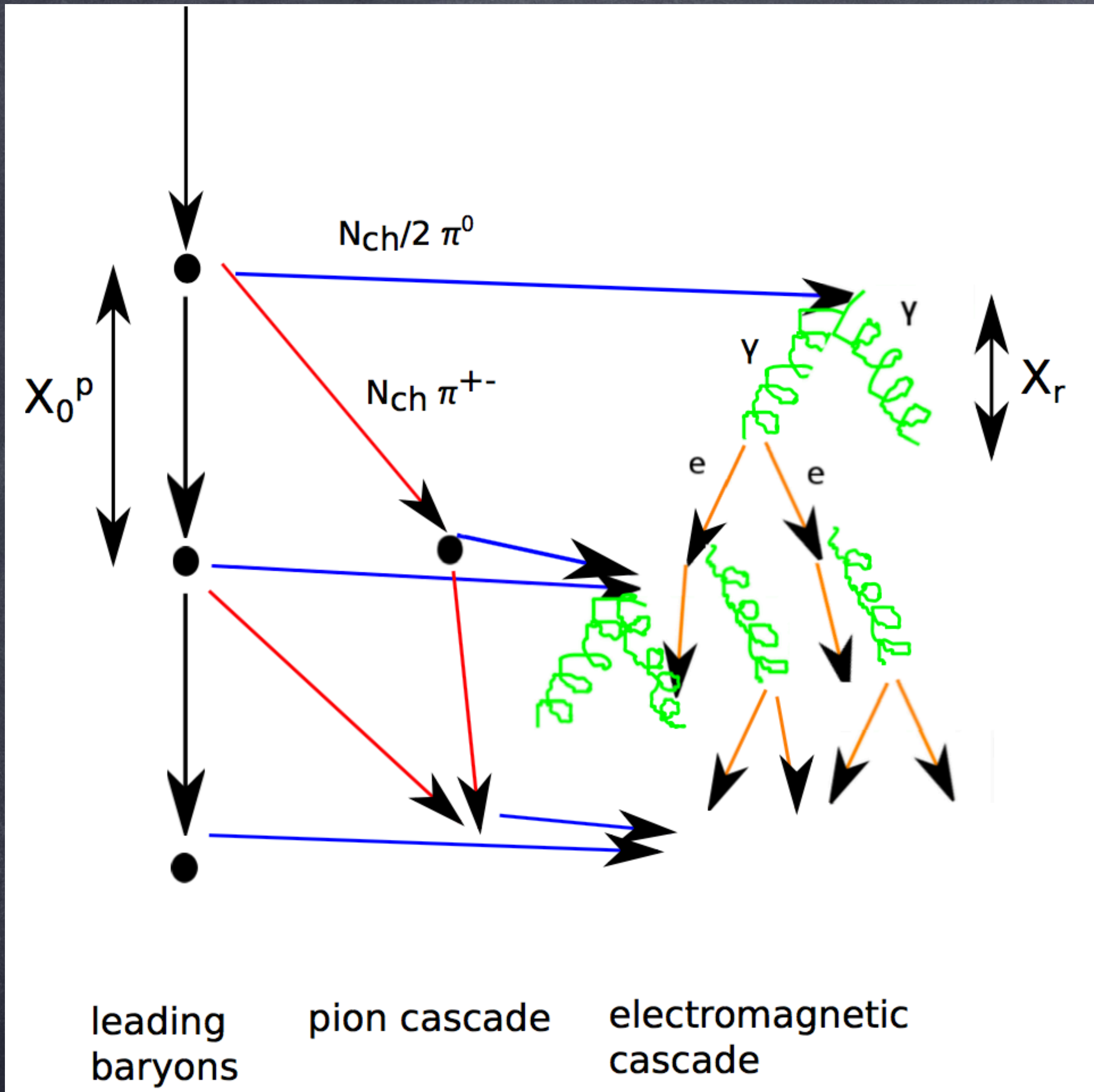

Fig. 5.2 A sketch of the first two generations of an hadronic cascade in the Heitler Matthews model [232] (left part) and of the first few generations of the electromagnetic cascade in the Heitler model [229] (right part). After each hadronic interaction length $X_0^p(E)$ the *leading baryon* produces $N_{ch}(E)$ charged pions and $N_{ch}(E)/2$ neutral pions. Neutral pions decay into two $\gamma-$rays instantaneously whereas charged pions interact again after column depth $\simeq X_0^p(E)$, producing further pions. High energy $\gamma-$rays produce electron-positron pairs after one radiation length X_r which in turn recreate $\gamma-$rays by bremsstrahlung after a similar length scale.

In this simple picture for a primary energy E_p the depth of shower maximum is the depth of first interaction X_0 plus the radiation length X_r times the number of generations n,

$$X_{max} \sim X_0 + X_r \log (E_p/E_c)$$

where E_c is some critical energy

Cosmic ray versus neutrino induced air showers

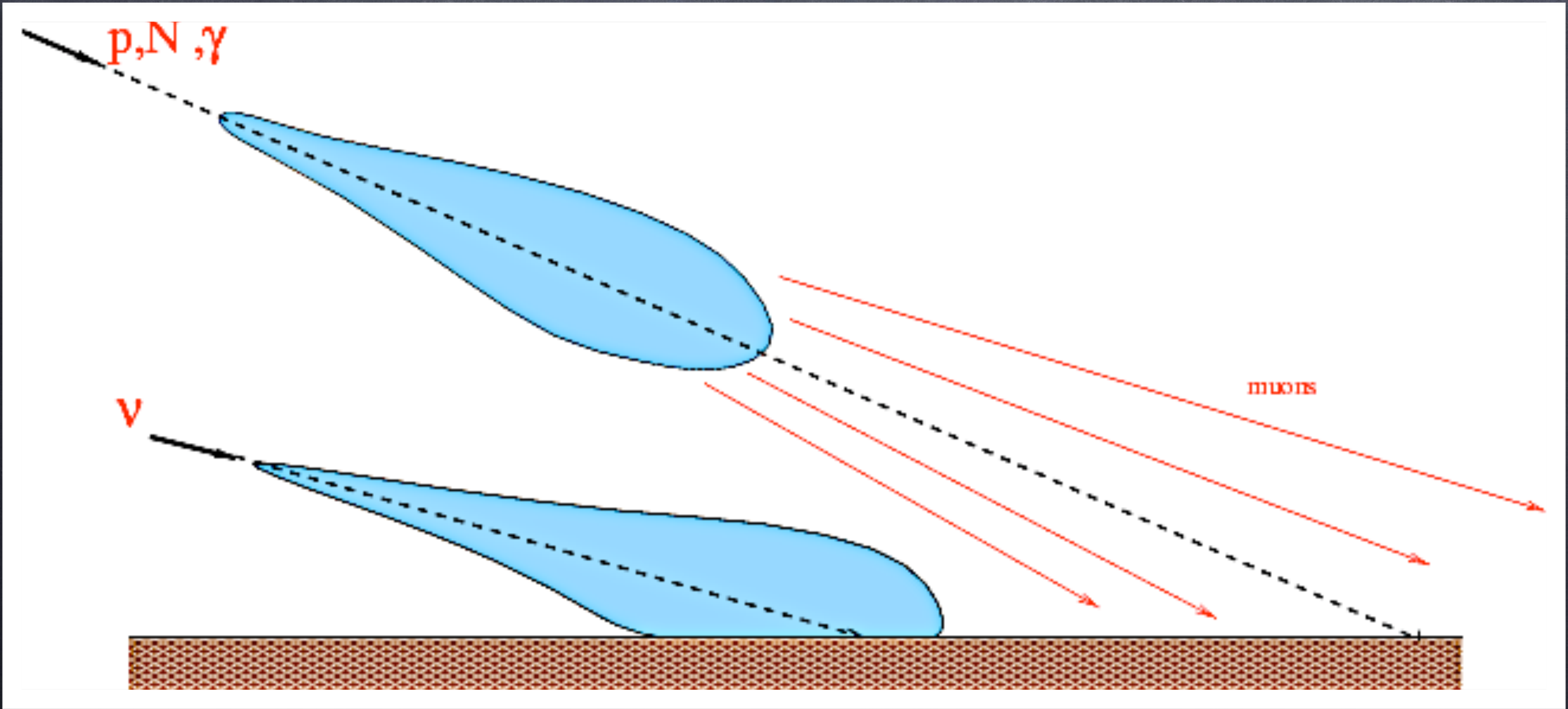

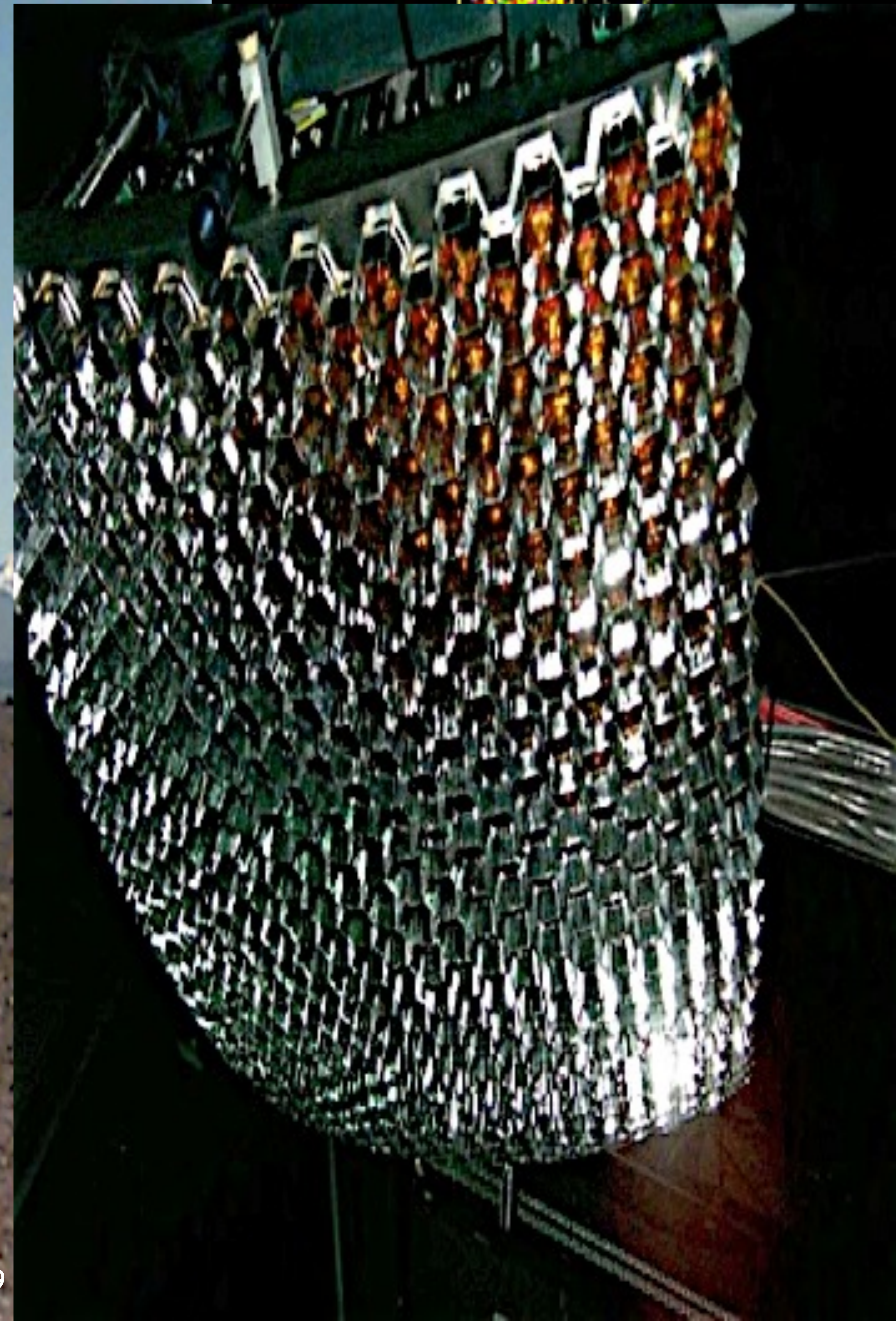

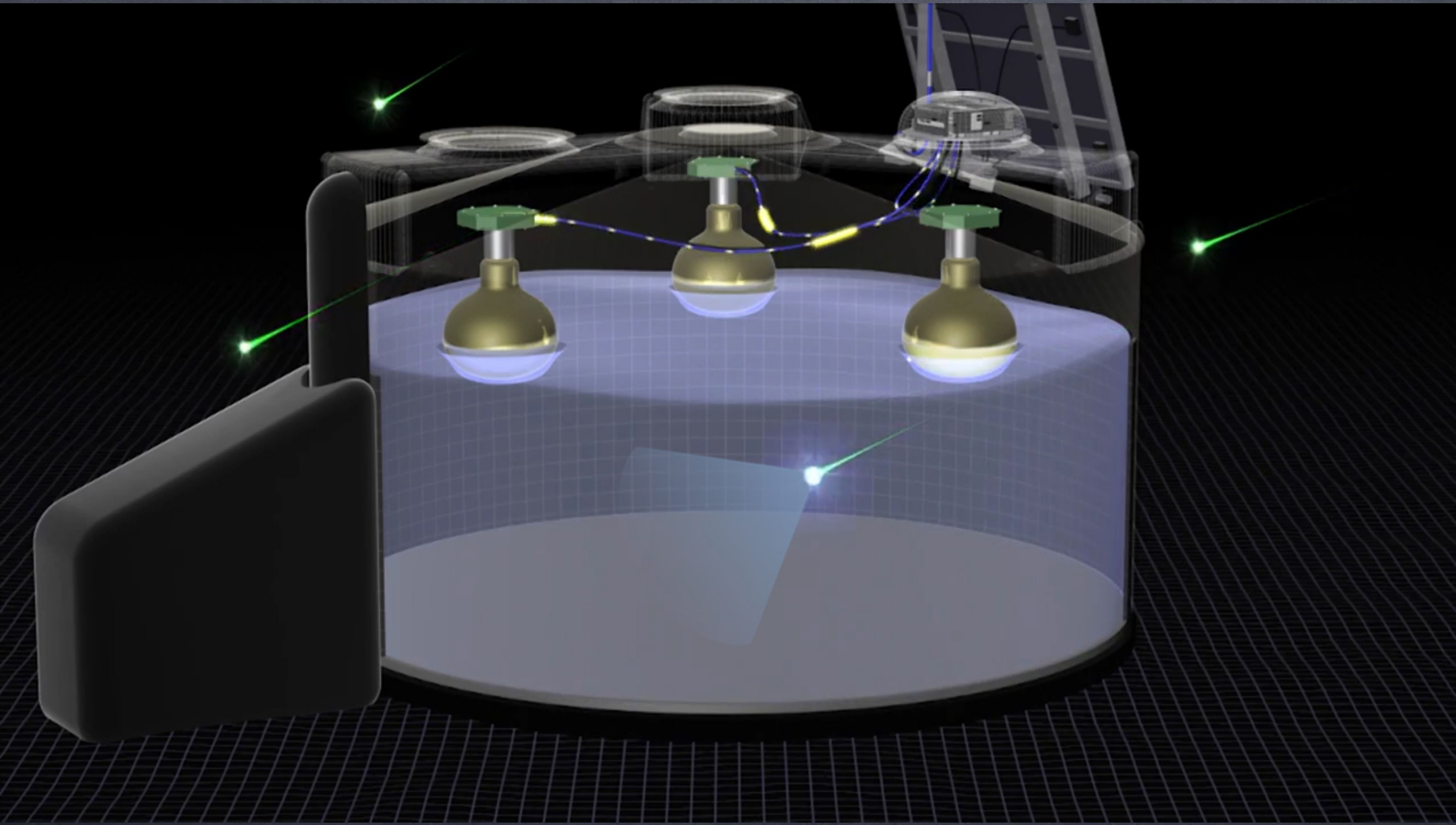

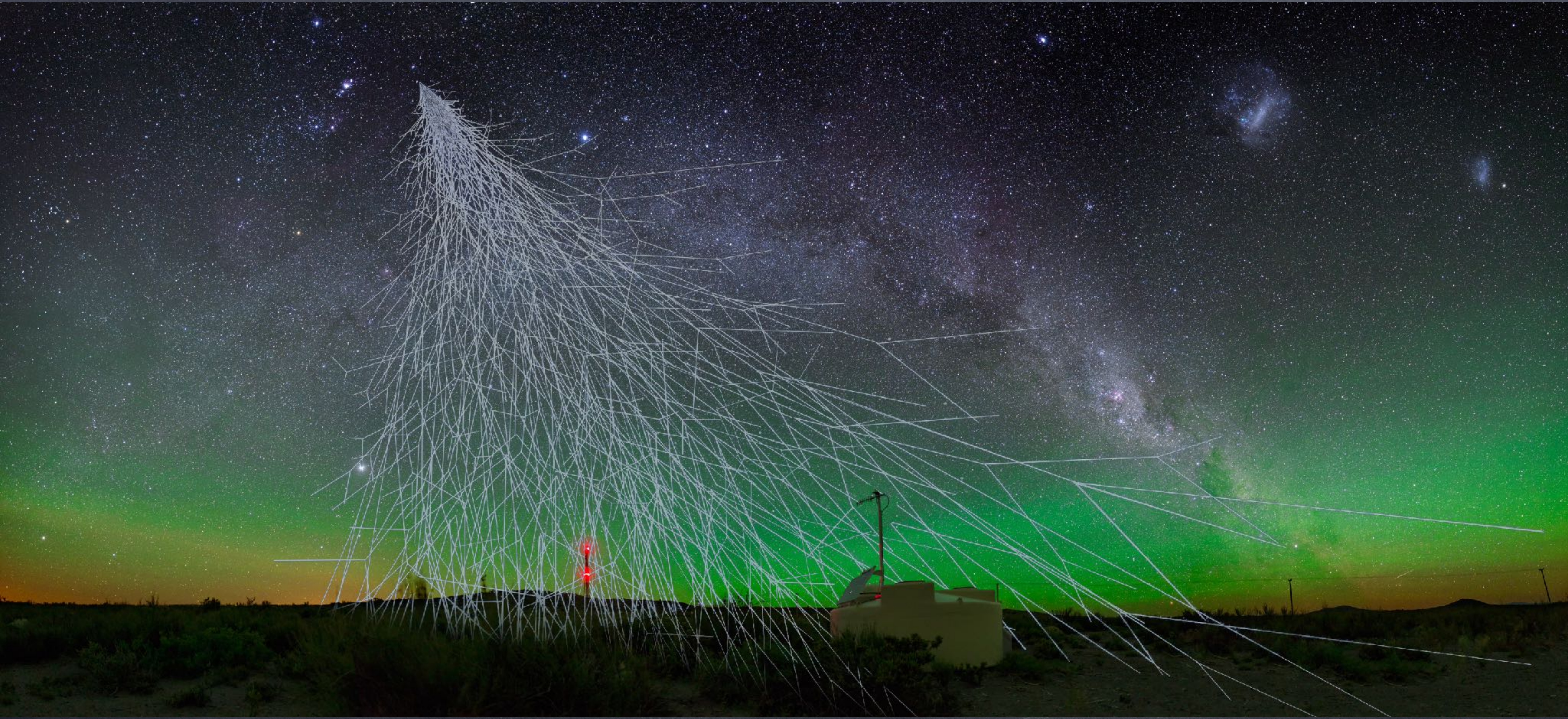

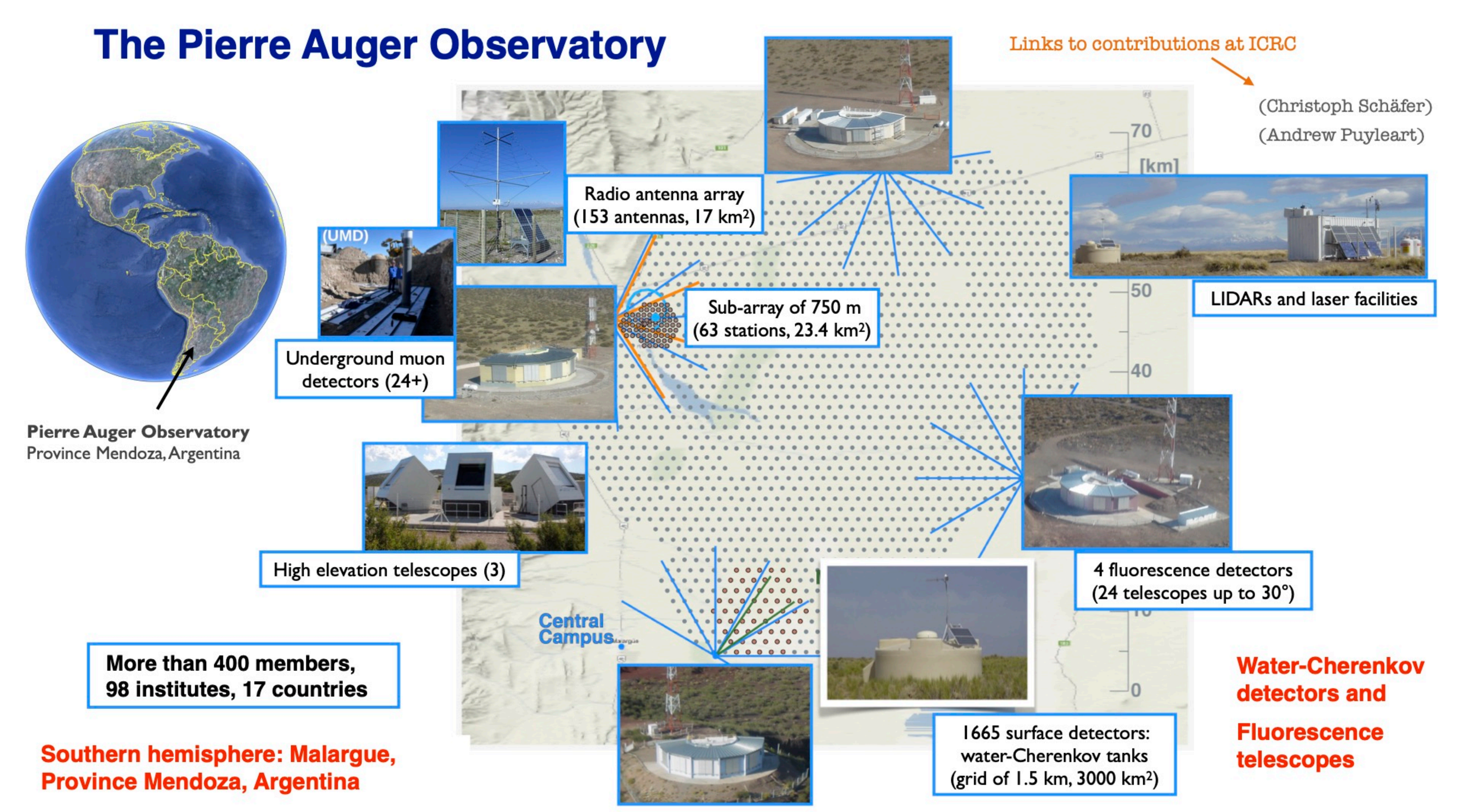

taken from R. Engel, Pierre Auger highlights, ICRC 2021

The Greisen-Zatsepin-Kuzmin (GZK) effect

Nucleons can produce pions on the cosmic microwave background

$$E_{\rm th} = \frac{2m_N m_\pi + m_\pi^2}{4\varepsilon} \simeq 4 \times 10^{19}\,{\rm eV}$$

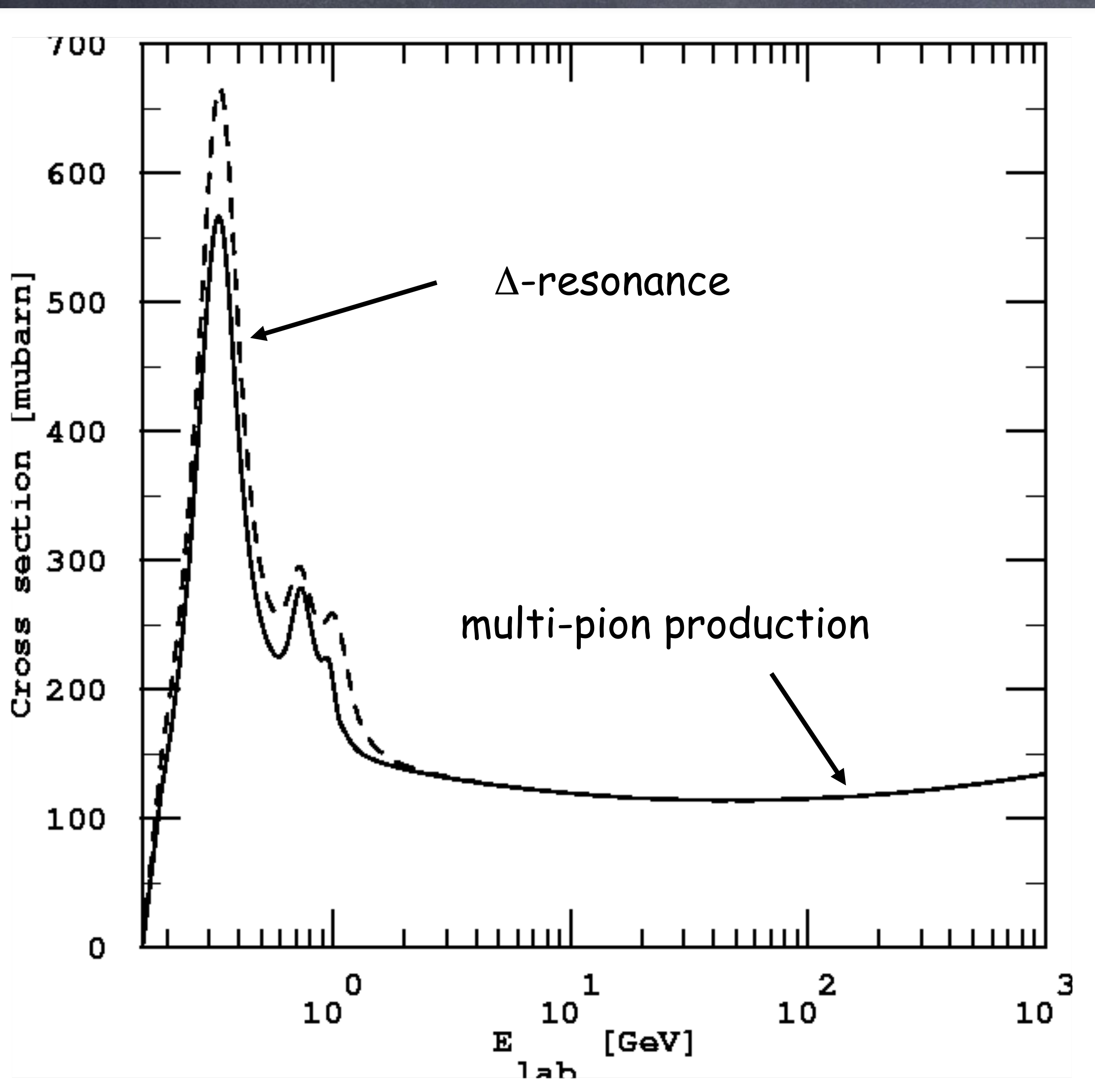

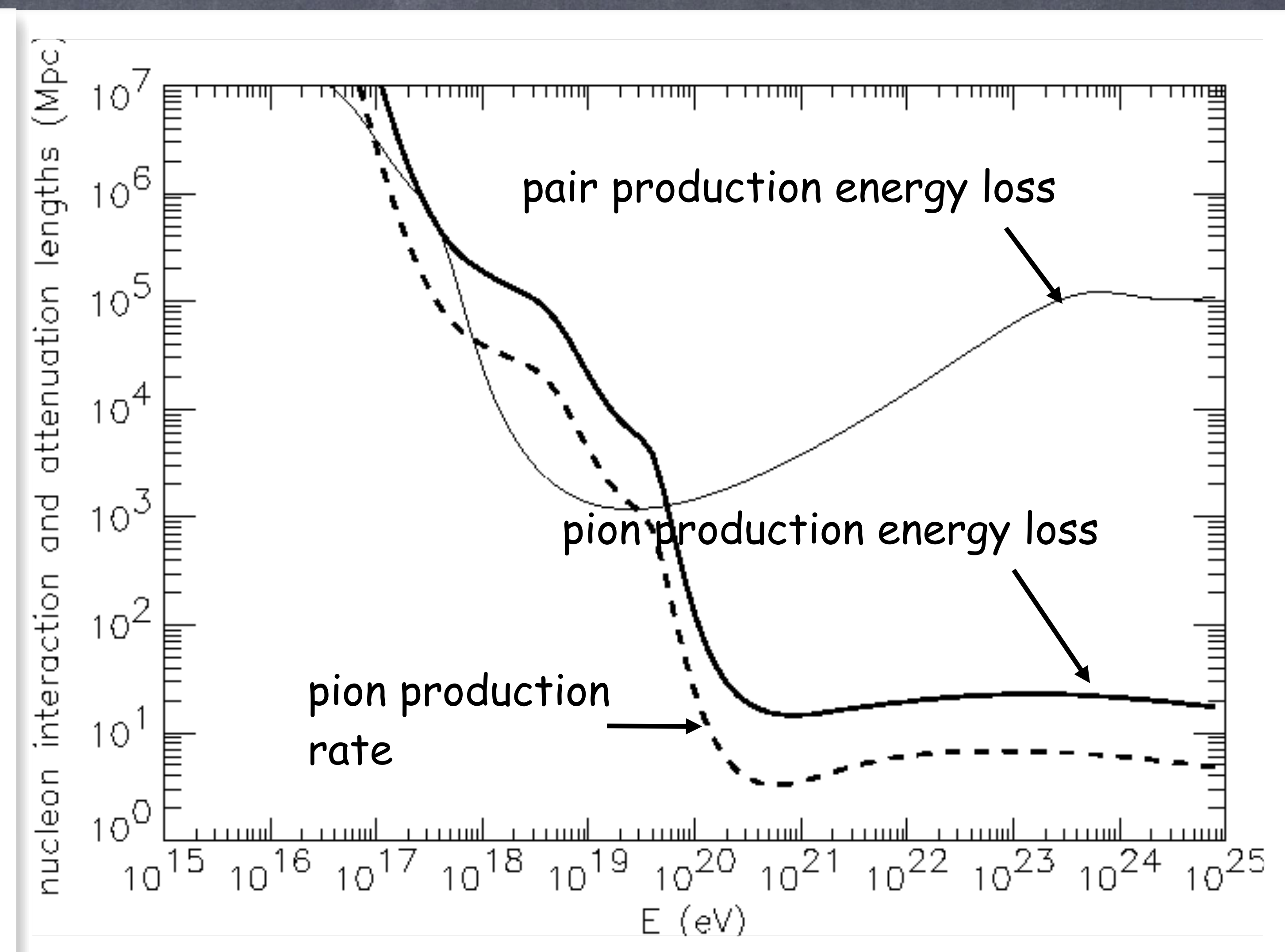

sources must be in cosmological backyard
Only Lorentz symmetry breaking at $\Gamma > 10^{11}$ could avoid this conclusion.

Length scales for relevant processes of a typical heavy nucleus

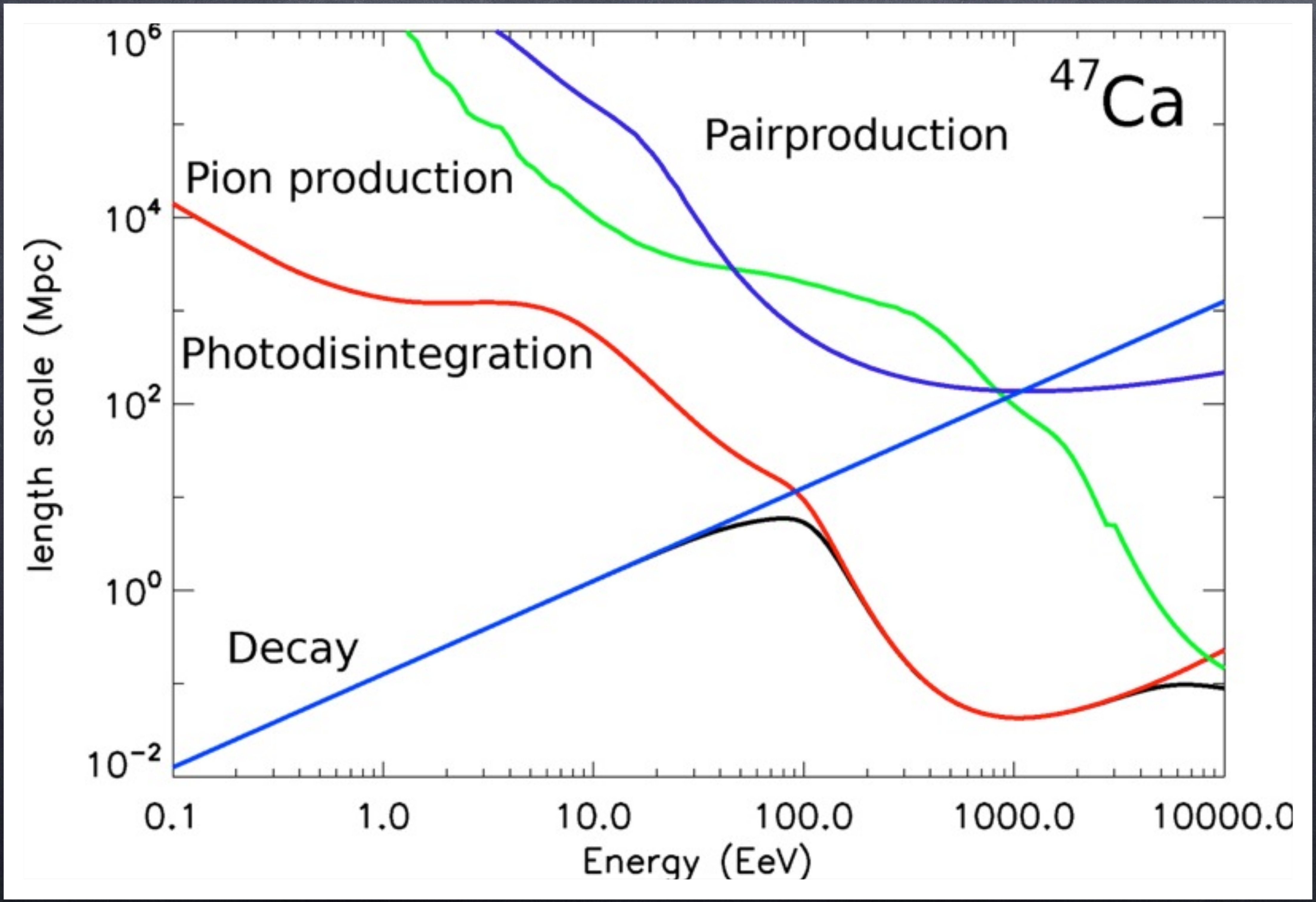

1^{st} Order Fermi Shock Acceleration

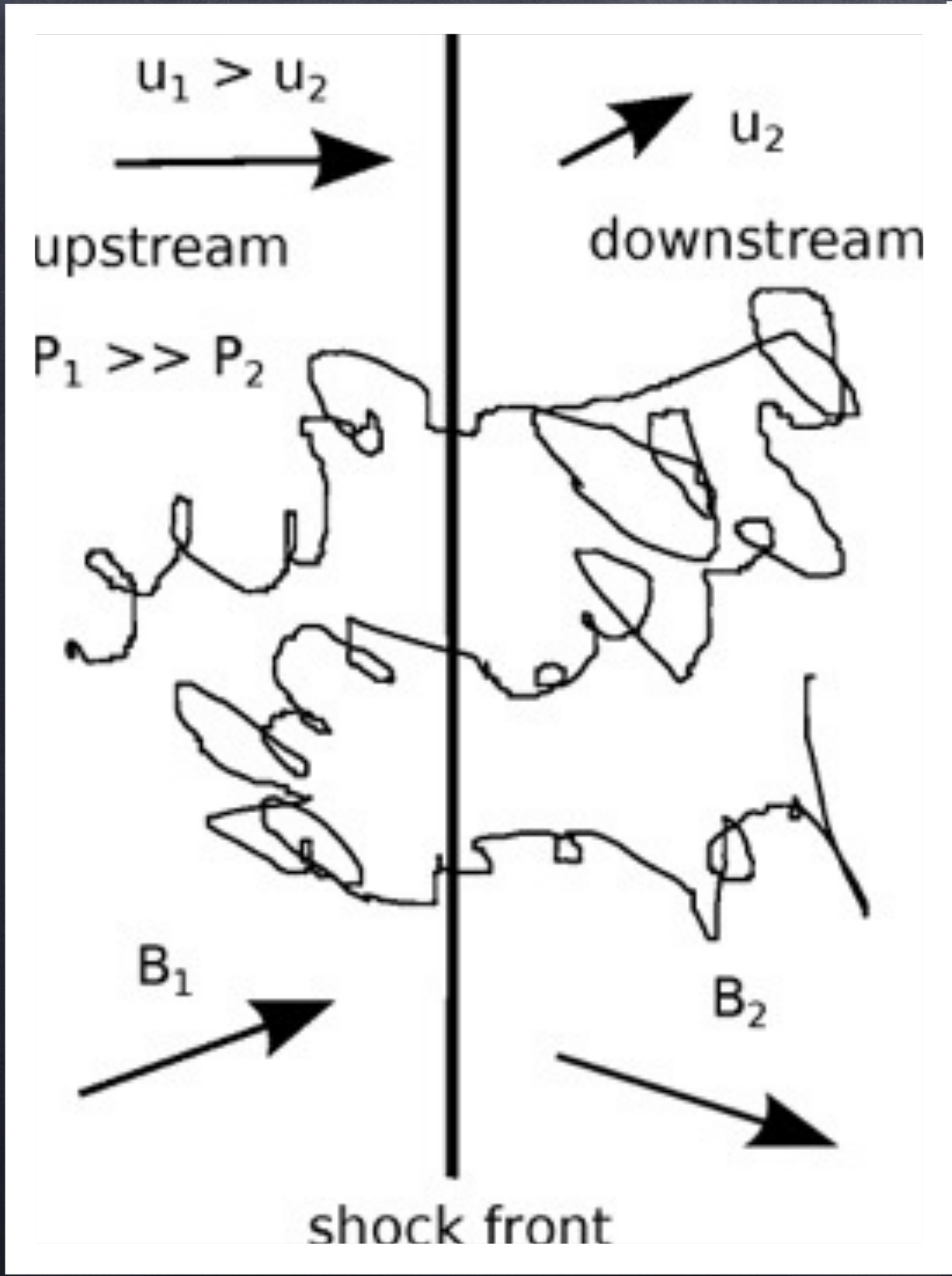

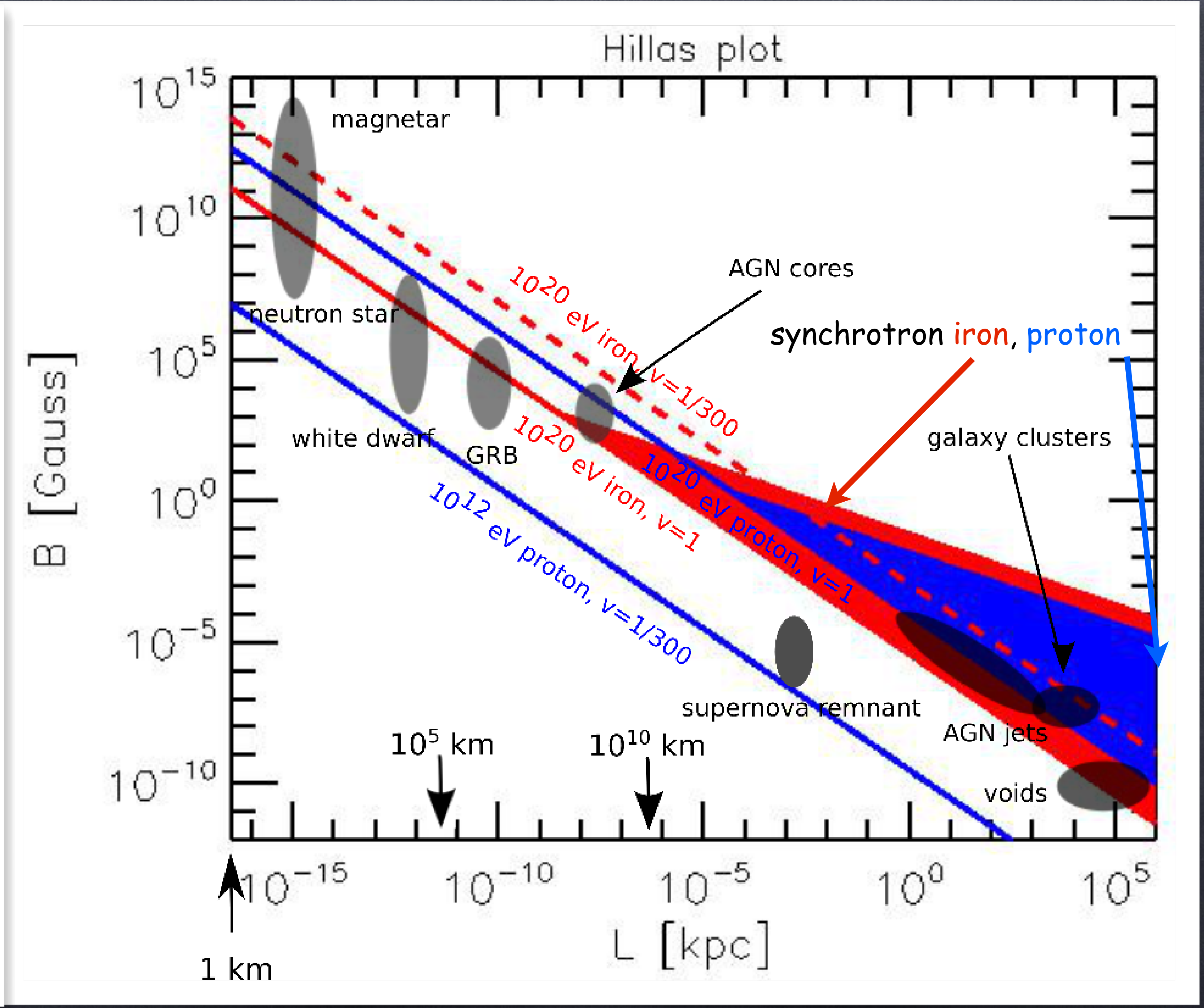

Fractional energy gain per shock crossing $\sim u_1 - u_2$ on a time scale r_L/u_2 .

Together with downstream losses this leads to a spectrum E^{-q} with $q > 2$ typically.

Confinement, gyroradius < shock size, and energy loss times define maximal energy

Shell-type supernova remnant RCW 86 seen by HESS

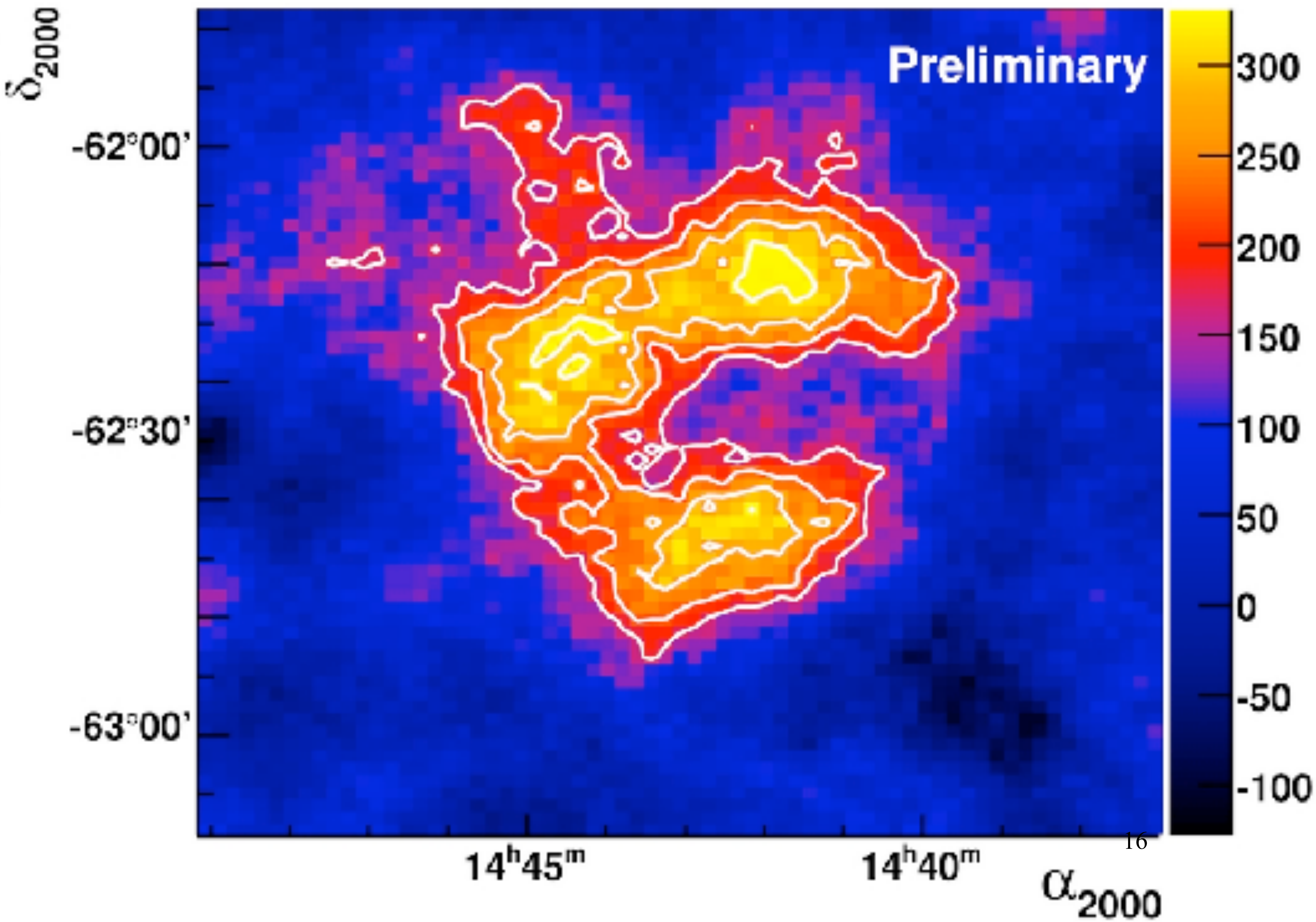

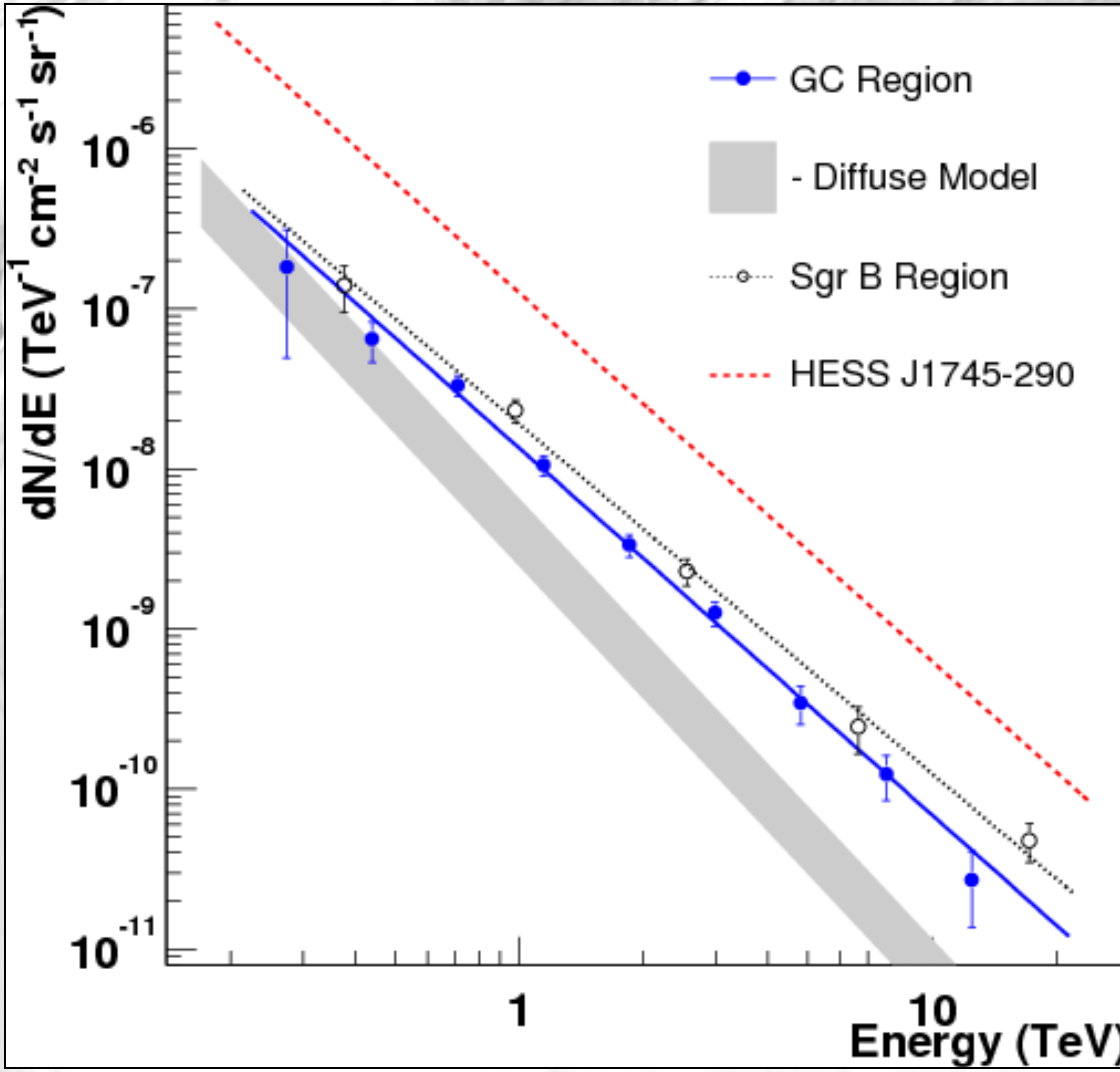

Given the observed spectrum $E^{-2.3}$, this can be interpreted as photons from π^0 decay produced in pp interactions where the TeV protons have the same spectrum and could have been produced in a SN event.

Note that this is consistent with the source spectrum both expected from shock acceleration theory and from the cosmic ray spectrum observed in the solar neighborhood, $E^{-2.7}$, corrected for diffusion in the galactic magnetic field, $j(E) \sim Q(E)/D(E)$.

Some general Requirements for Sources

Accelerating particles of charge eZ to energy E_{max} requires induction $\varepsilon > E_{max}/eZ$. With $Z_0 \sim 100\Omega$ the vacuum impedance, this requires dissipation of minimum power of

$$L_{\rm min} \sim \frac{\epsilon^2}{Z_0} \simeq 10^{45}\, Z^{-2} \left(\frac{E_{\rm max}}{10^{20}\,{\rm eV}}\right)^2 \,{\rm erg\,s^{-1}}$$

This „Poynting" luminosity can also be obtained from $L_{min} \sim (BR)^2$ where BR is given by the „Hillas criterium":

$$BR > 3\times10^{17}\,\Gamma^{-1}\left(\frac{E_{\rm max}/Z}{10^{20}\,{\rm eV}}\right)\,{\rm Gauss\,cm}$$

where Γ is a possible beaming factor.
If most of this goes into electromagnetic channel, only AGNs and maybe gamma-ray bursts could be consistent with this.

A possible acceleration site associated with shocks in hot spots of active galaxies

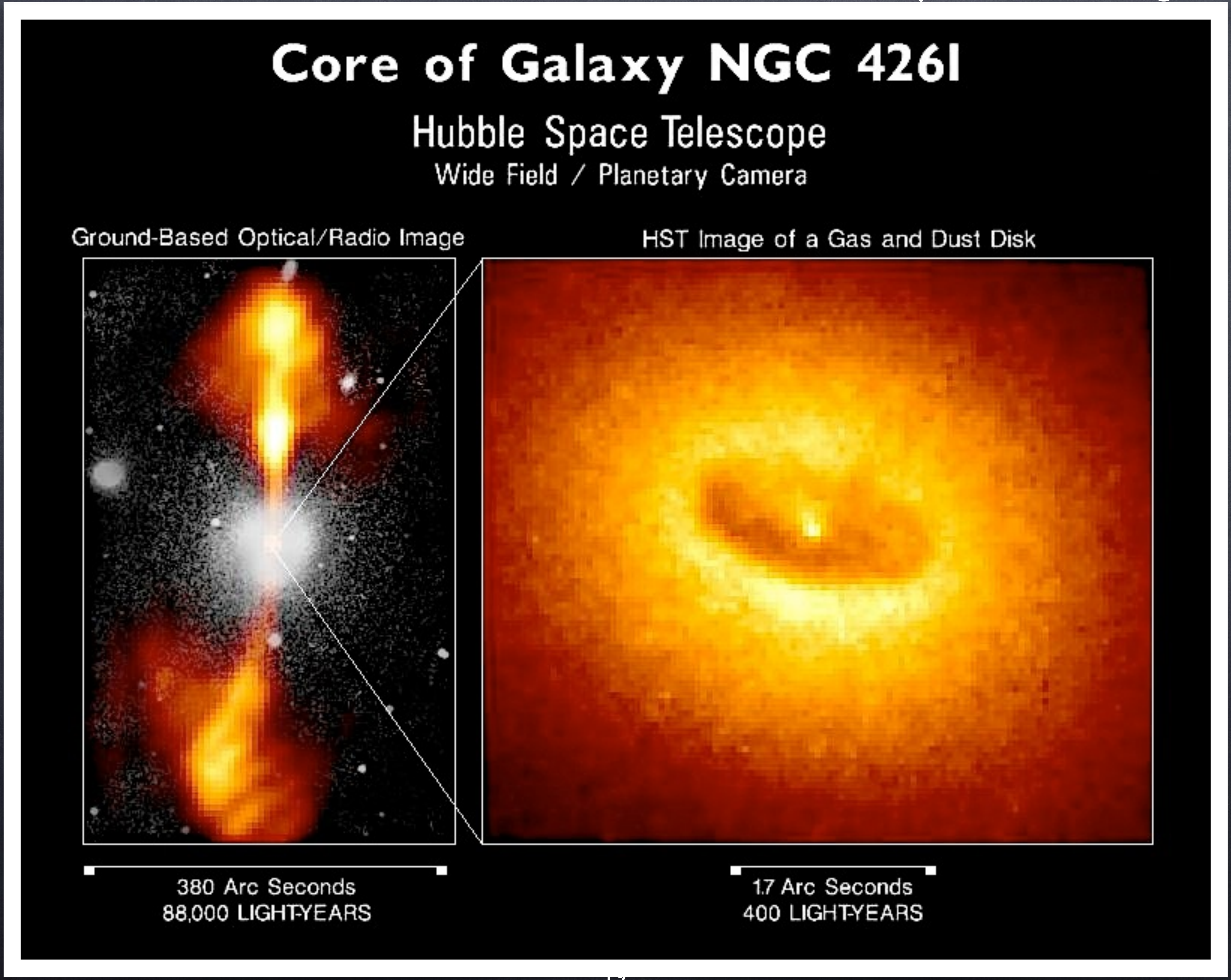

Or Cygnus A

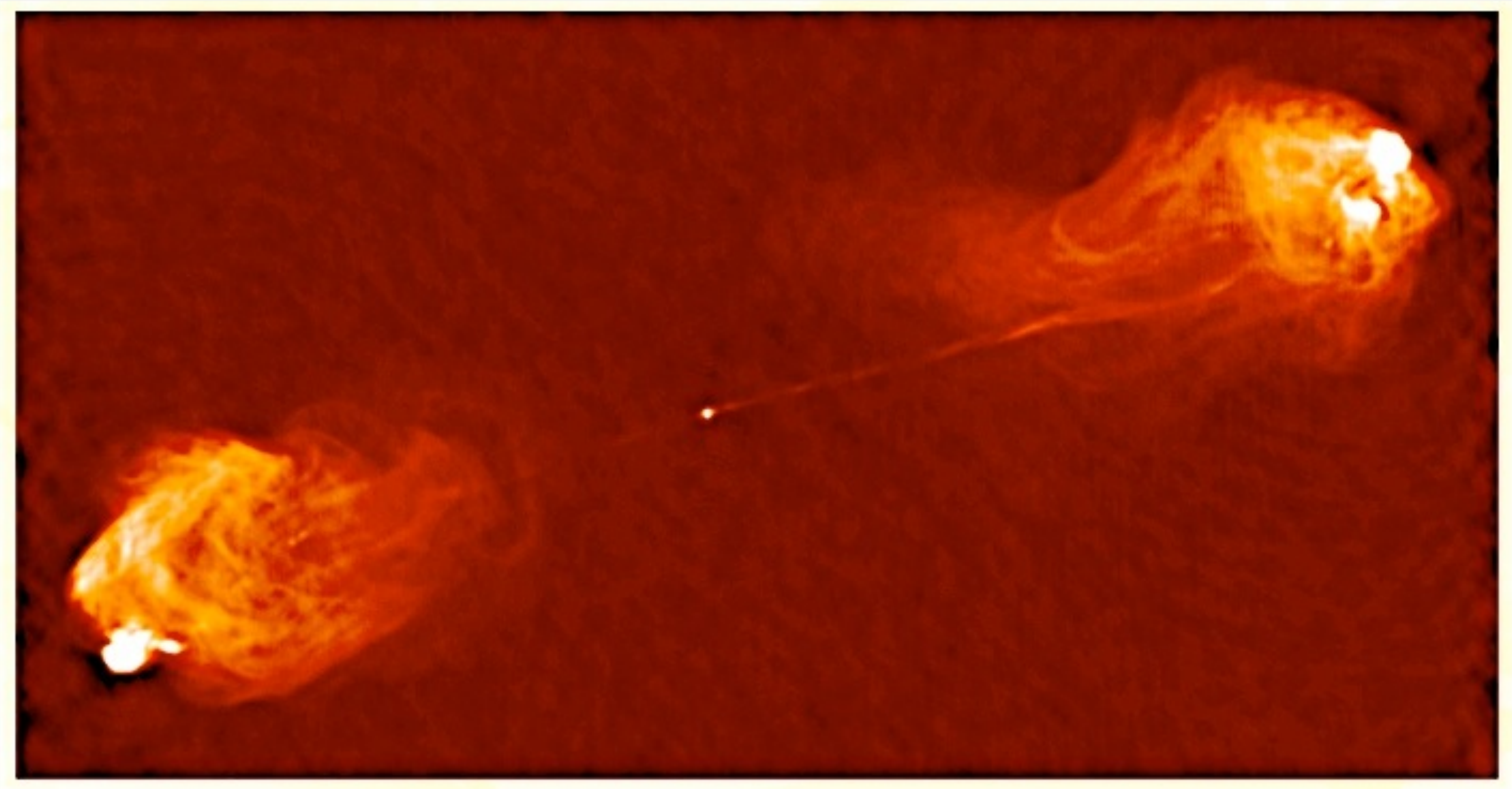

Mass Composition

Depth of shower maximum X_{max} and its distribution contain information on primary mass composition

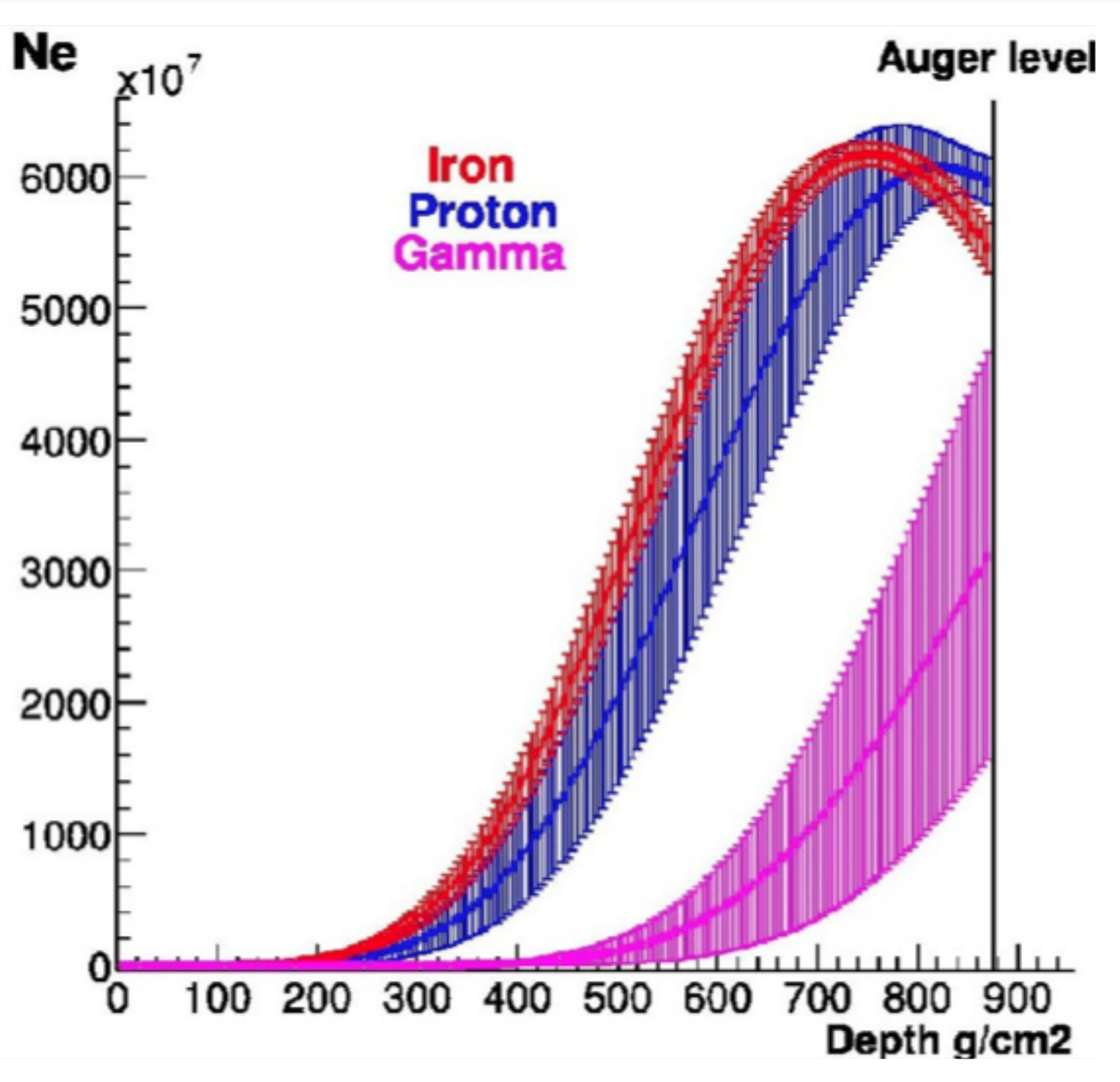

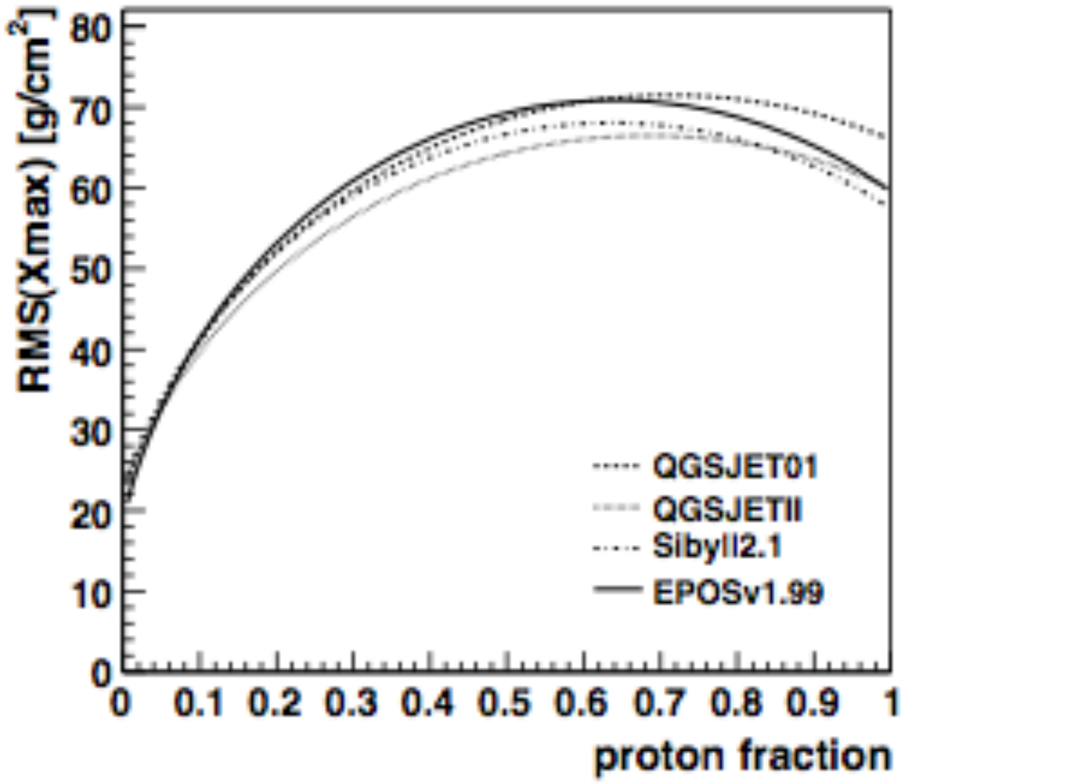

FIGURE 1. RMS(X_{max}) from different hadronic interaction models [23] and a two-component p/Fe composition model ($E = 10^{18}$ eV).

Pierre Auger data suggest a heavier composition toward highest energies:

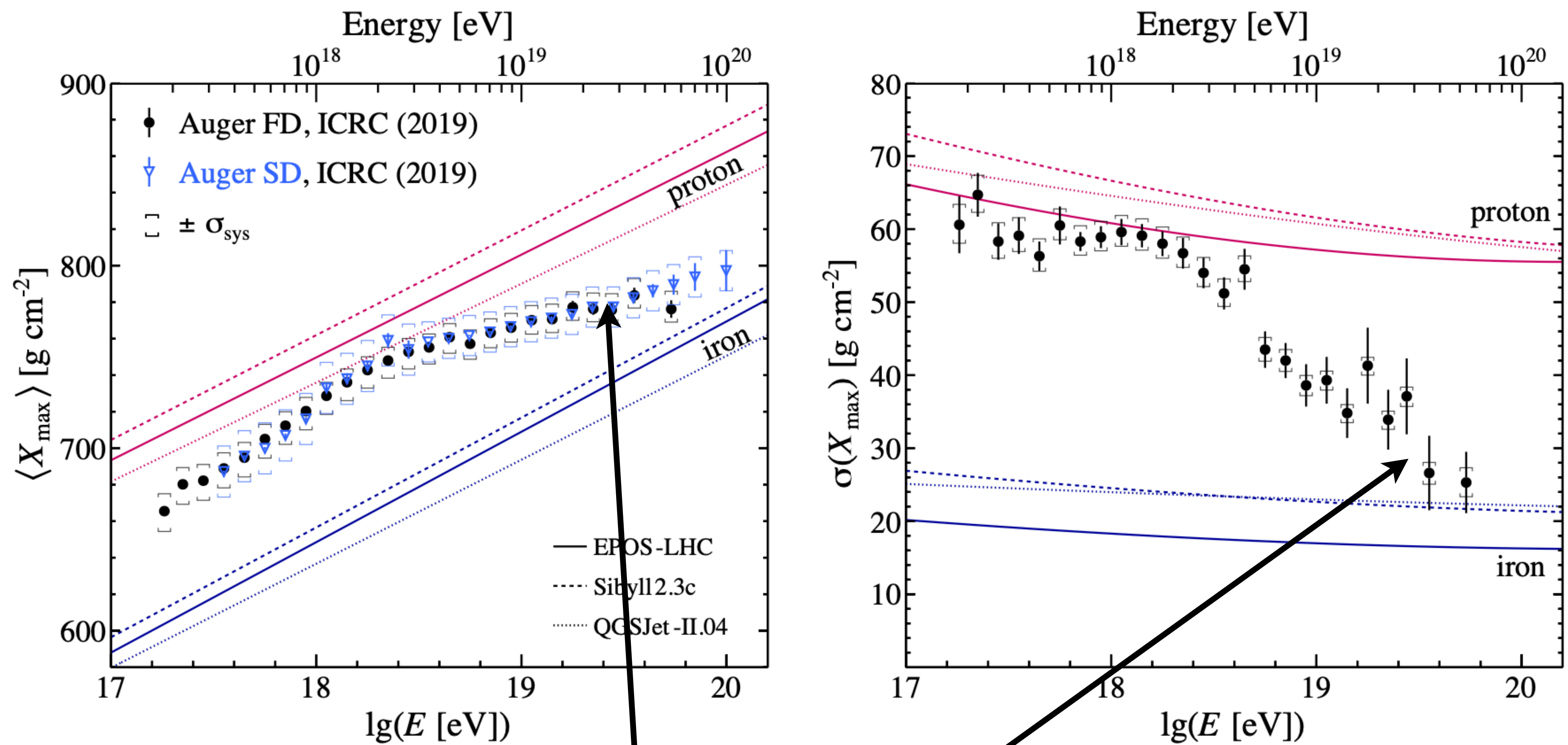

taken from R. Engel, Pierre Auger highlights, ICRC 2021

Important: LHC-tuned interaction models used for interpretation

(Phys. Rev. D90 (2014), 122005 & 122005, updated ICRC 2019) (Phys. Rev. D96 (2017), 122003)

potential tension with air shower simulations and some hadronic interaction models because a mixed composition would predict larger RMS(X_{max})

but not confirmed on the northern hemisphere by HiRes and Telescope Array which appear consistent with protons

Muon number measured are systematically higher than predicted

Hybrid events and inclined showers

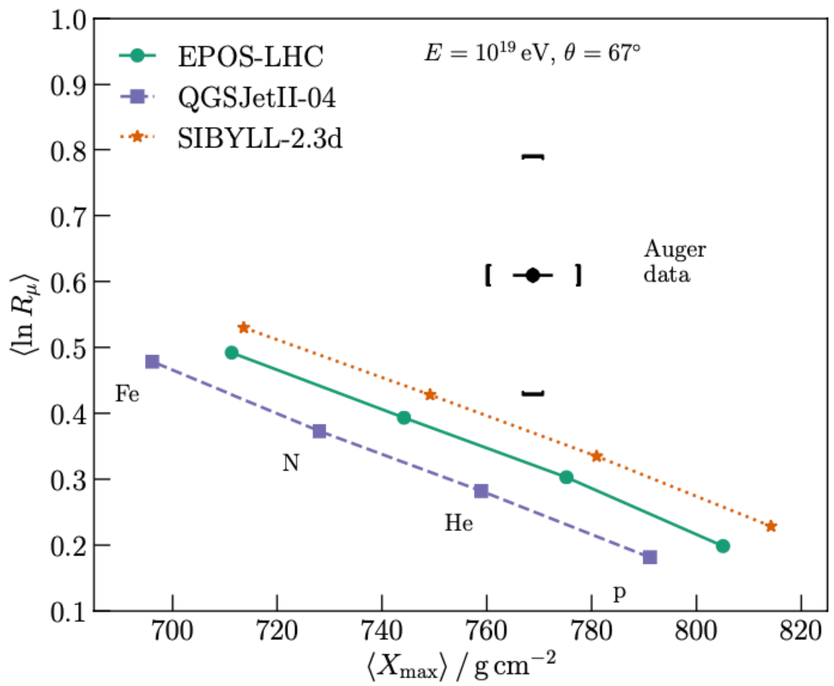

(Phys. Rev. Lett. 117 (2016) 192001, Phys. Rev. D91 (2015) 032003)

Muon counters and vertical

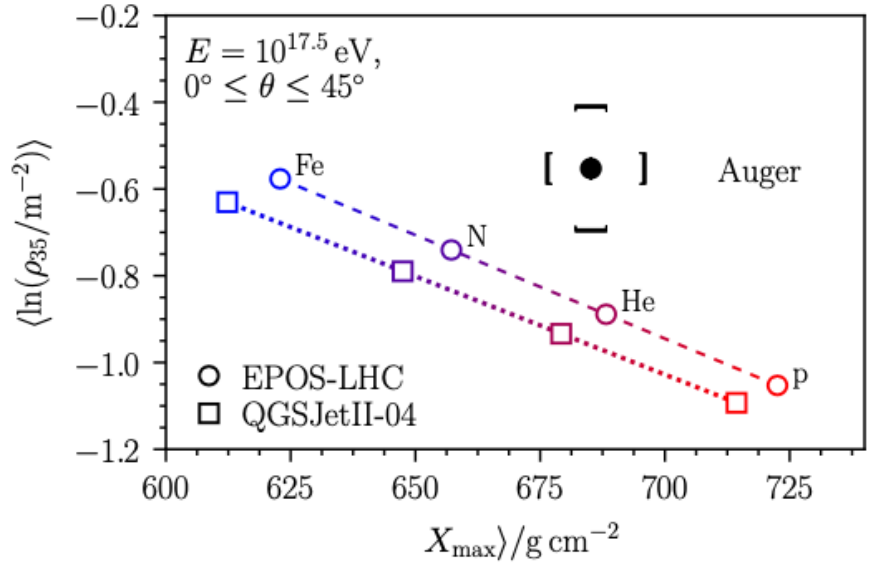

(Eur. Phys. J. C80 (2020) 751)

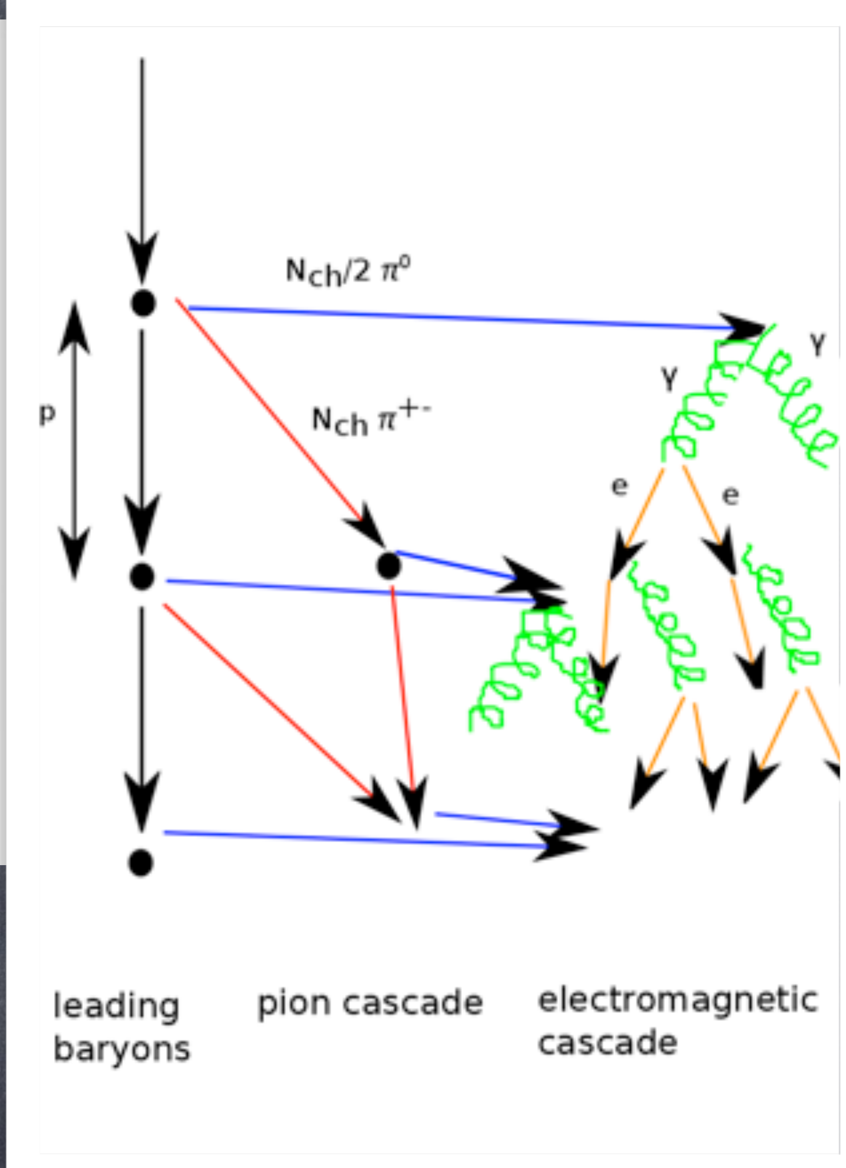

Pierre Auger Collaboration highlights, R. Engel, ICRC 2021

The muon number scales as

$$N_\mu \propto E_{\text{had}} \propto (1 - f_{\pi^0})^N ,$$

with the fraction going into the electromagnetic channel $f_{\pi^0} \simeq \frac{1}{3}$ and the number of generations N strongly constrained by $X_{\max}$. Larger N_μ thus requires smaller f_{π^0} ! The production of ρ^0 could also play a role.

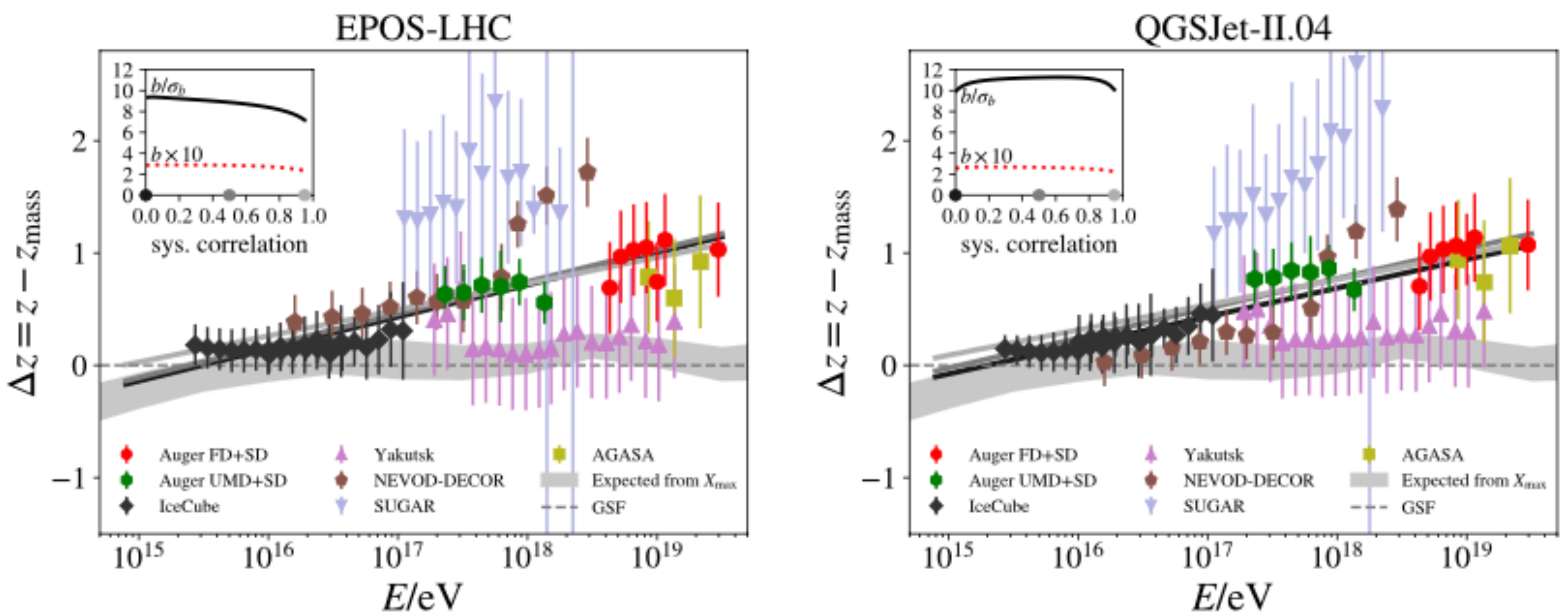

D. Soldin, arXiv:2108.08431, ICRC 2021

Figure 5: Linear fits to the $\Delta z = z - z_{\rm mass}$ distributions, as described in Eq. (3). Shown in the inset are the slope, b, and its deviation from zero in standard deviations for an assumed correlation of the point-wise uncertainties within each experiment. Examples of the fits are shown for a correlation of 0.0, 0.5, and 0.95.

$$\Delta z \equiv \frac{\ln \left\langle N_\mu \right\rangle - \ln \left\langle N^{\rm det}_{\mu,\rm p} \right\rangle}{\ln \left\langle N^{\rm det}_{\mu,\rm Fe} \right\rangle - \ln \left\langle N^{\rm det}_{\mu,\rm p} \right\rangle} - \frac{\langle \ln A \rangle}{56}$$

where N_μ is the measured muon number, $N^{\rm det}_{\mu,i}$ is the muon number predicted to be detected for species i and $\langle \ln A \rangle$ is composition deduced from measured $X_{\rm max}$. A consistent hadronic model would give $\Delta z = 0$ within the superposition approximation.

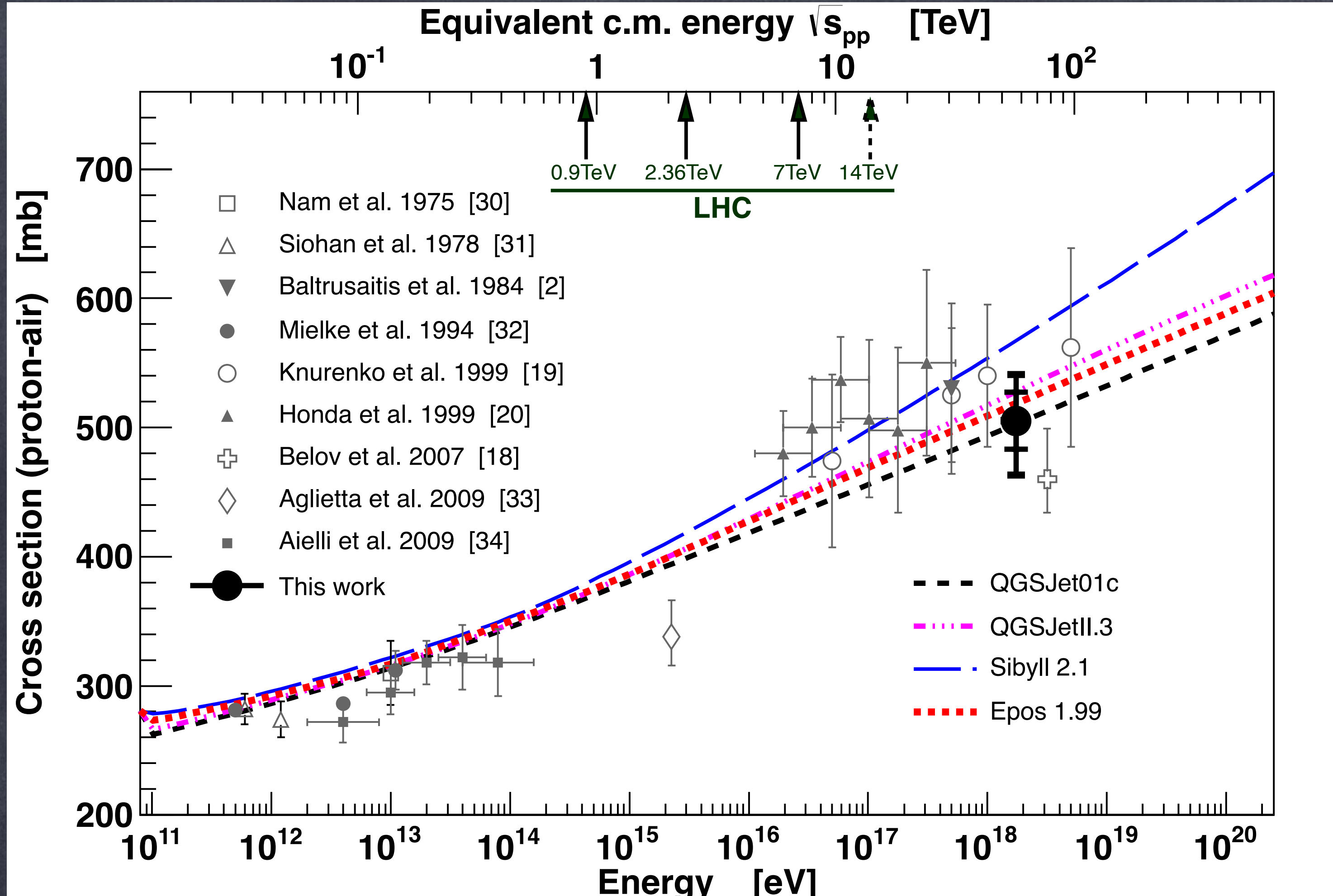

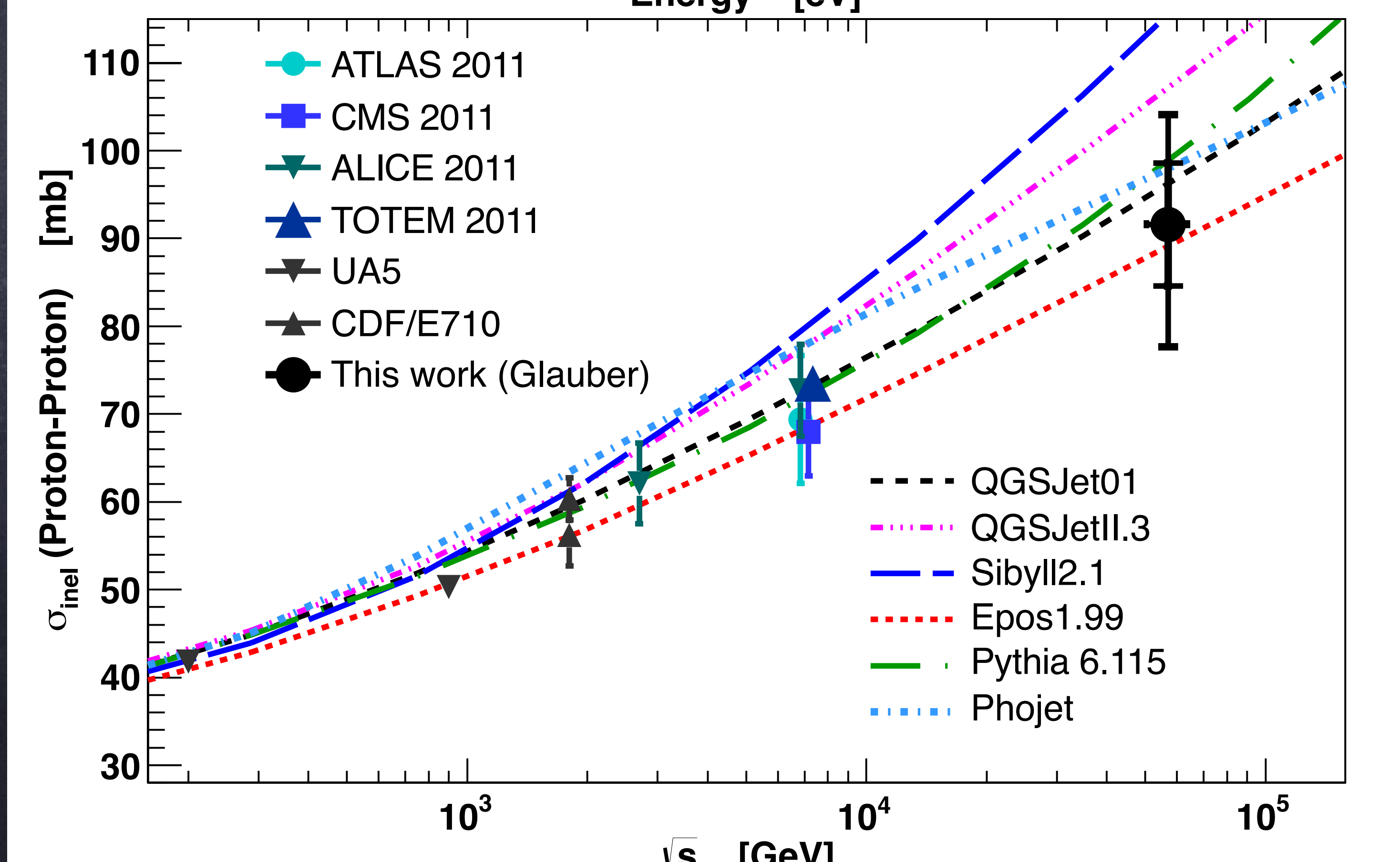

p-air cross section derived from exponential tail of depth of shower maxima: probability for not having interacted up to X_{max} ~ $\exp(-\sigma X_{max}/m_N)$

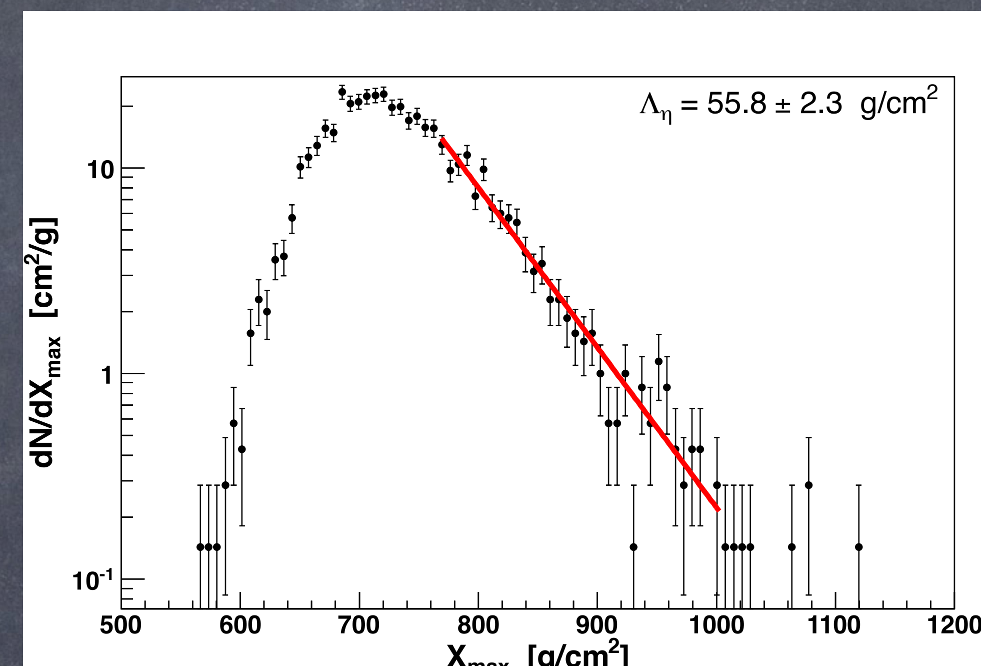

pp cross section derived from Glauber model

Pierre Auger Collaboration, PRL 109, 062002 (2012)

Global Picture on Mass Composition

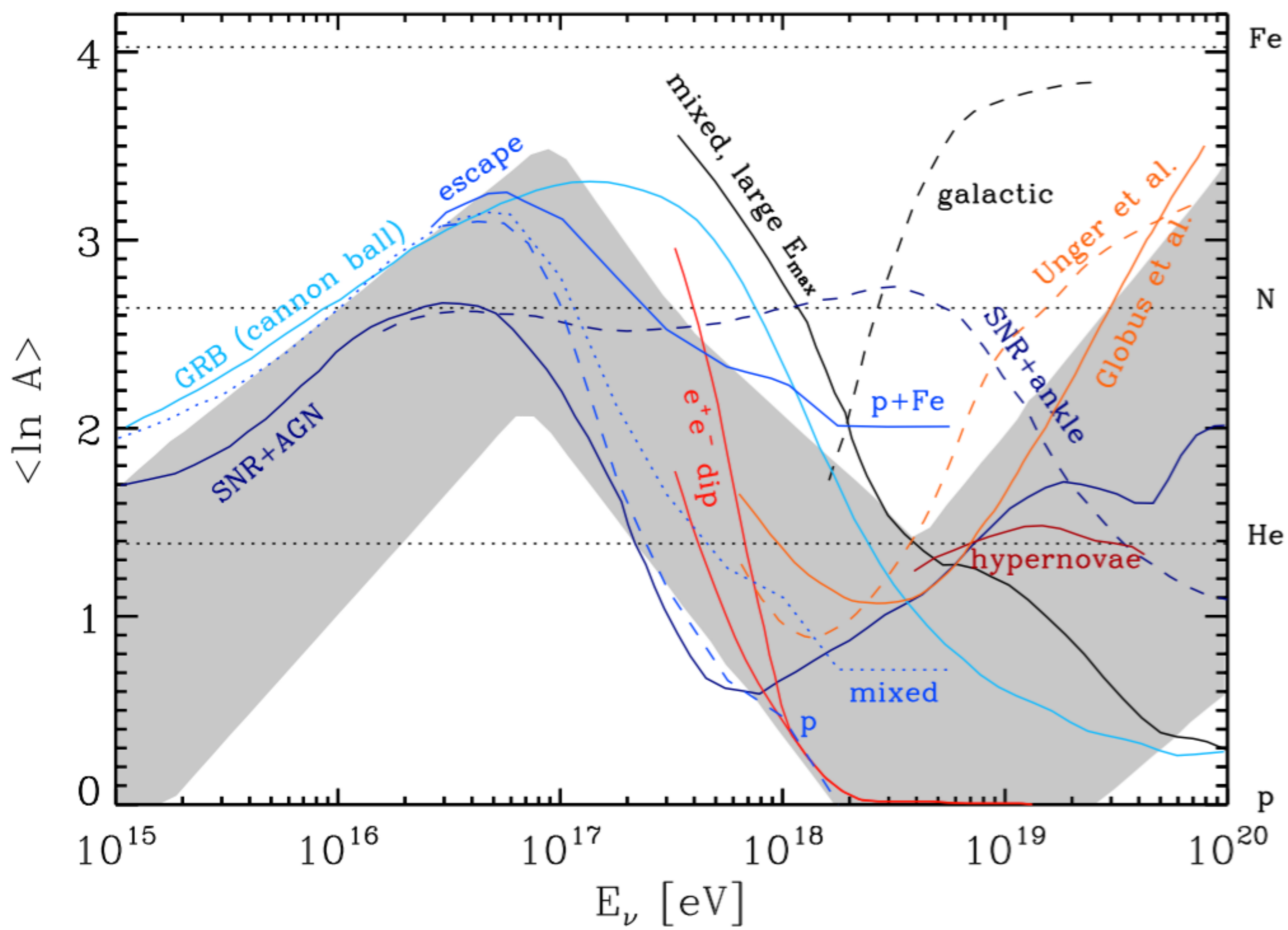

Fig. 5.8 The energy dependence of the average logarithmic mass predicetd by various models, as indicated and explained in more details in the text. The grey band represents the combined uncertainties resulting from systematic experimental errors and hadronic model uncertainties, based on data such as the ones shown in Fig. 5.7. The first minimum in $\langle \ln A \rangle$ at $\simeq 3 \times 10^{15}$ eV corresponds to the CR knee and the first maximum in $\langle \ln A \rangle$ at $\simeq 10^{17}$ eV corresponds to the *second knee*. Both the knee and the second knee could signify a rigidity dependent Peters cycle either due to the maximal rigidity reached at acceleration in supernova remnants or due to a transition to a propagation regime leading to faster CR leakage from the Galaxy. Finally, the second minimum in $\langle \ln A \rangle$ at $\simeq 5 \times 10^{18}$ eV signifies the *ankle*. Compare the CR spectrum shown in Fig. 5.6. Inspired by Ref. [231].

Indications of "Peters cycles" for galactic and extragalactic sources whose maximal energies are proportional to the charge Z and extend up to ~ 10^{17} and 10^{20} eV, respectively

G. Sigl, book "Astroparticle Physics: Theory and Phenomenology", Atlantis Press/Springer 2016

see also K.-H.Kampert and M.Unger, Astropart.Phys. 35 (2012) 660

Interpretation of flux and composition data (i)

Mass composition at Earth

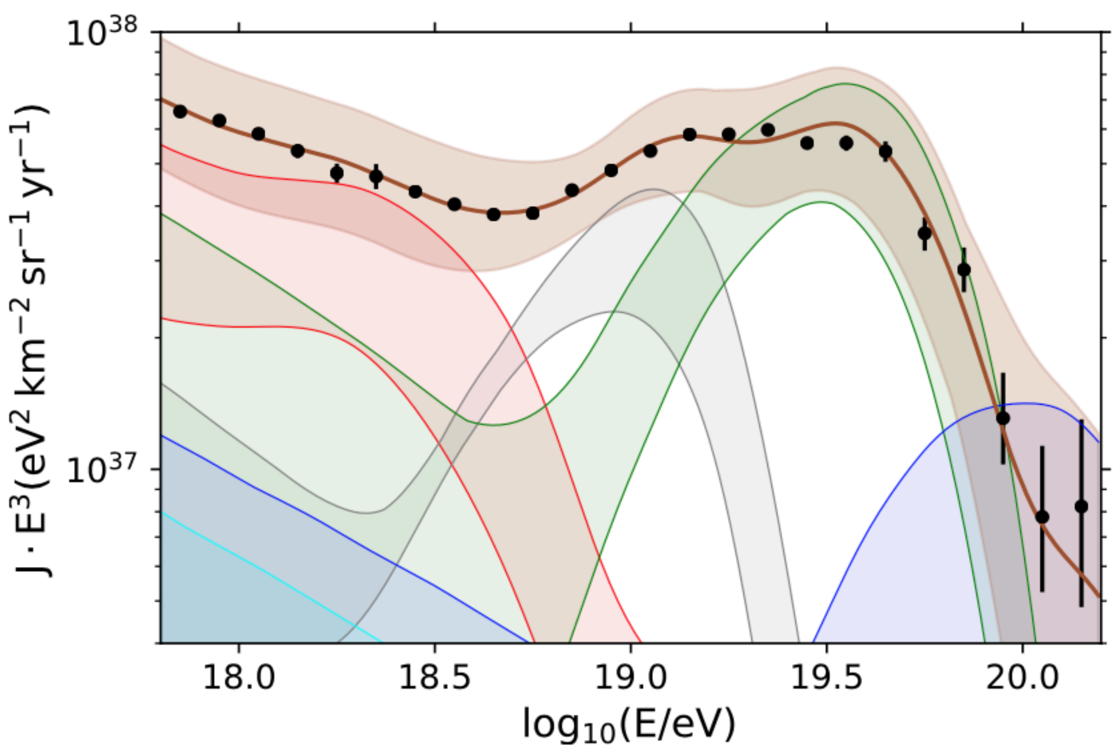

$A = 1$
$1 < A < 5$
$4 < A < 23$
$22 < A < 39$
$38 < A < 57$

Bands:
Experimental uncertainties
(model uncertainties smaller)

Energy scale: $\sigma_{\mathrm{sys}}(E)/E = 14\,\%$
X_{max} scale: $\sigma_{\mathrm{sys}}(X_{\mathrm{max}}) = 6 \div 9\ \mathrm{g\,cm}^{-2}$

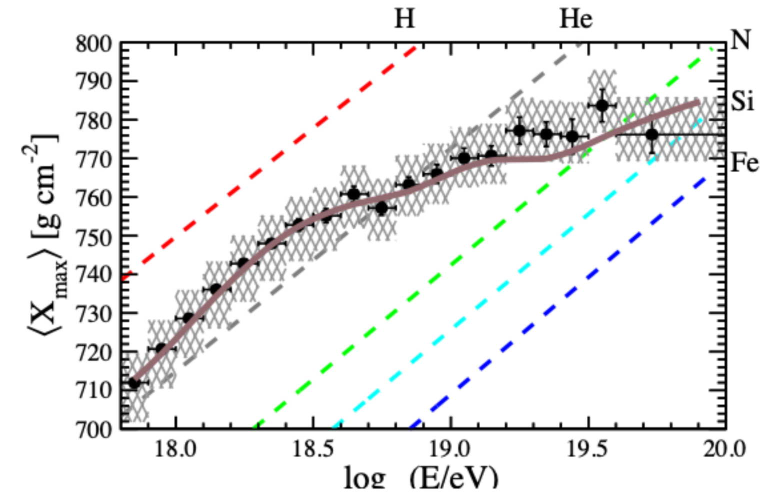

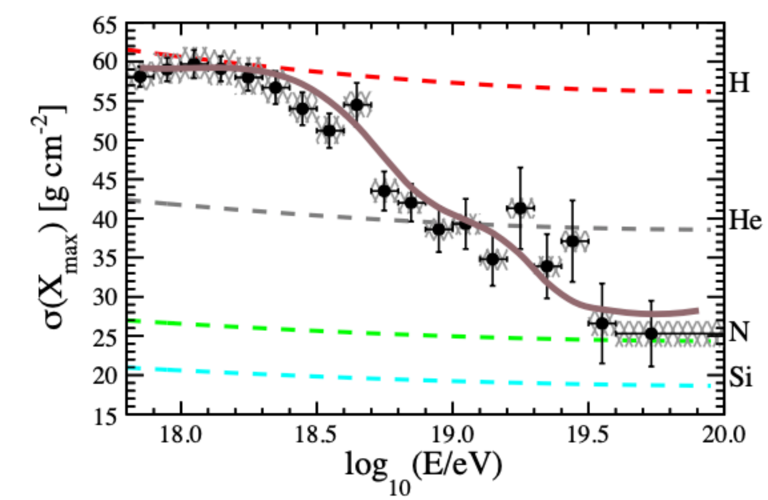

Different model scenarios considered for low-energy part
(transition to galactic component), similar results for total composition obtained

$$J(E) = \sum_A f_A \cdot J_0 \cdot \left(\frac{E}{E_0}\right)^{-\gamma} \cdot \begin{cases} 1, & E < Z_A \cdot R_{\mathrm{cut}}; \\ \exp\left(1 - \frac{E}{Z_A \cdot R_{\mathrm{cut}}}\right), & E > Z_A \cdot R_{\mathrm{cut}}. \end{cases}$$

$$R_{\mathrm{cut}} = 1.4 \ldots 1.6 \times 10^{18}\,\mathrm{V}$$

Flux suppression superposition
of injection maximum energy
and propagation energy losses

Extragalactic index very hard, but no really good handle on this parameter

(Eleonora Guido)

taken from R. Engel, Pierre Auger highlights, ICRC 2021

Spectrum and Composition

fits to spectrum and composition for a homogeneous source distribution neglecting deflection (which generally is a good approximation for the solid angle integrated flux) tend to favor very hard injection spectra with low cut-off rigidities

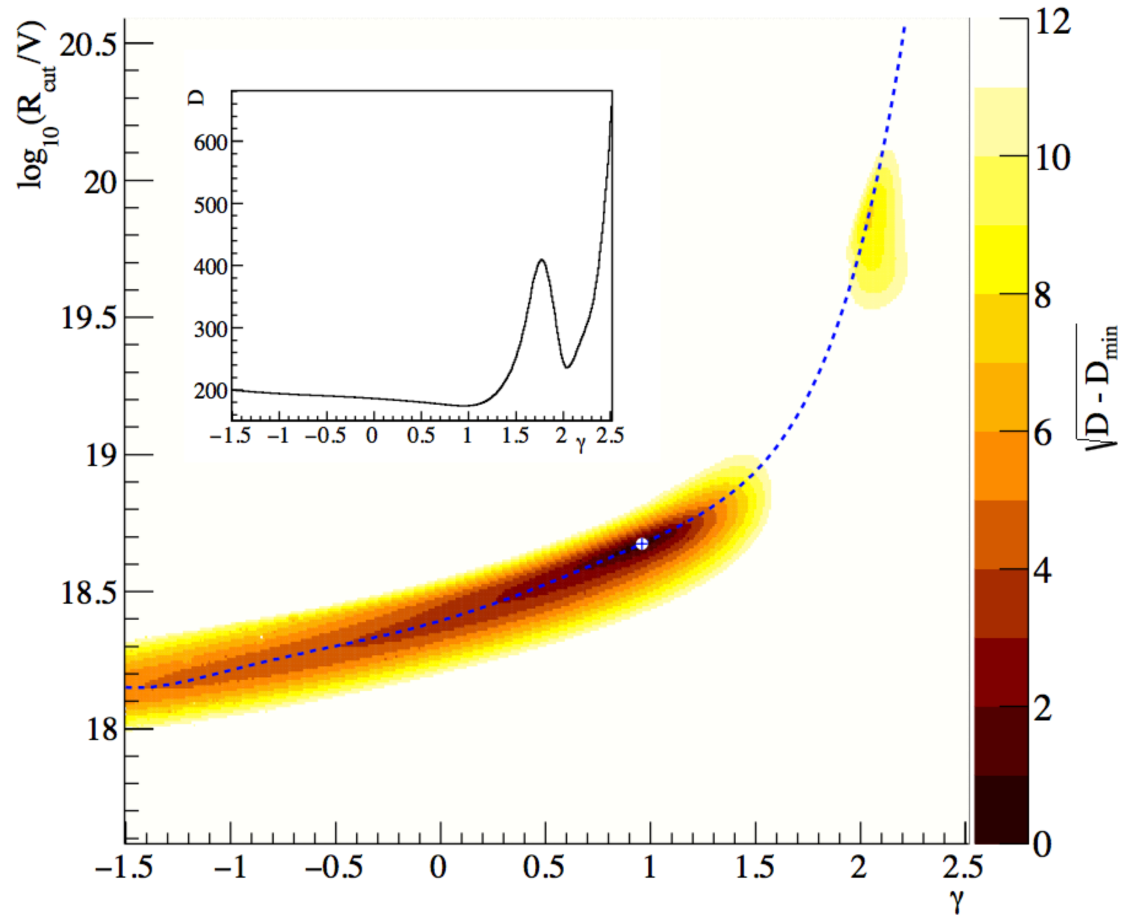

Pierre Auger collaboration, JCAP 1704 (2017) 028 [arXiv:1612.07155]

Figure 1. Deviance $\sqrt{D - D_{\rm min}}$, as function of γ and $\log_{10}(R_{\rm cut}/{\rm V})$. The dot indicates the position of the best minimum, while the dashed line connects the relative minima of D (valley line). In the inset, the distribution of $D_{\rm min}$ in function of γ along this line.

AugerPrime extension aims at event-by-event measurement of composition; other future experiments include space-based missions JEM-EUSO, POEMMA, ..

Newest Results on Anisotropy

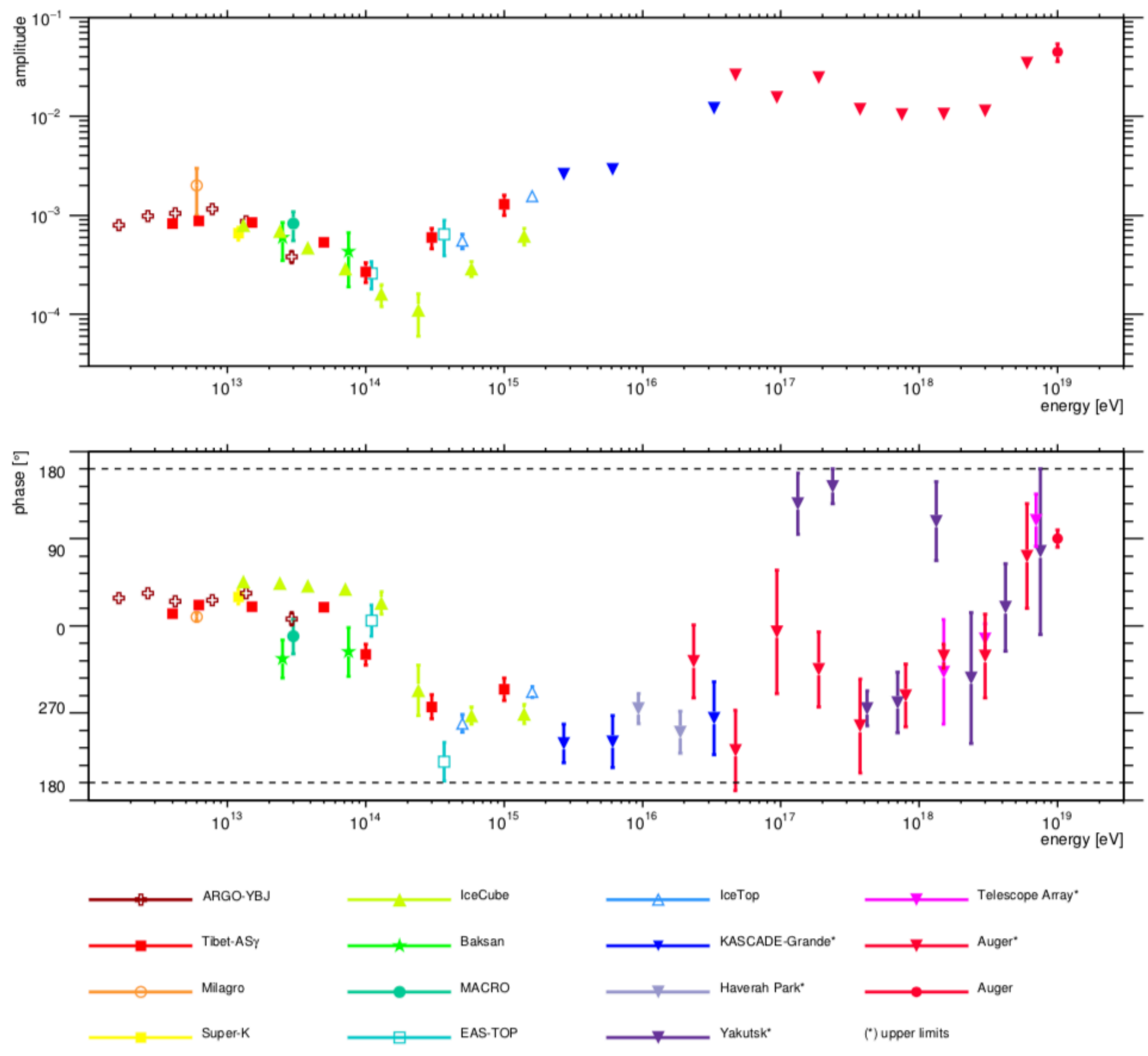

Figure 7: Amplitude (top) and phase (bottom) measurements of the first harmonic in right ascension as a function of energy, from various reports. Amplitudes drawn as triangles with apex pointing down are the most stringent upper limits up to date in the considered energy ranges.

Amplitude and phase of dipole as function of energy

O. Deligny, Astropart. Phys. 104 (2019) 13 [arXiv:1808.03940]

Do Cosmic Ray Anisotropies at 1-100 TeV reveal the Sources ?

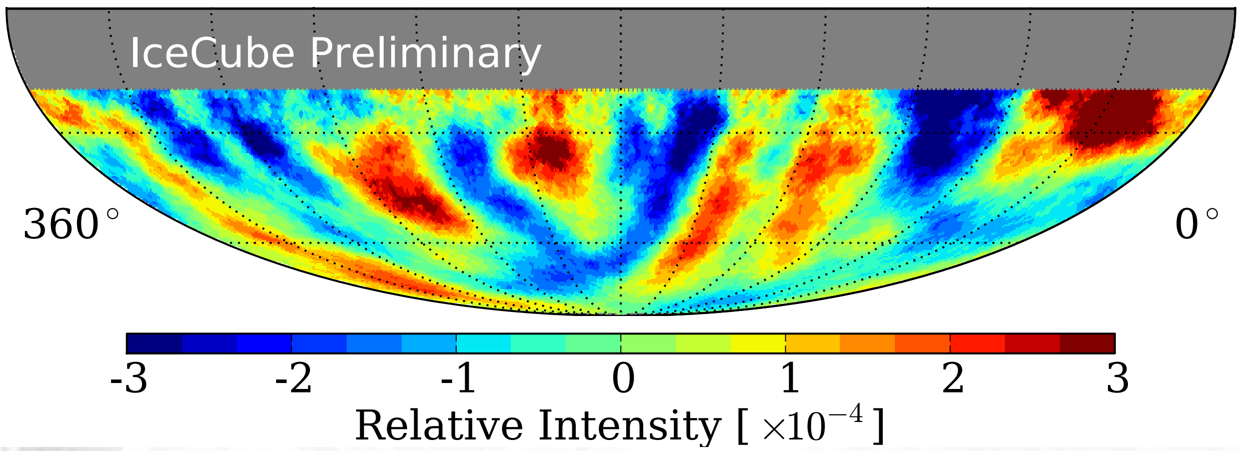

@20 TeV after dipole subtraction

P. Desiati et al, ICECUBE collaboration, arXiv:1308.0246

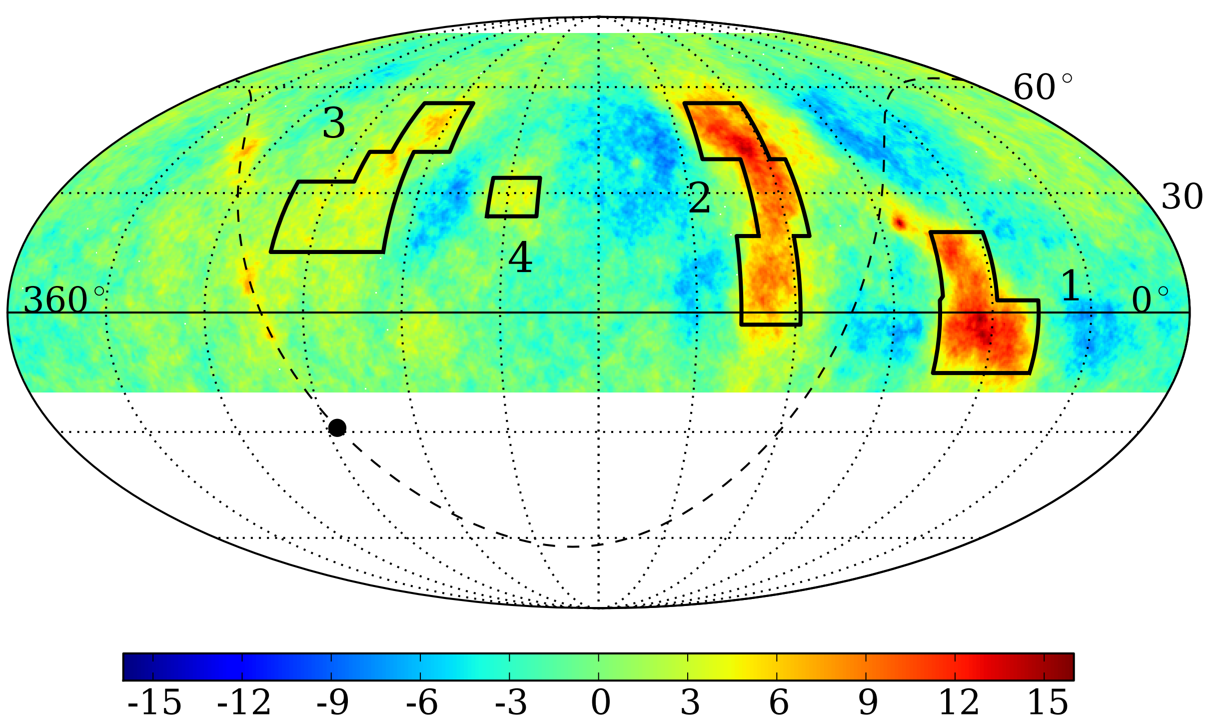

B. Bartoli et al, ARGO-YBJ collaboration, arXiv:1309.6182

Observed by Milagro, ARGO-YBJ, IceCube

Observed level ~ 10^{-3} is surprisingly high and difficult to explain:

wrong structure for Compton-Getting effect

too large for sources like Vela and beyond (> 100 pc) because gyro-radius < 0.1 pc

propagation mode, magnetic field structure ?

Anisotropy Patterns are strongly Energy dependent

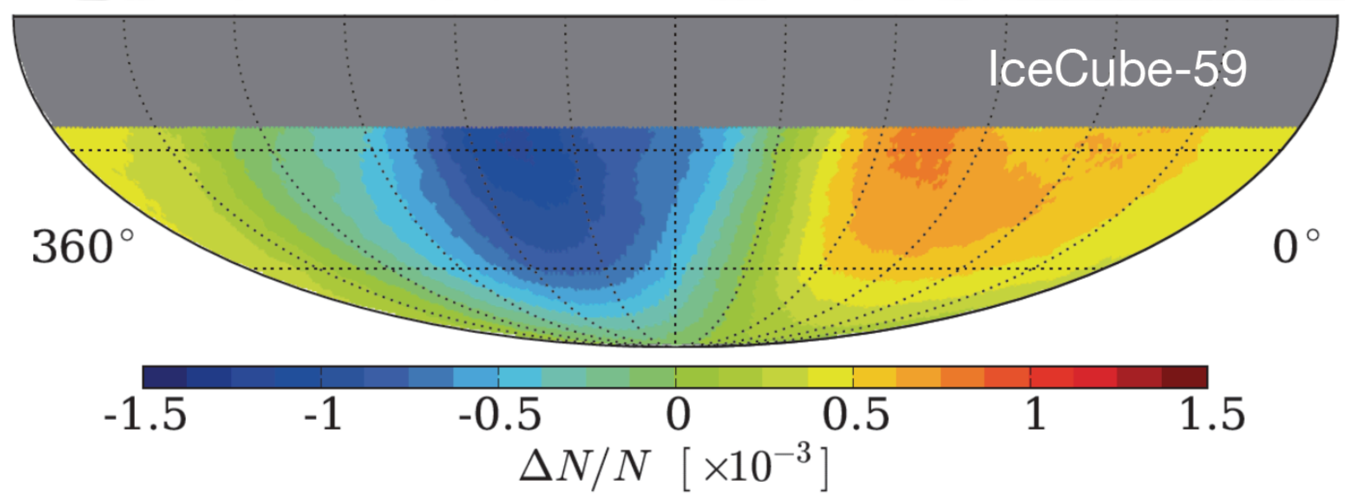

@20 TeV

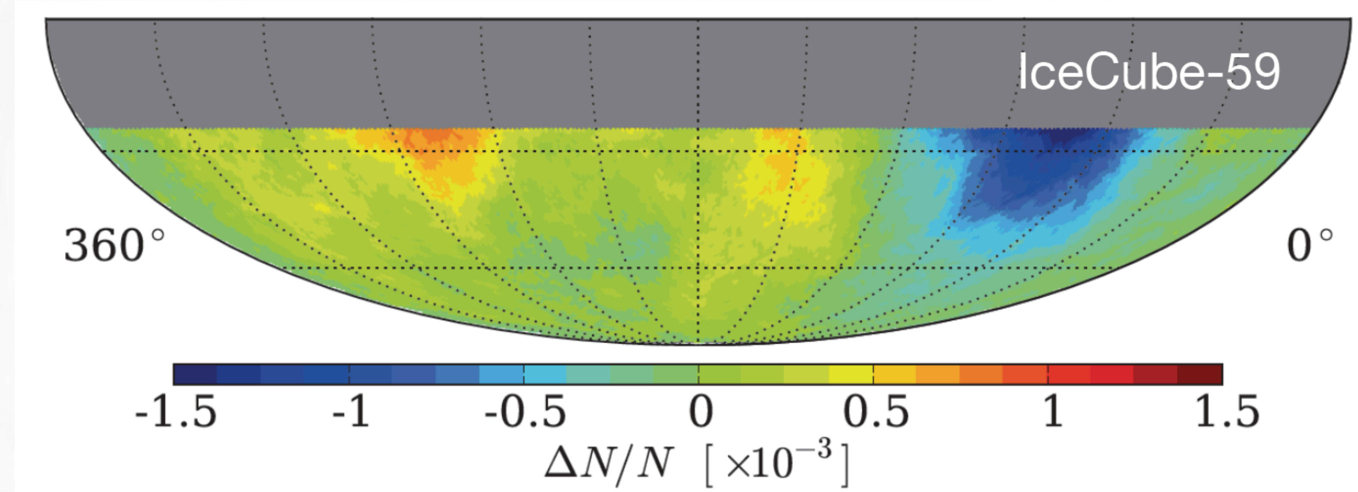

@400 TeV

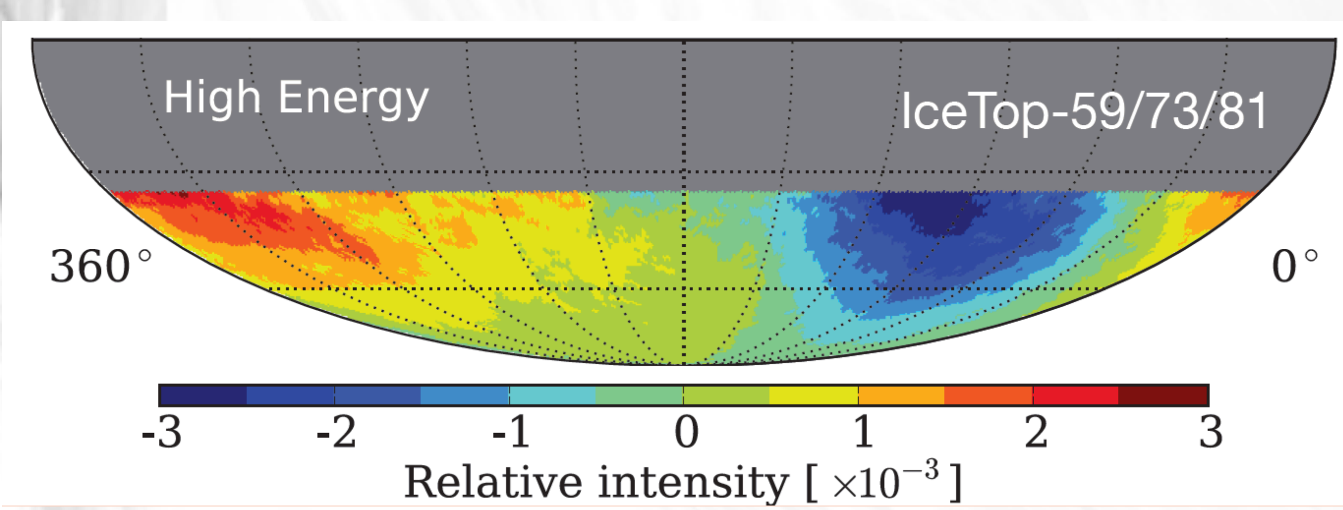

@400 TeV

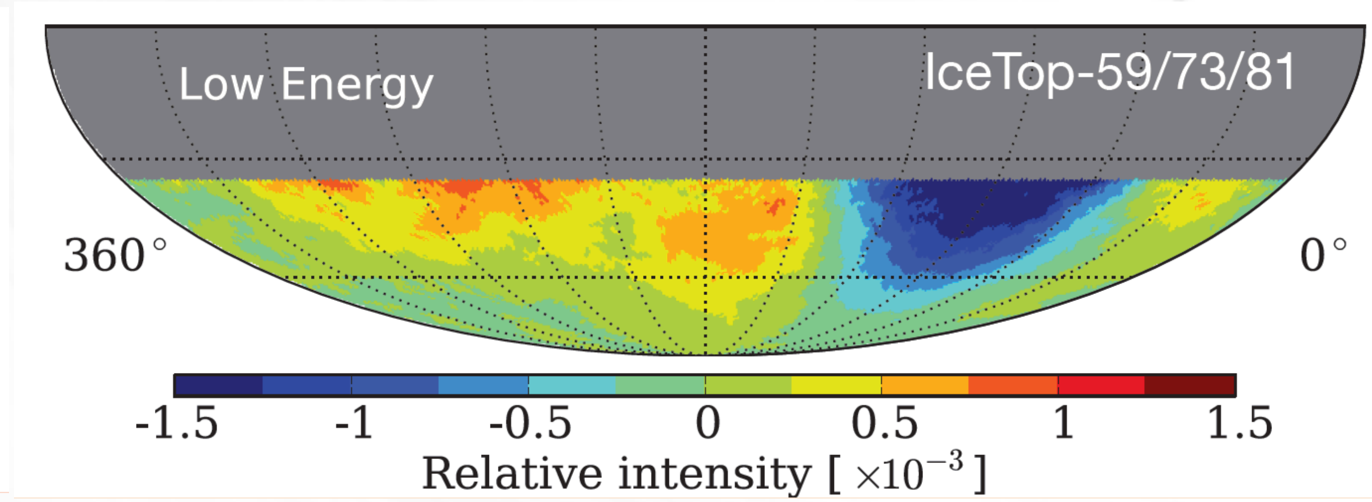

@2 PeV

The anisotropies may reflect the structure of the magnetic field within one scattering length (on magnetic inhomogeneities) around the observer. This structure is "missed" in the diffusion approximation which averages over magnetic field ensembles.

G.Giacinti and G.Sigl, PRL 109 (2012) 071101, M.Ahlers, arXiv:1310.5712

A Significant Anisotropy around 8×10^{18} eV is now seen

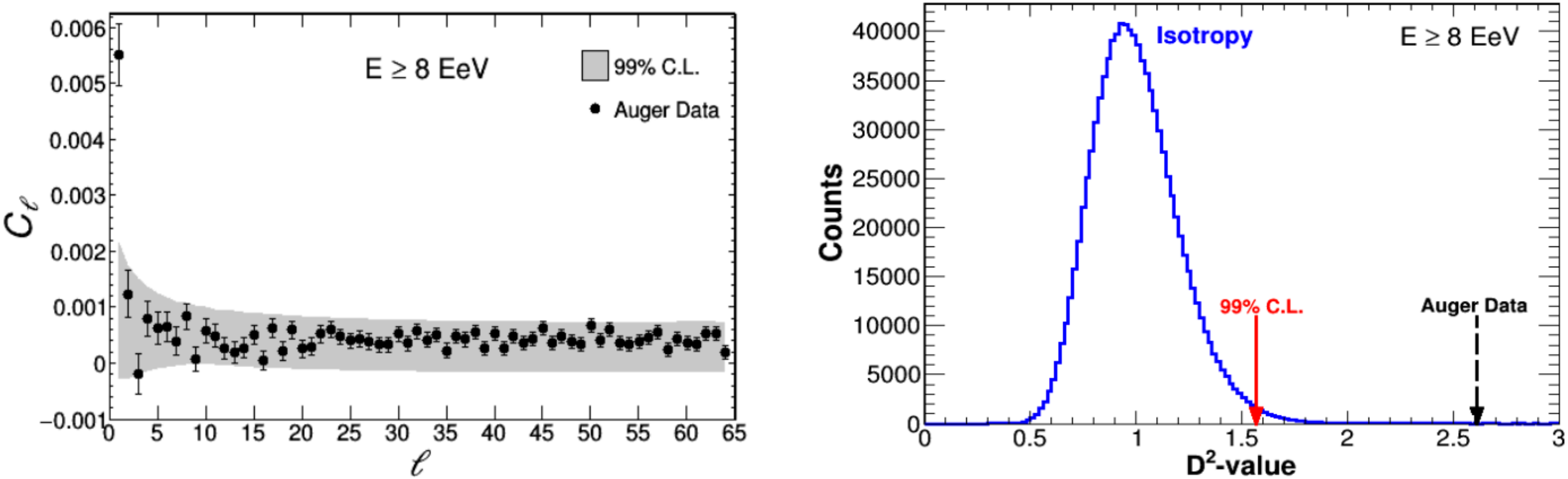

Figure 3: Angular power spectrum for $E \geq 8$ EeV. On the left a clear indication for a departure from isotropy is captured in the dipole scale. On the right the D^2-value distribution from 1,000,000 isotropic sky maps is shown. The D^2-value from data, represented by the black (dashed) arrow, is larger than the threshold of isotropy presenting an indication of anisotropy with > 99% C.L..

Pierre Auger Collaboration, JCAP 1706 (2017) 026 [arXiv:1611.06812]

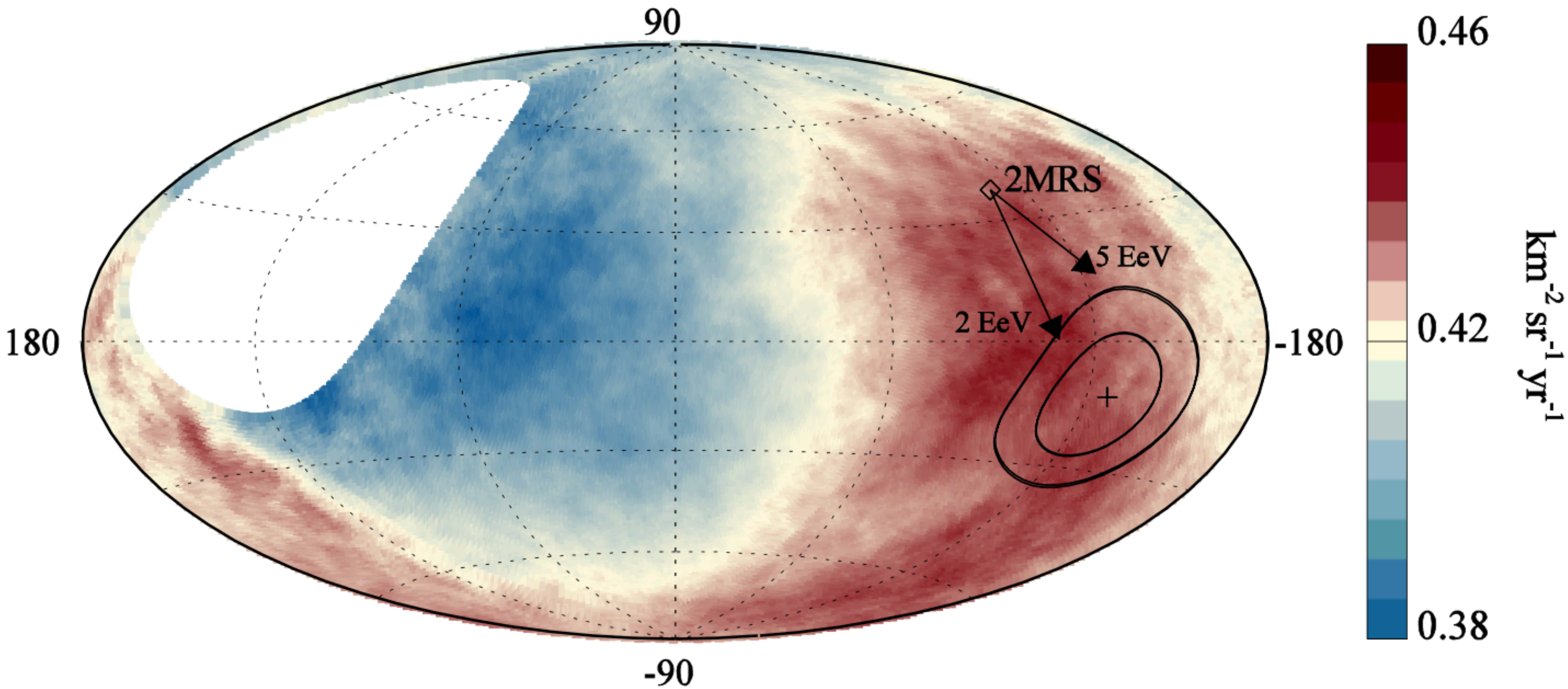

Fig. 3. Map showing the fluxes of particles in Galactic coordinates. Sky map in Galactic coordinates showing the cosmic-ray flux for $E \geq 8$ EeV smoothed with a 45° top-hat function. The Galactic center is at the origin. The cross indicates the measured dipole direction and the contours the 68% and 95% confidence-level regions. The dipole in the 2MRS galaxy distribution is indicated, while arrows show the deflections expected for a particular model of the Galactic magnetic field (*8*), for *E/Z*=5 EeV or 2 EeV.

Pierre Auger Collaboration, Science 357 (22 September 2017) 1266 [arXiv:1709:07321]

Anisotropy searches at highest energies – catalogs

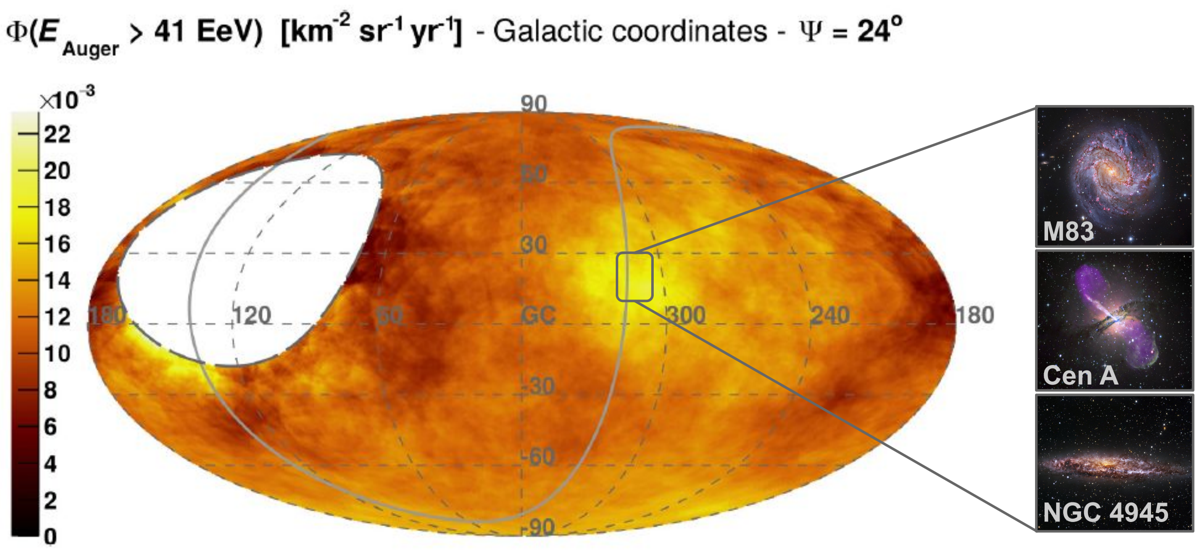

Direction fixed to that of Cen A, free E_{th} and Ψ

$E_{th} > 41$ EeV, $\Psi = 27°$: **3.9σ post-trial** deviation from isotropy (5% excess)

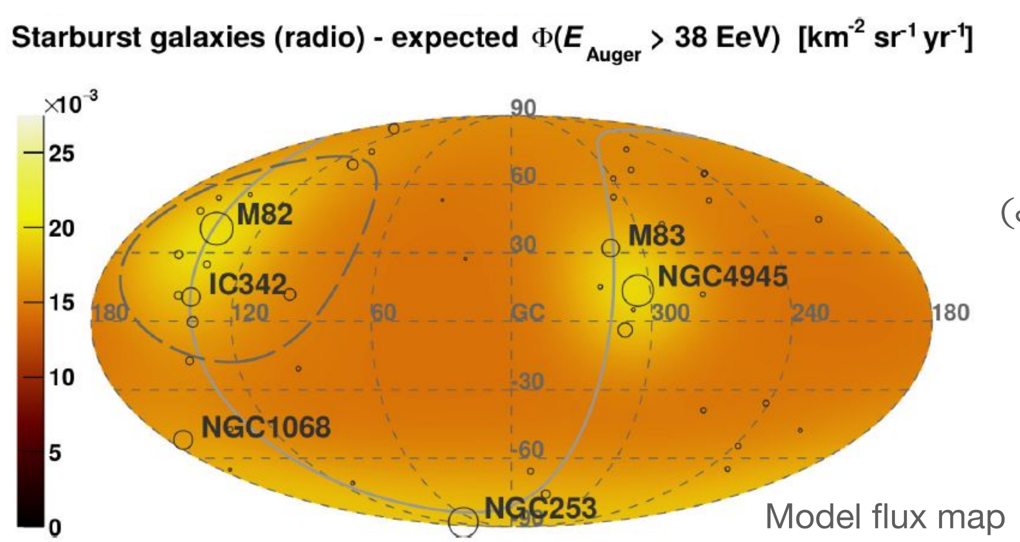

(Jonathan Biteau)

All data until end of 2020, optimized quality cuts: 120,000 km² sr yr

Catalog	E_{th} [EeV]	Ψ [deg]	α [%]	TS	Post-trial p-value
All galaxies (IR)	40	24^{+16}_{-8}	15^{+10}_{-6}	18.2	6.7×10^{-4}
Starbursts (radio)	38	25^{+11}_{-7}	9^{+6}_{-4}	24.8	3.1×10^{-5}
All AGNs (X-rays)	41	27^{+14}_{-9}	8^{+5}_{-4}	19.3	4.0×10^{-4}
Jetted AGNs (γ-rays)	40	23^{+9}_{-8}	6^{+4}_{-3}	17.3	1.0×10^{-3}

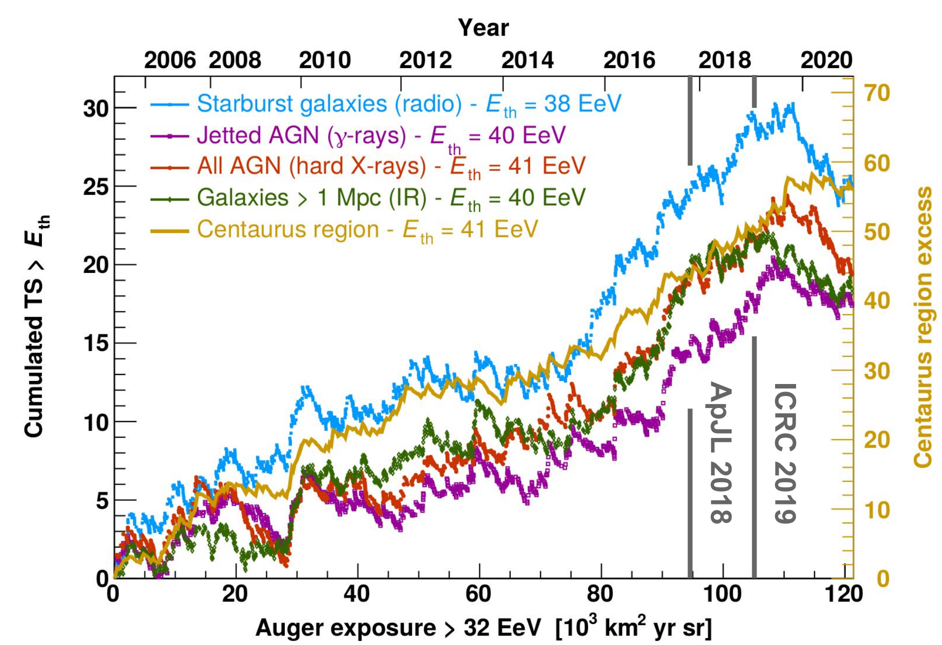

4.0σ

3.1σ

Growth of test statistic (TS) compatible with linear increase
Discovery threshold of 5σ expected in 2025 – 2030 (Phase II)
Other means to increase sensitivity (Auger 85% sky coverage)

21

taken from R. Engel, Pierre Auger highlights, ICRC 2021

Lobes of Centaurus A seen by Fermi-LAT

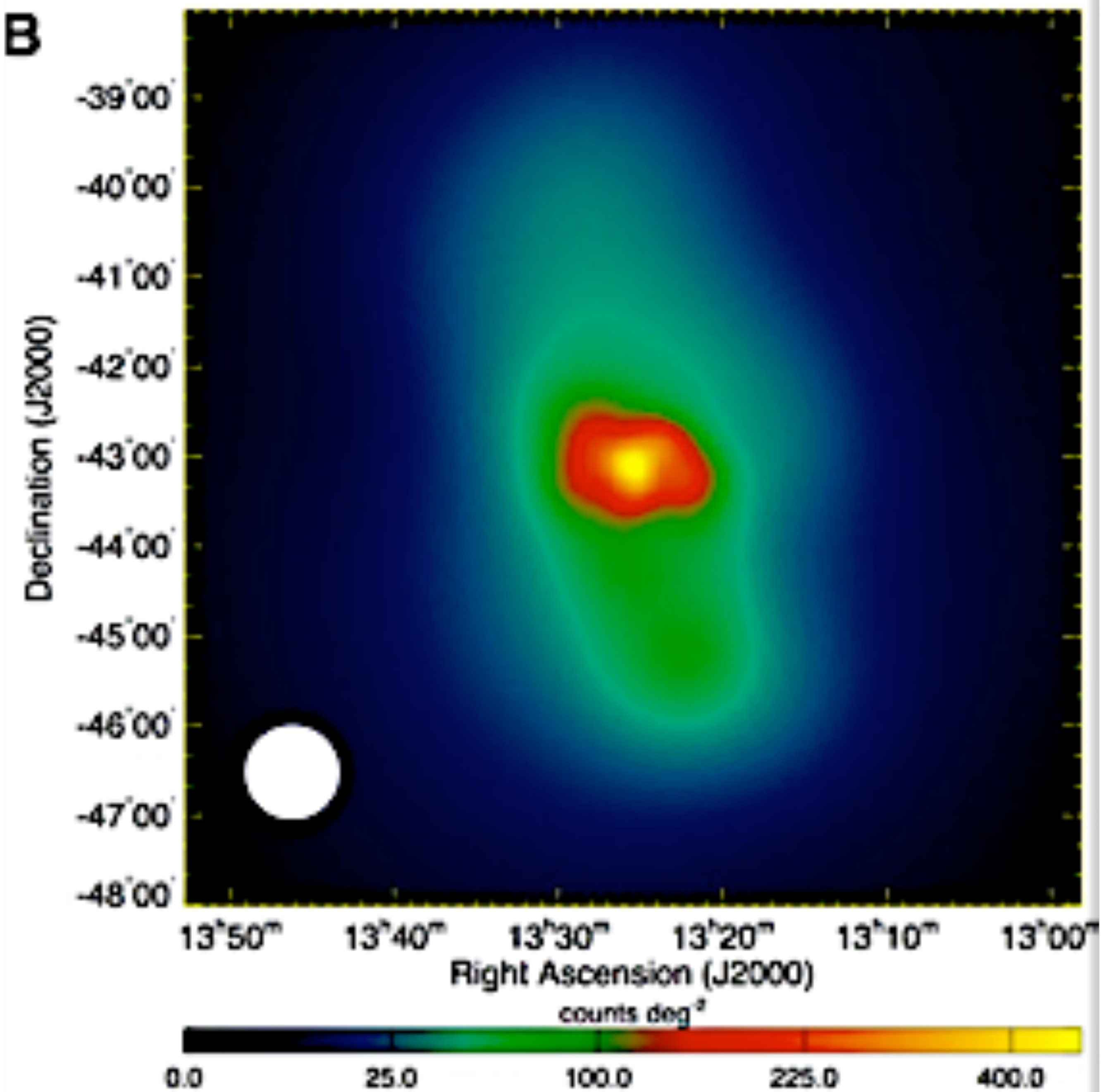

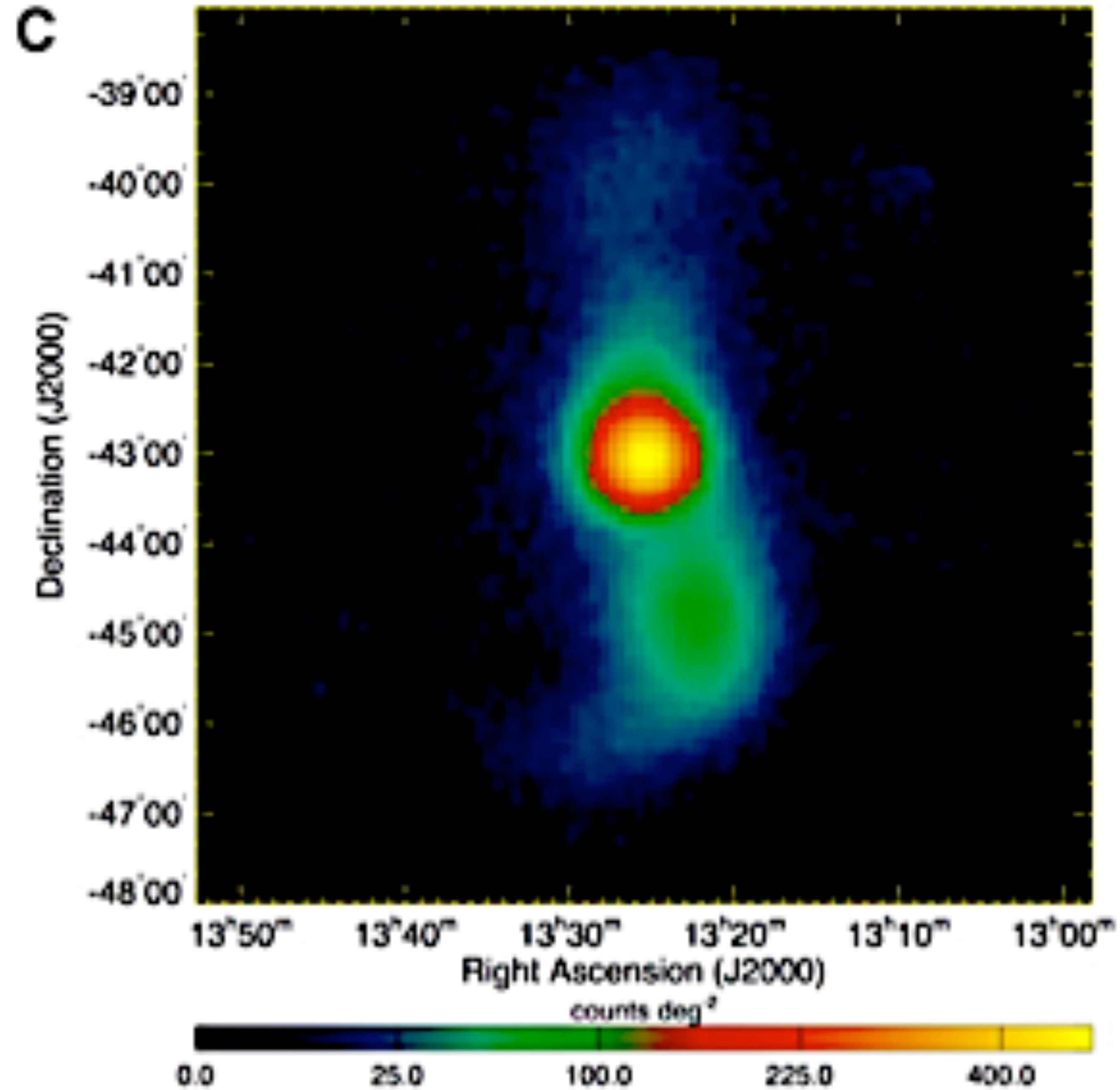

> 200 MeV γ-rays

Radio observations

Abdo et al., Science Express 1184656, April 1, 2010

Core of Centaurus A seen by Fermi-LAT

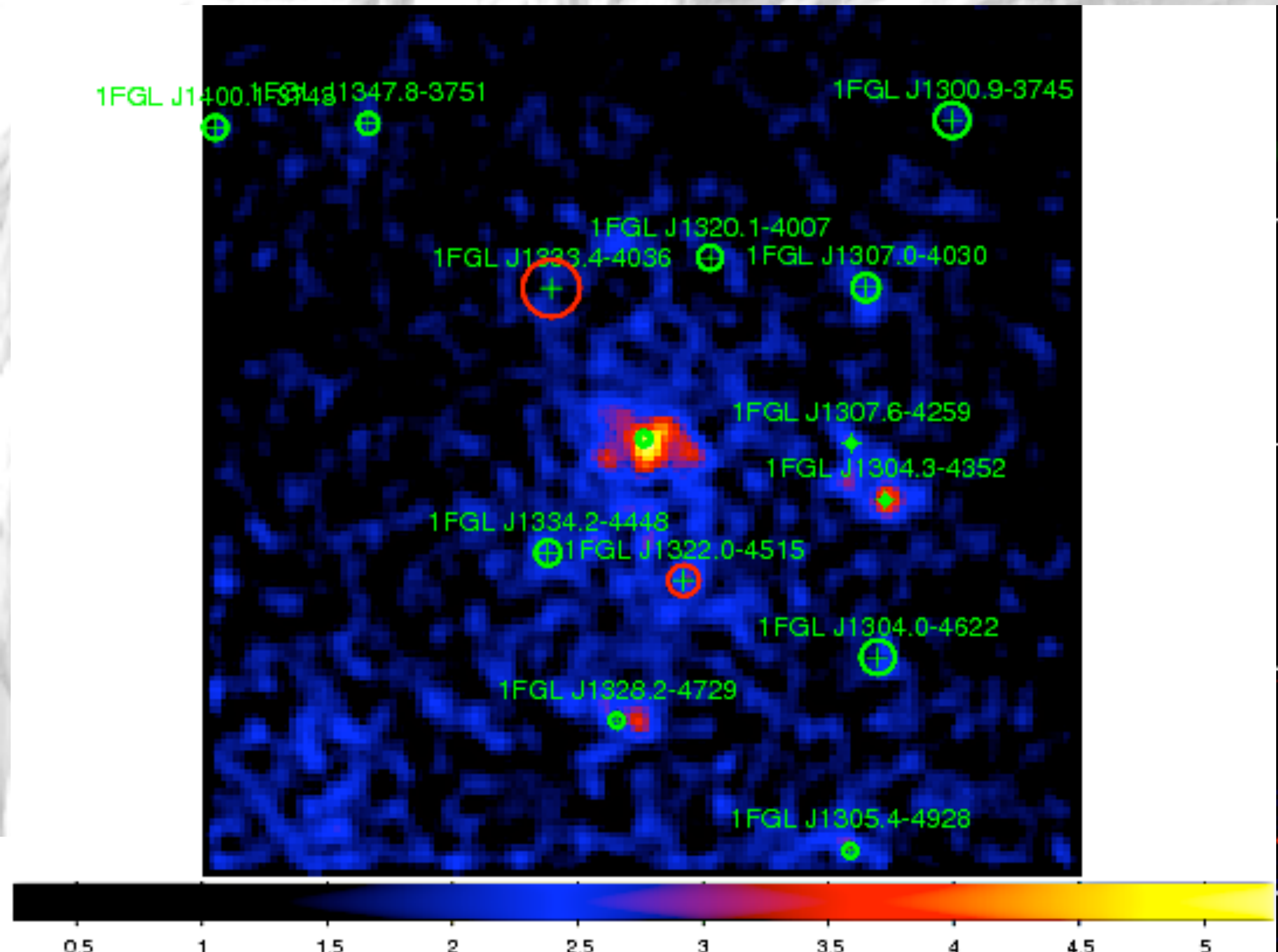

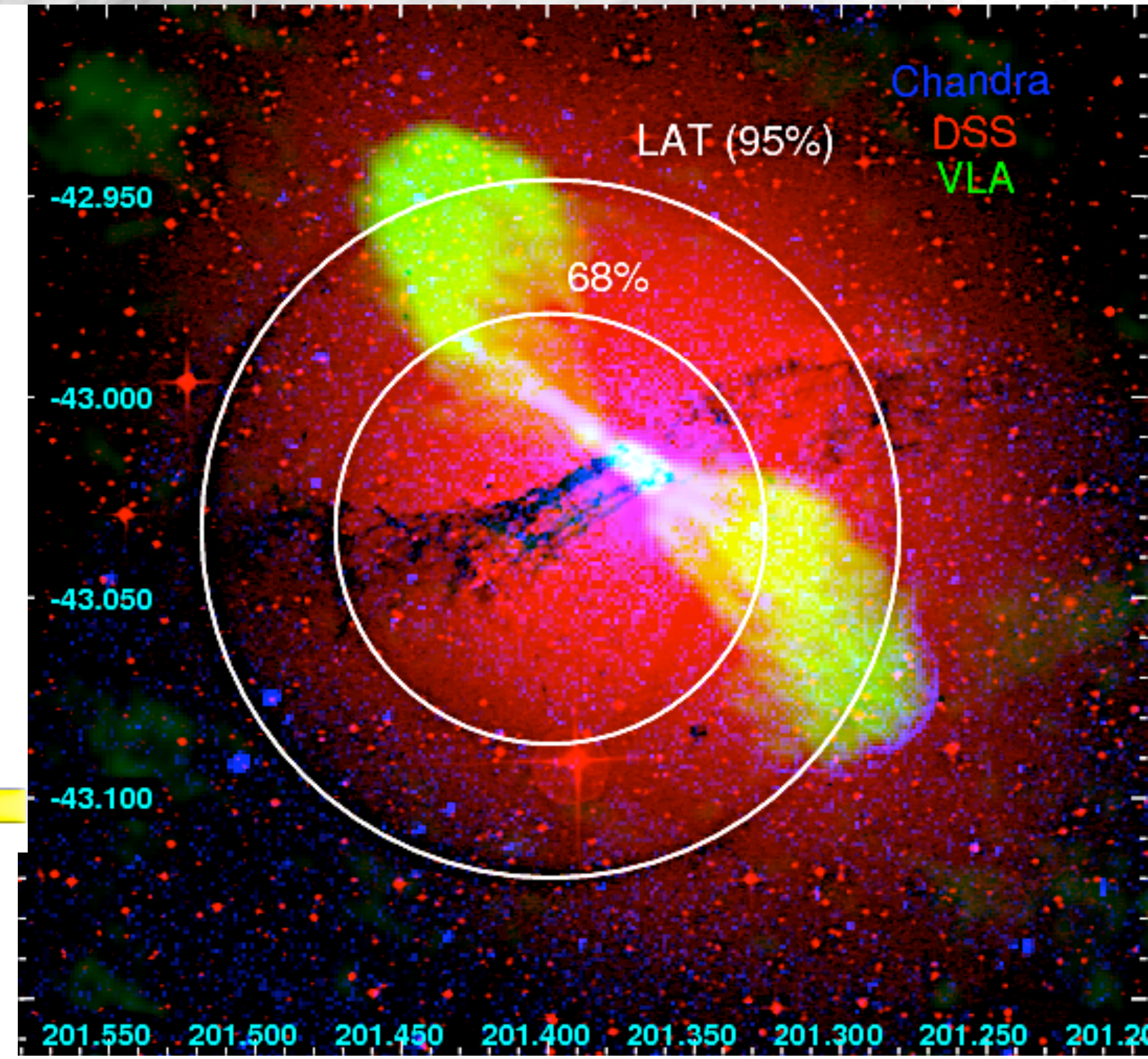

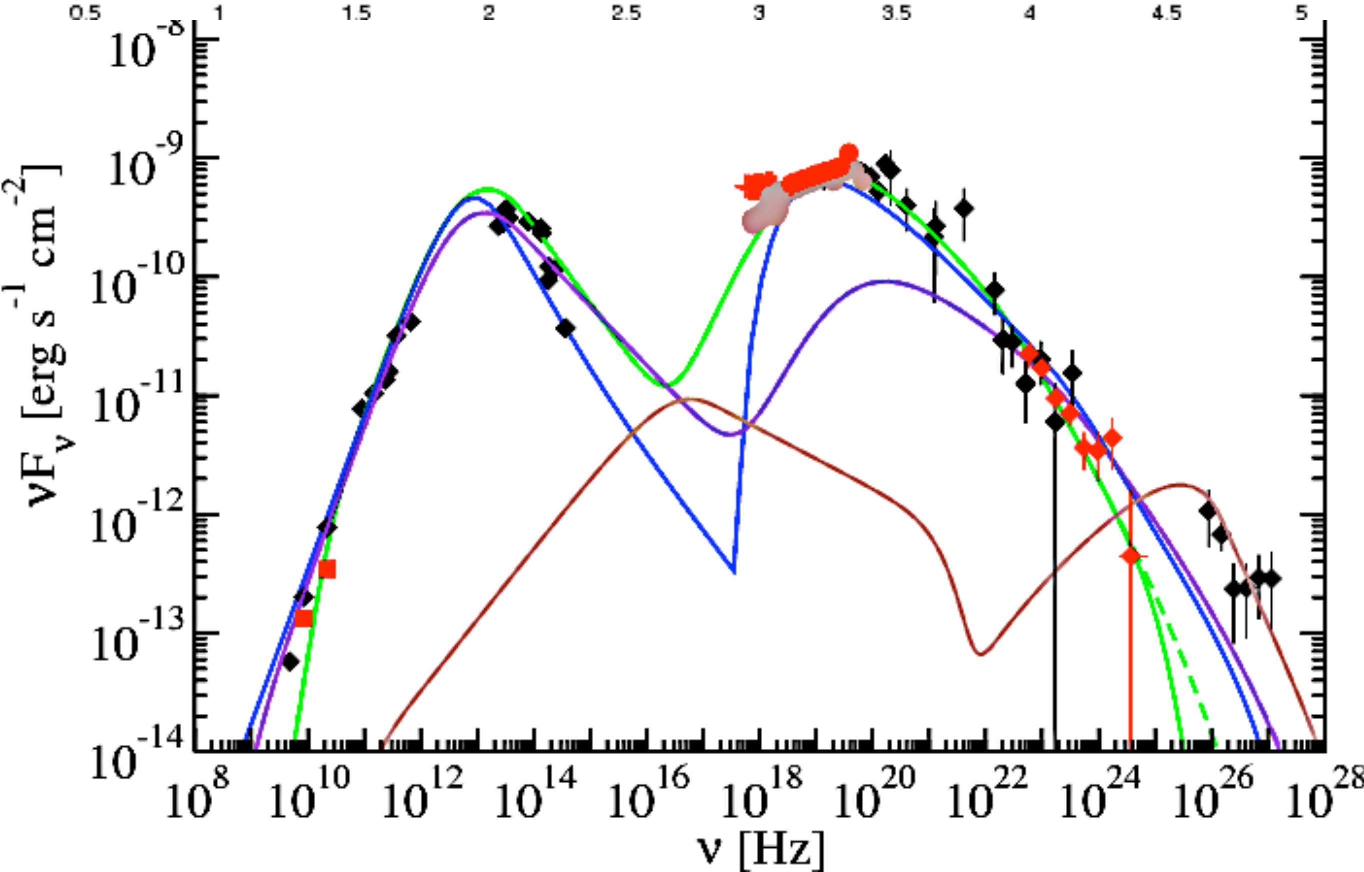

Can be explained by synchrotron self Compton except for HESS observation

Abdo et al., (Fermi LAT collaboration), arXiv:1006.5463

Centaurus A as Multimessenger Source: A Mixed hadronic+leptonic Model

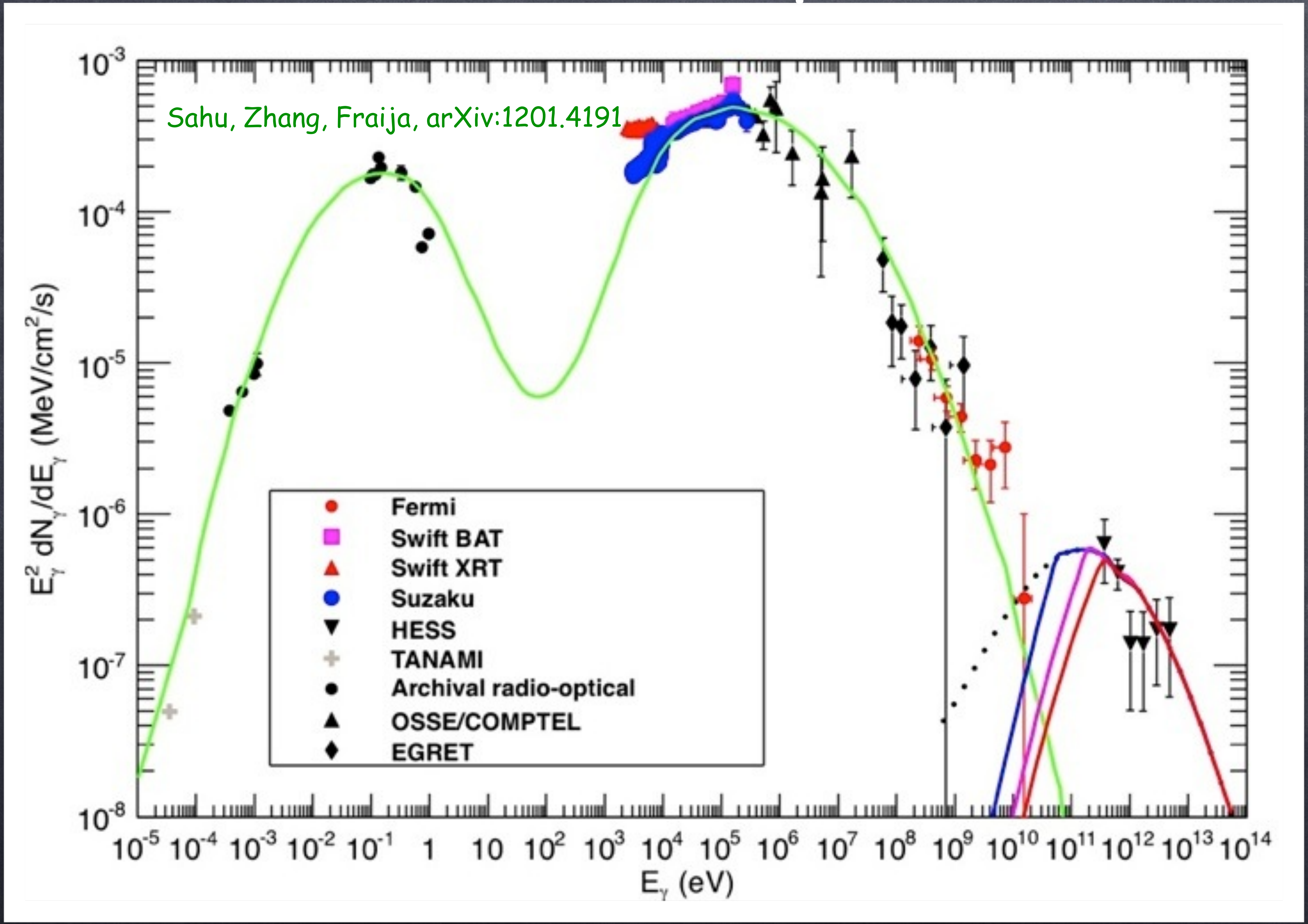

Low energy bump = synchrotron

high energy bump = synchrotron self-Compton

TeV-γ-rays: pγ interactions of shock-accelerated protons

Constraints on UHECR sources

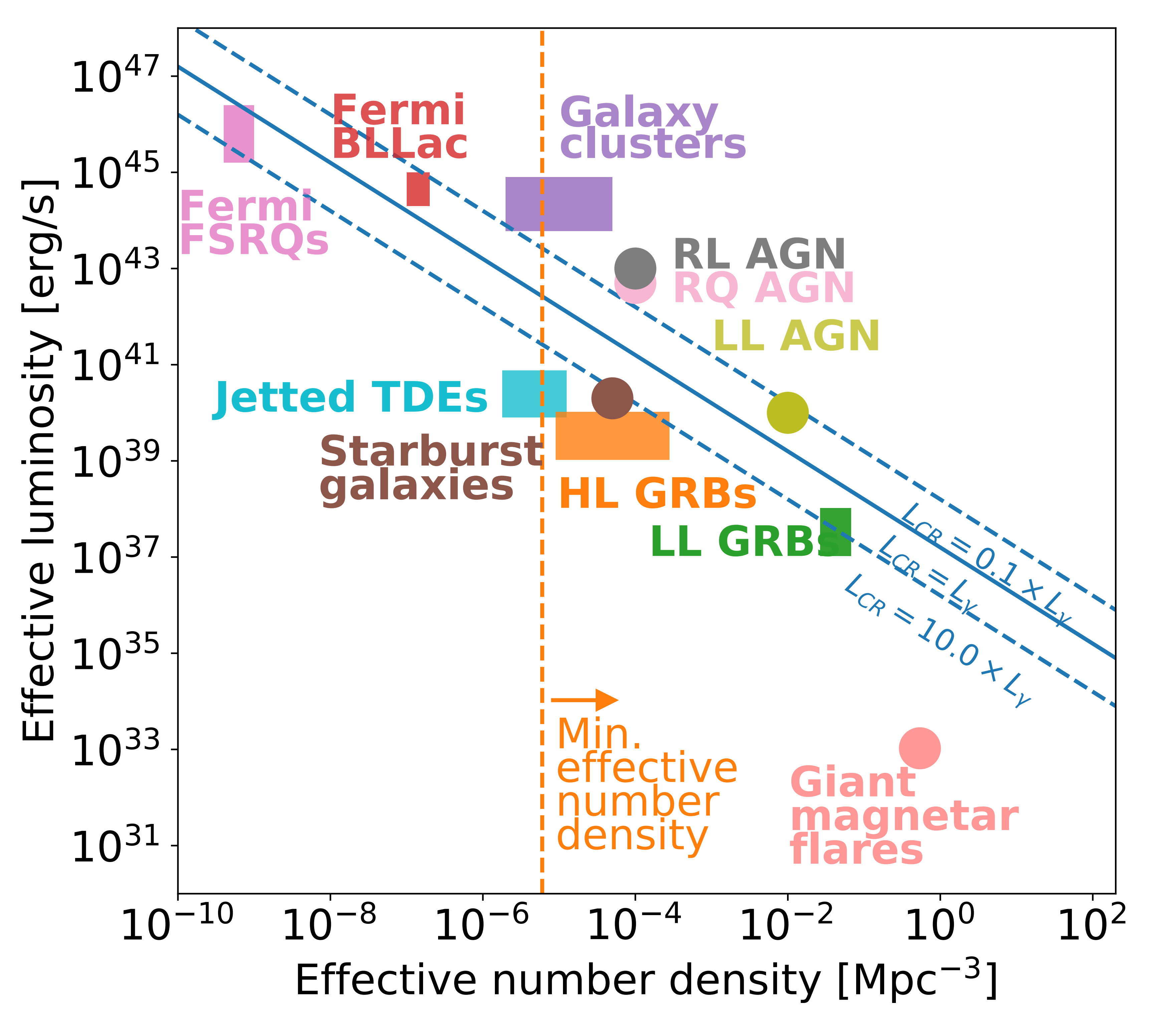

luminosity versus number density for continuous sources or (total energy released)/T versus (rate per volume)*T for intermittent sources with effective time delay T=3x10^5 y:

diagonal lines from UHECR flux, minimal number density from lack of significant UHECR clustering

Alves Batista et al., ``Open Questions in Cosmic Ray Research at ultra-high energies'', Front.Astron.Space Sci. 6 (2019) 23 [arXiv:1903.06714]

3-Dimensional Effects in Propagation

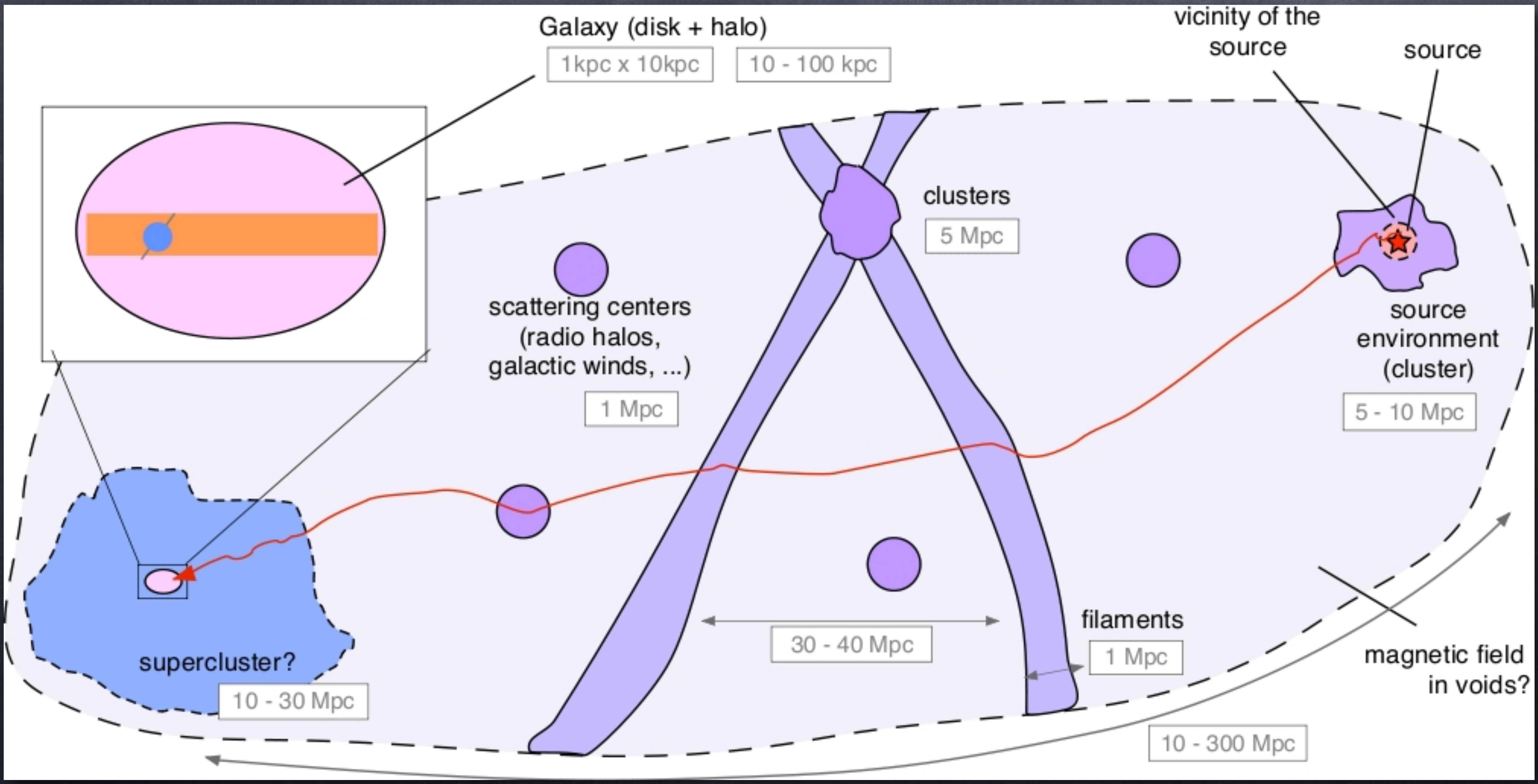

Kotera, Olinto, Ann.Rev.Astron.Astrophys. 49 (2011) 119

Extragalactic Magnetic Field Filling Factors from recent Simulations

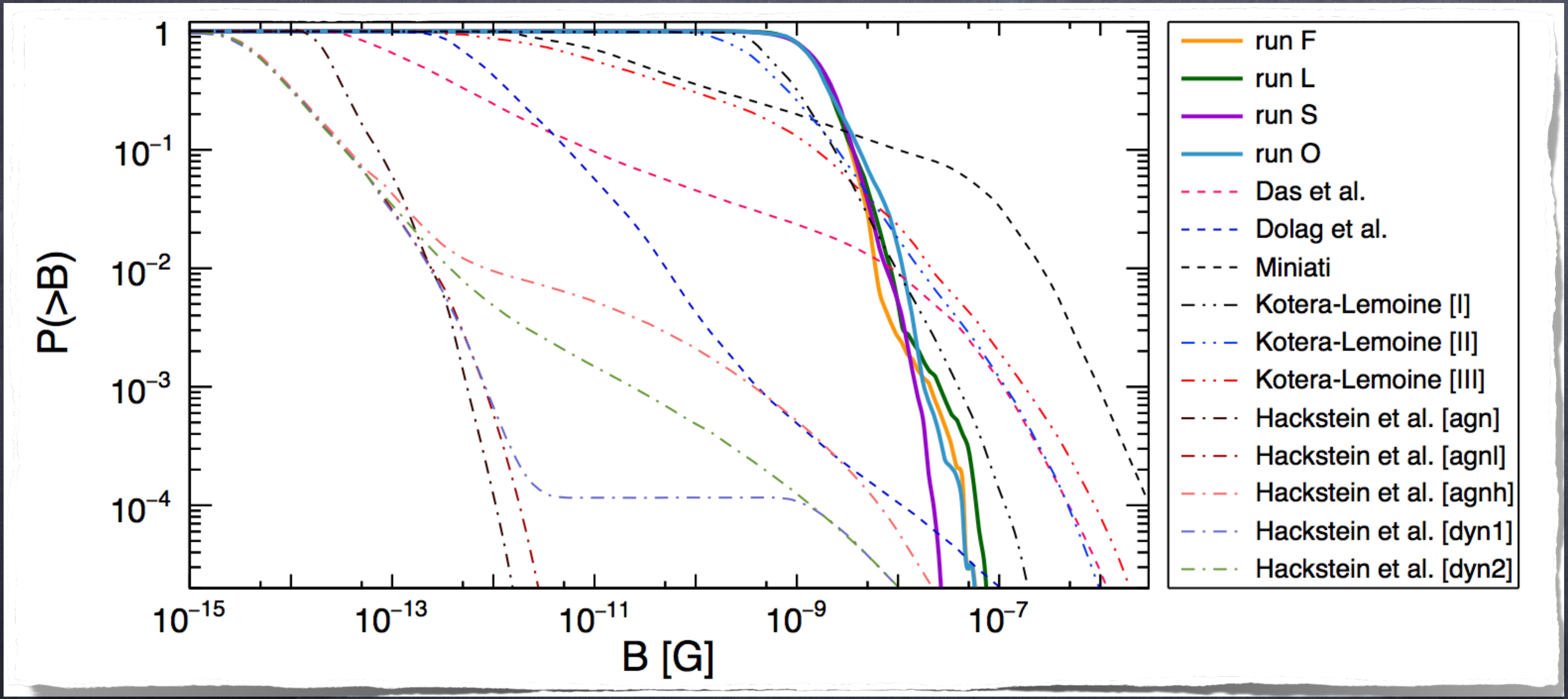

Alves Batista et al, PRD 96 (2017) 023010 [arXiv:1704.05869]

Extragalactic iron propagation produces nuclear cascades in structured magnetic fields:

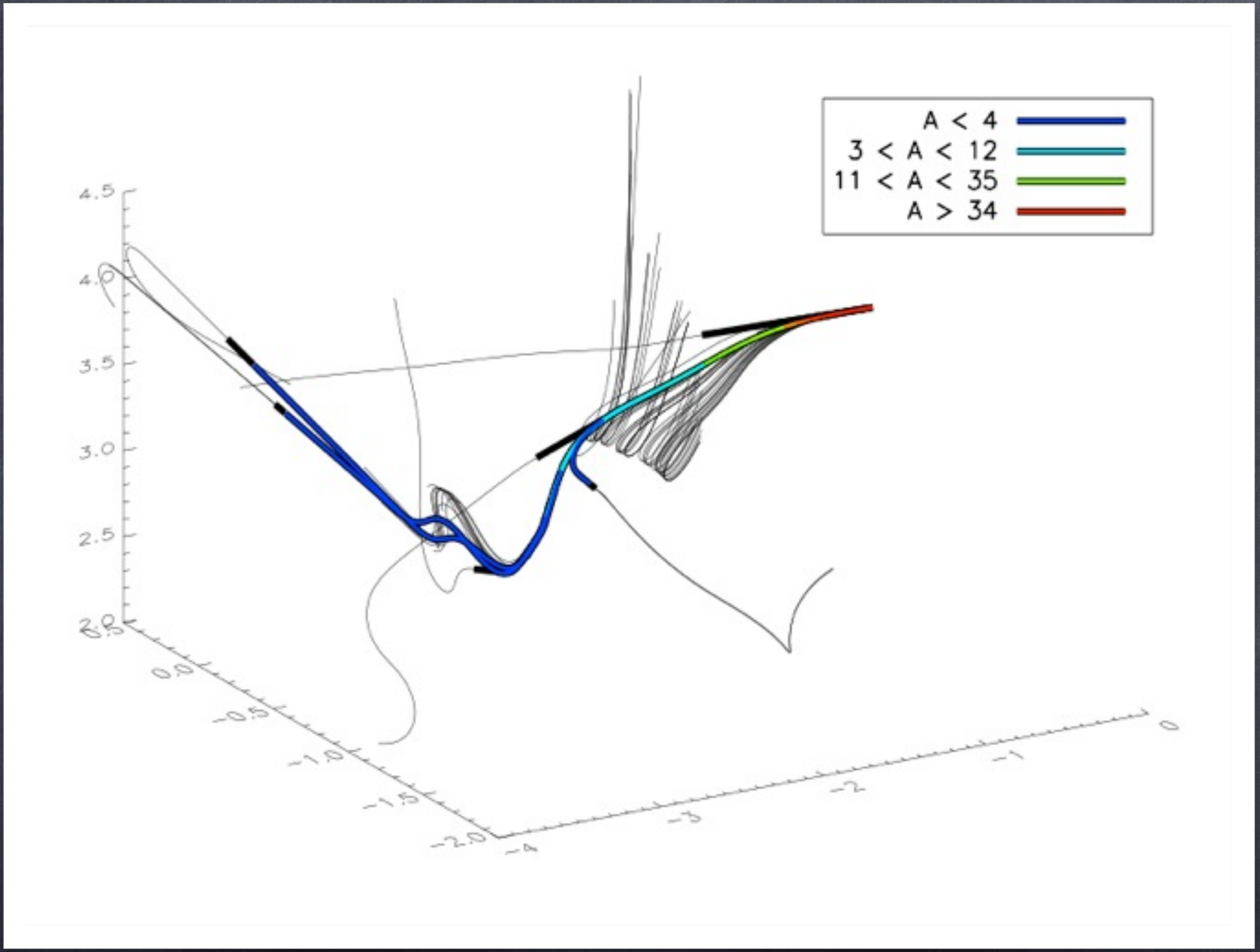

Initial energy 1.2 x 10^{21} eV, magnetic field range 10^{-15} to 10^{-6} G. Color-coded is the mass number of secondary nuclei

CRPropa 2.0/3.0

CRPropa is a public code for UHE cosmic rays, neutrinos and γ-rays being extended to heavy nuclei and hadronic interactions

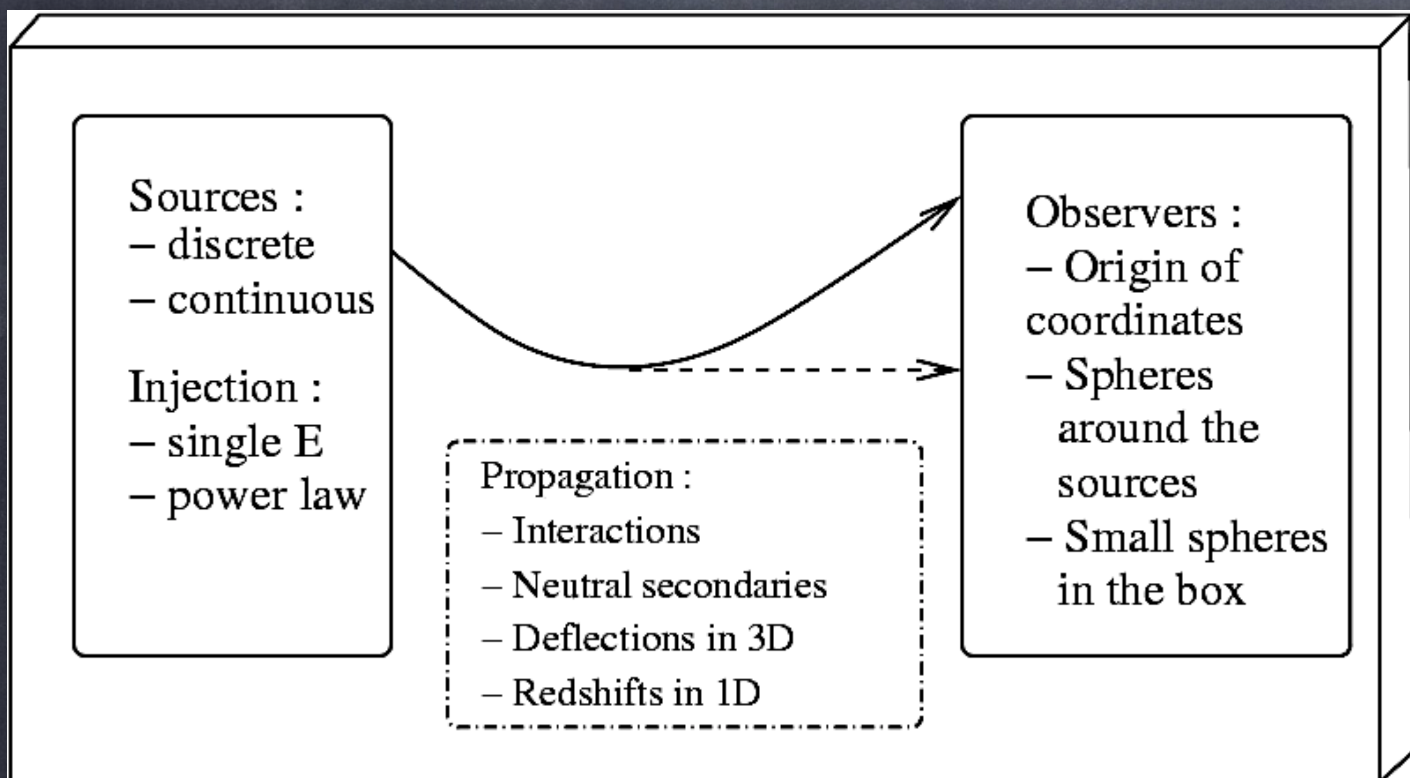

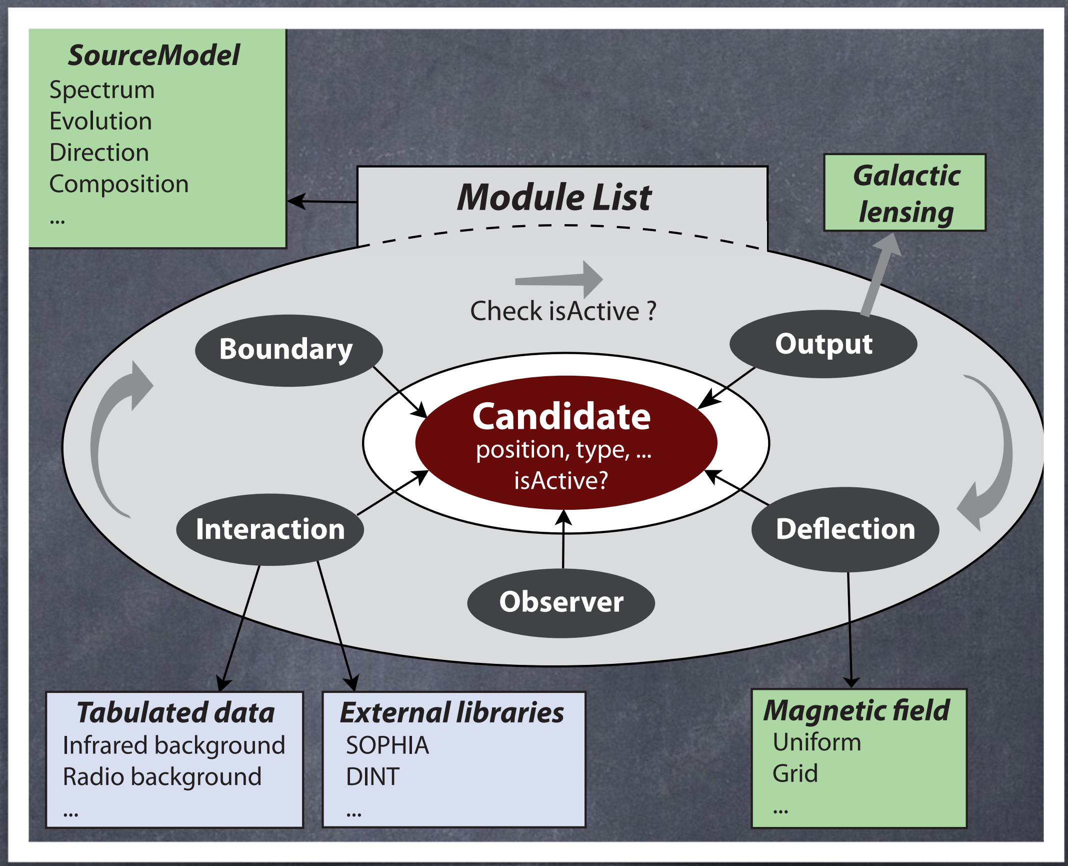

Version 1.4: Eric Armengaud, Tristan Beau, Günter Sigl, Francesco Miniati, Astropart.Phys.28 (2007) 463.

https://crpropa.desy.de/Main_Page

https://github.com/CRPropa/CRPropa3/

Version 2.0: Luca Maccione, Rafael Alves Batista, David Walz, Gero Müller, Nils Nierstenhoefer, Karl-Heinz Kampert, Peter Schiffer, Arjen van Vliet Astroparticle Physics 42 (2013) 41

Discrete Sources in nearby large scale structure

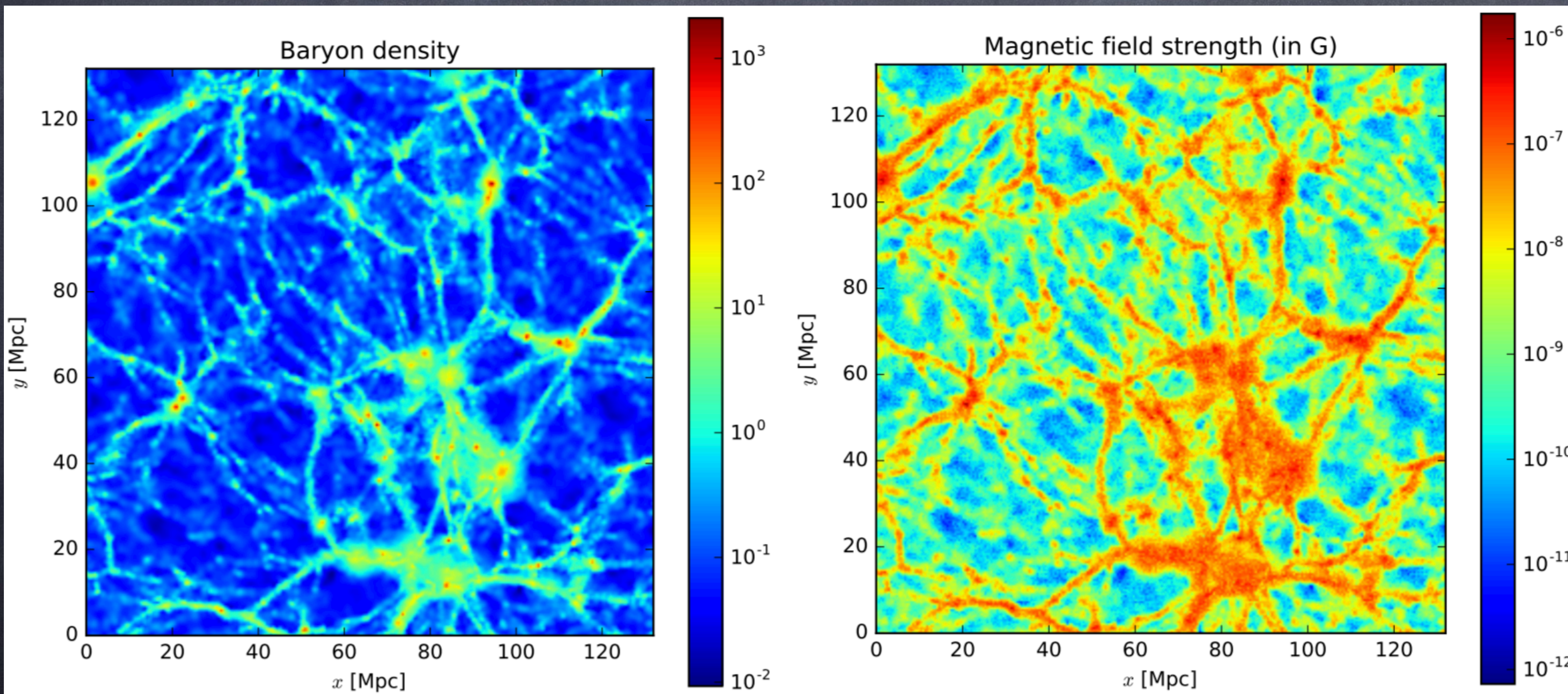

Building Benchmark Scenarios

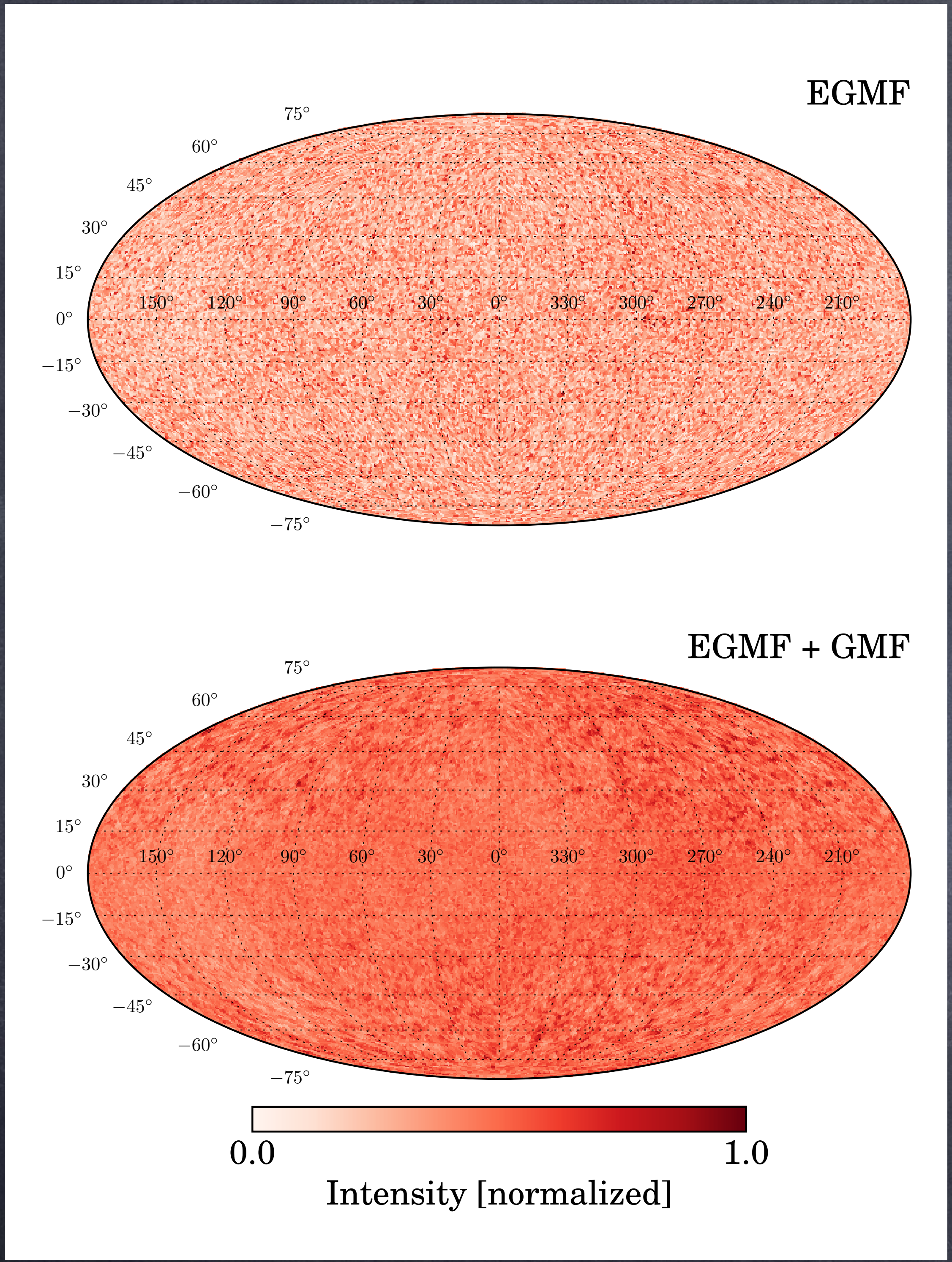

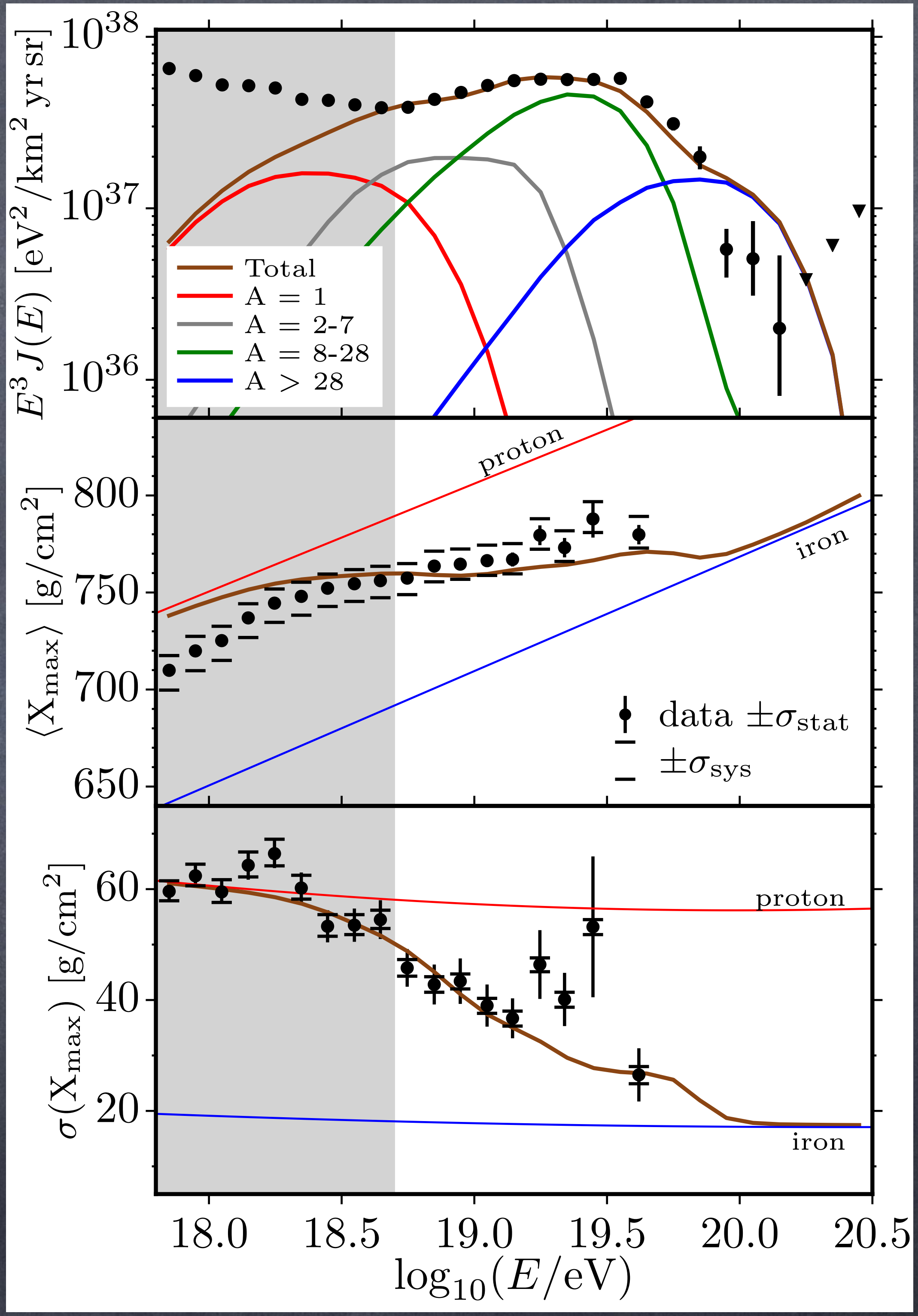

combining spectral and composition information with anisotropy can considerably strengthen constraints on source characteristics, distributions and magnetization

Very High High Energy Neutrinos

The „grand unified" differential neutrino number spectrum

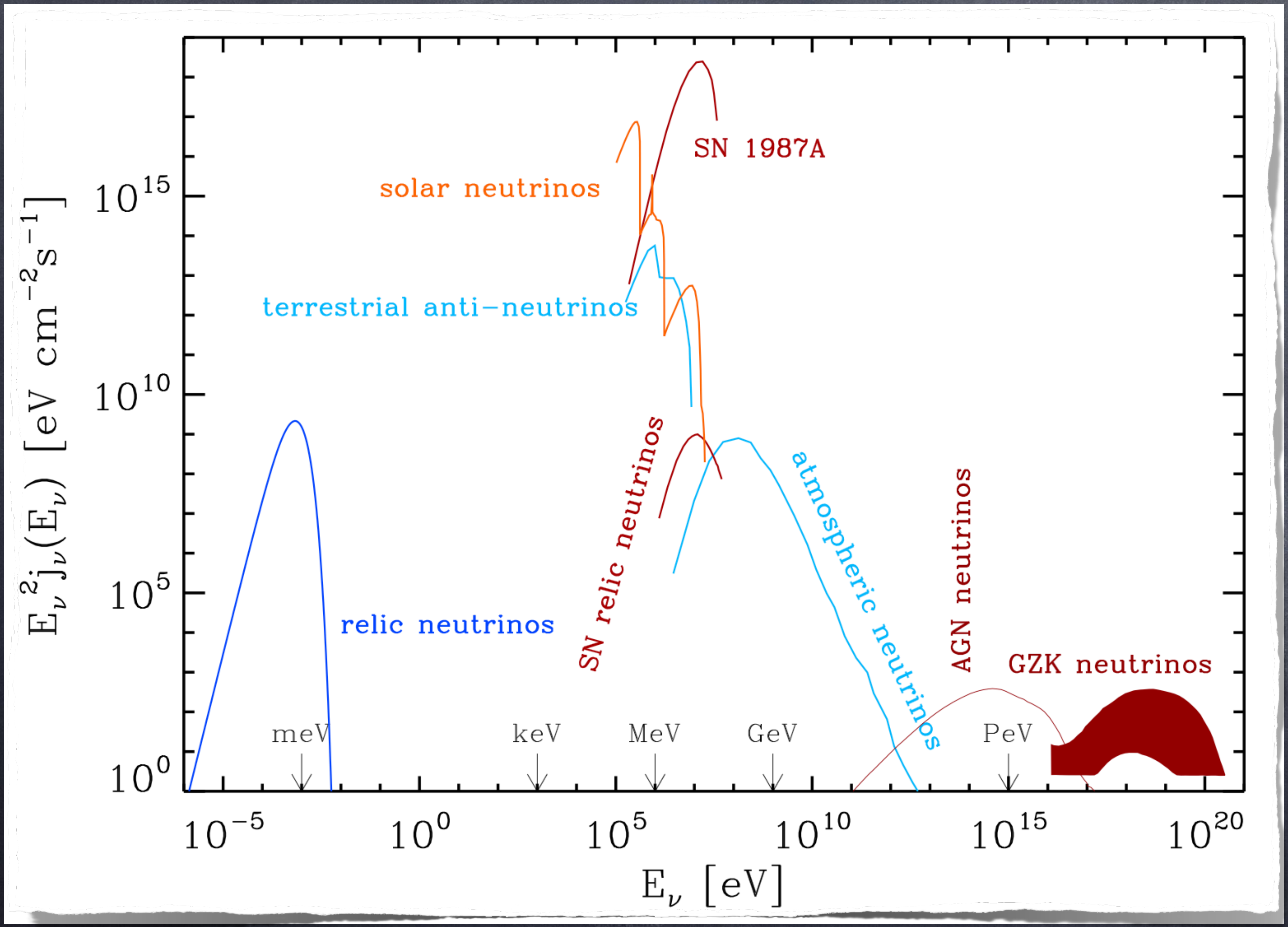

G. Sigl, book "Astroparticle Physics: Theory and Phenomenology", Atlantis Press/Springer 2016

Summary of neutrino production modes

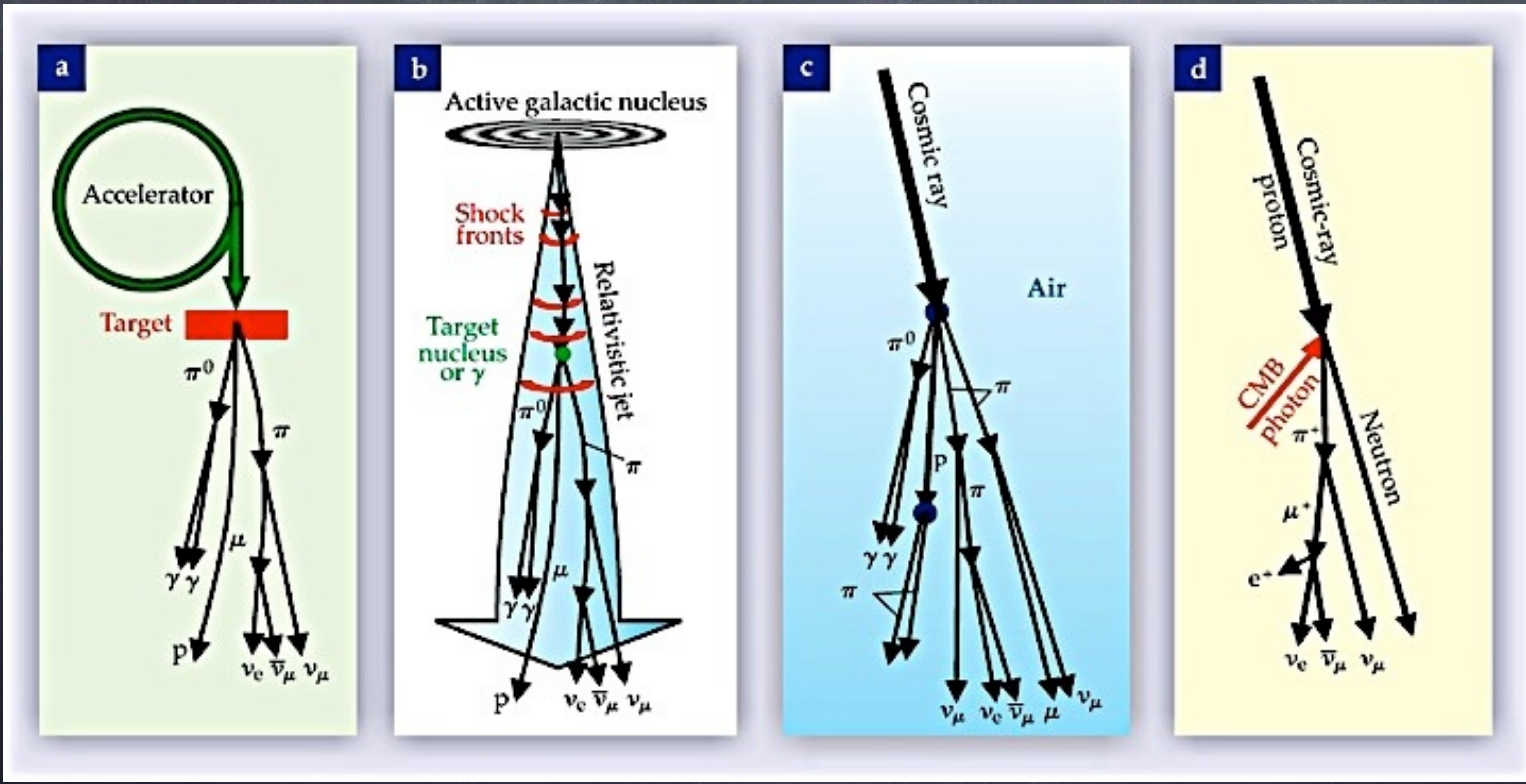

From Physics Today

The IceCube Neutrino Observatory

- 5160 PMTs
- 1 km³ volume
- 86 strings
- 17 m vertical spacing
- 125 m string spacing
- Completed 2010
- Fully operational since 2011

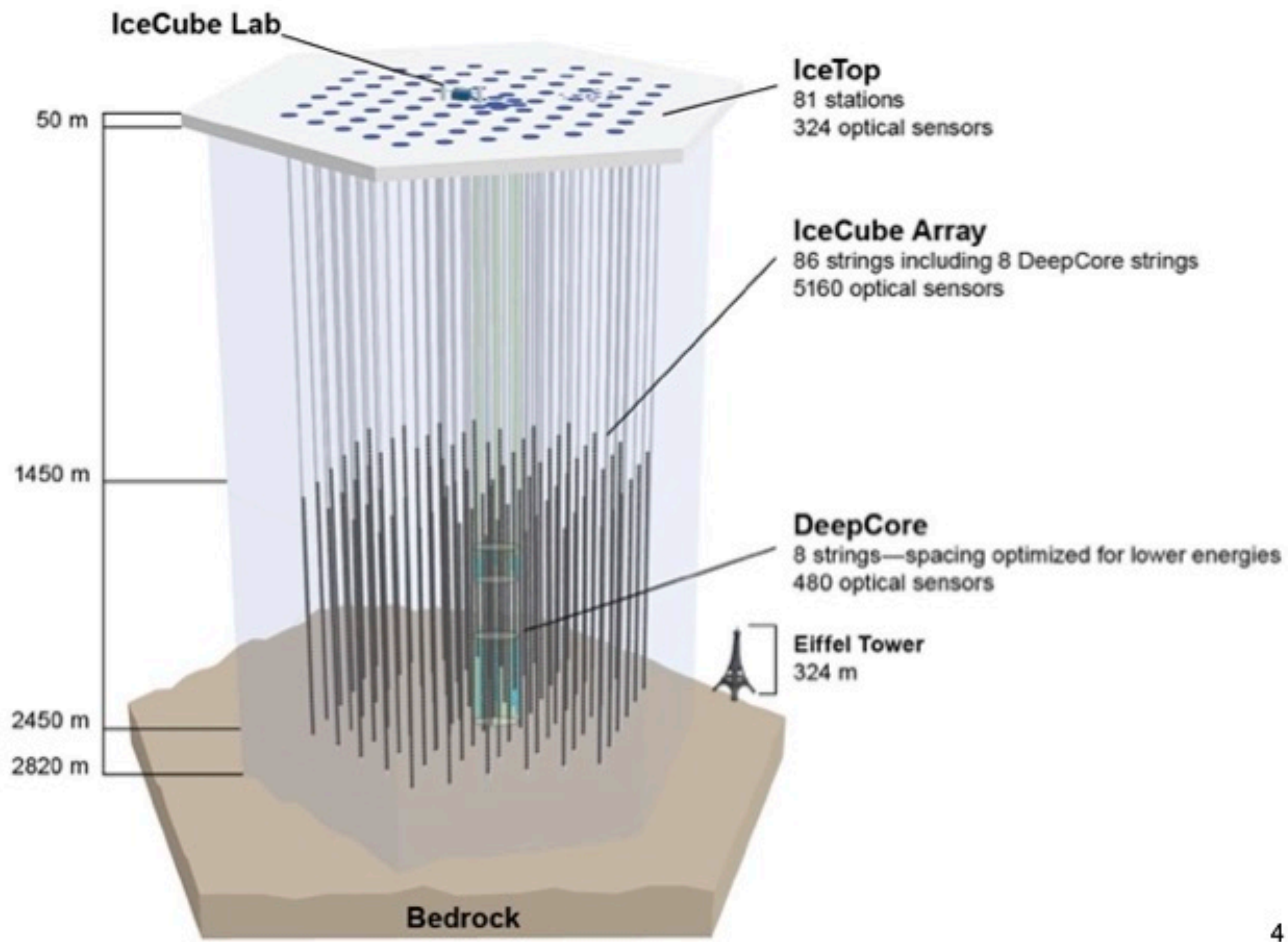

The first decade of discoveries

4

taken from M. Kowalski, IcCube, ICRC 2021

Neutrino Signatures in IceCube

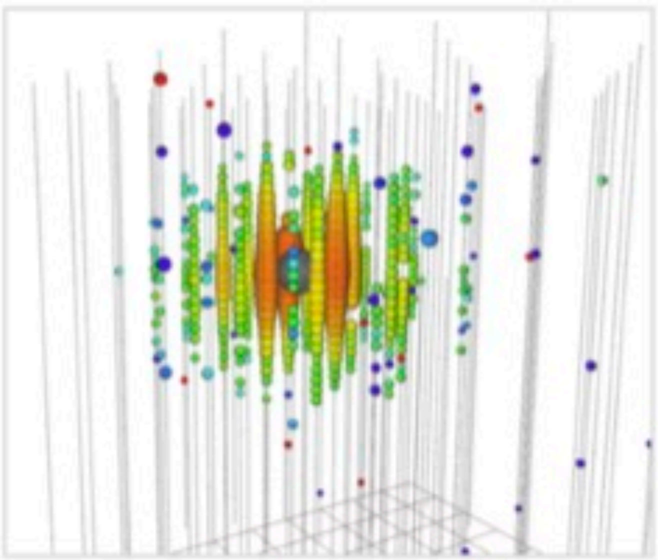

Electron neutrinos:
isolated cascades

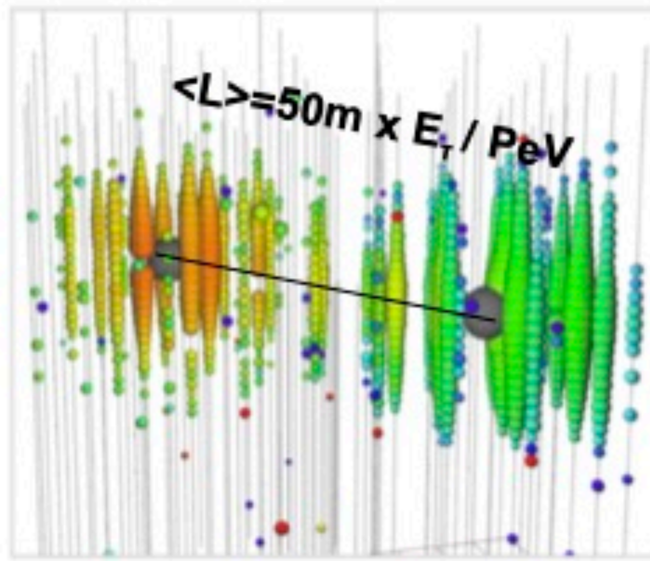

Tau neutrinos:
"double bang"

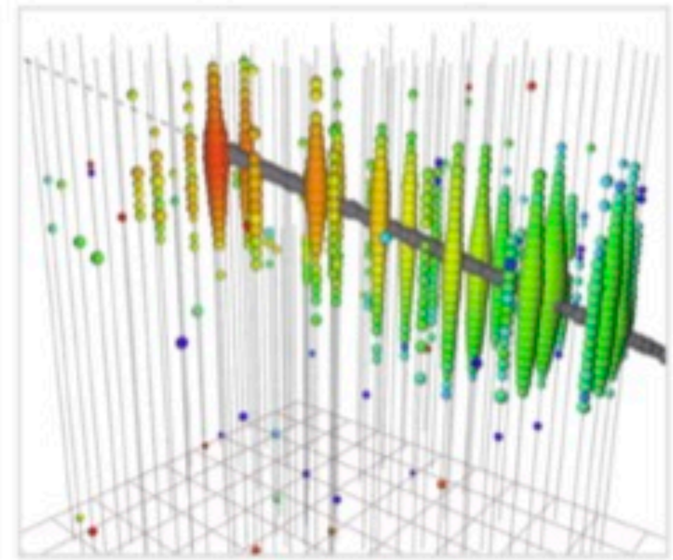

Muon neutrinos:
track-like events

The first decade of discoveries

5

taken from M. Kowalski, IcCube, ICRC 2021

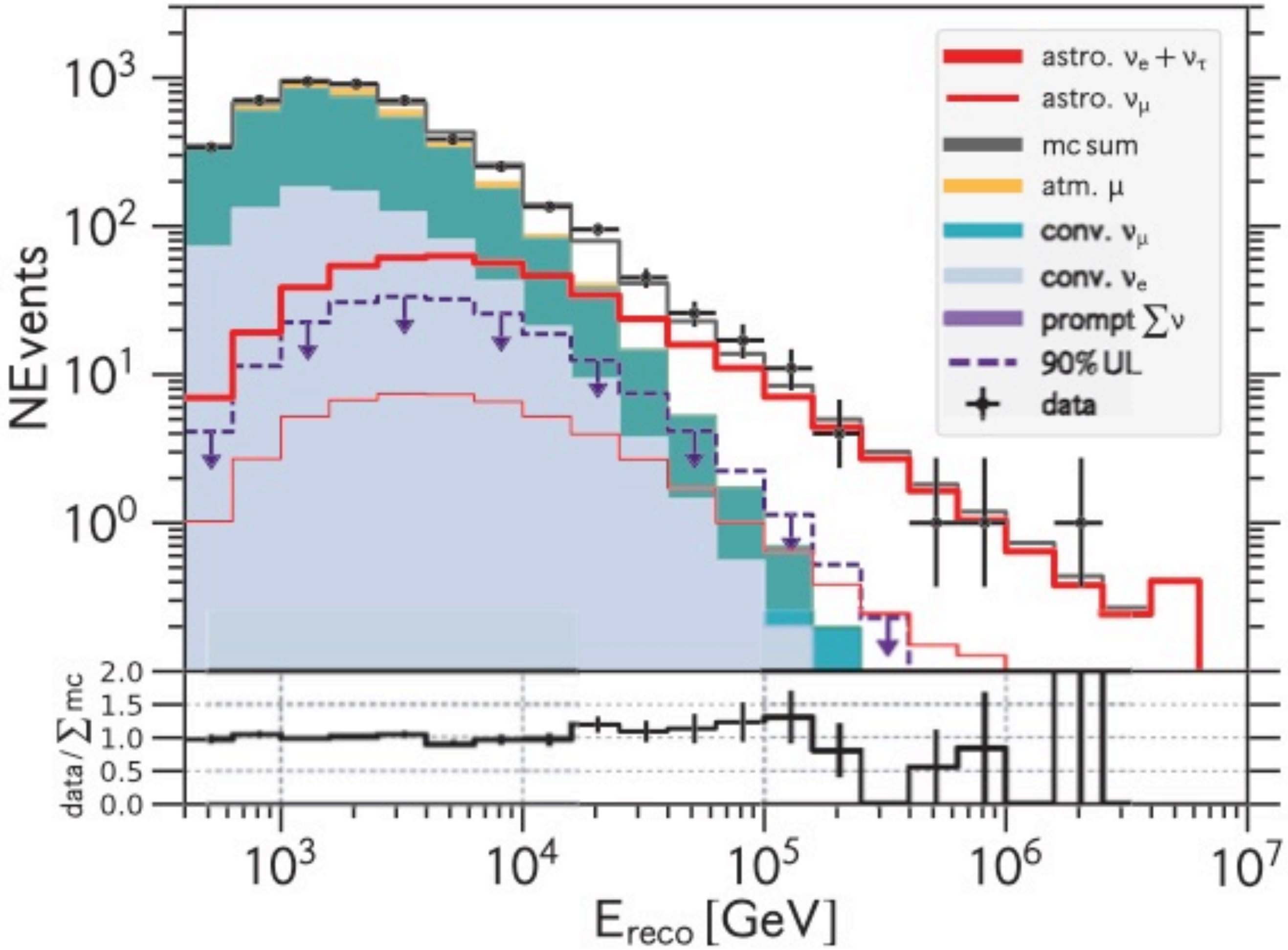

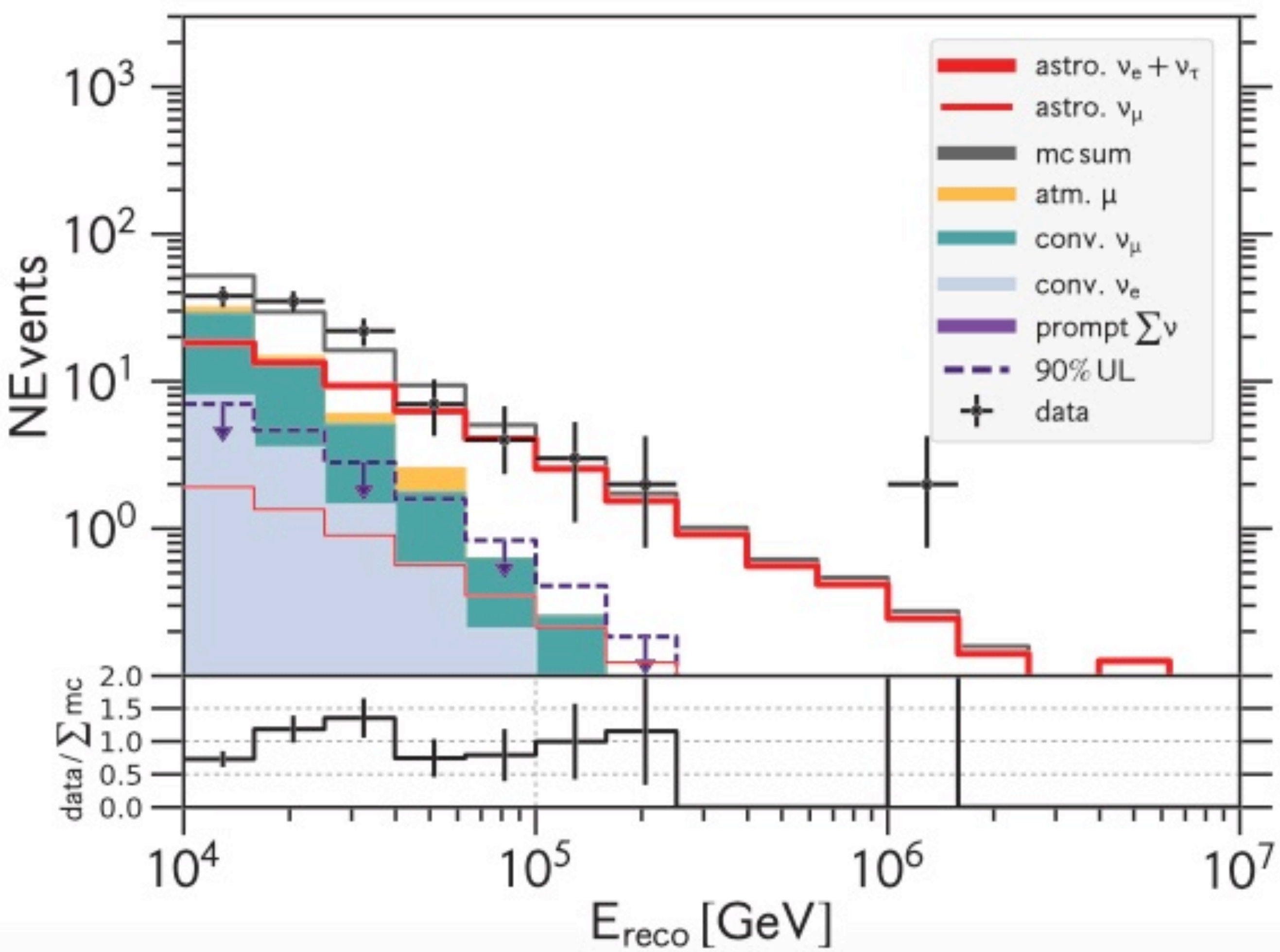

Components of the Diffuse Spectrum

astrophysical neutrinos have a harder spectrum than atmospheric neutrinos which have a spectrum steeper by one power of energy than cosmic ray spectrum due to energy-dependent decay probability of pions, thus $\sim E^{-3.7}$

flavour ratio $(\nu_e + \bar{\nu}_e)/(\nu_\mu + \bar{\nu}_\mu) \sim 1$ for astrophysical neutrinos, but $(\nu_e + \bar{\nu}_e)/(\nu_\mu + \bar{\nu}_\mu) \sim 0.3(10\,\mathrm{GeV}/E_\nu)$ for $E_\nu \gtrsim \mathrm{GeV}$ due to energy-dependent decay probability of muons; flavour ratio saturates at few percent level above ~ 100 GeV due to kaon production.

Aartsen et al [IceCube collaboration], PRL 125 (2020) 121104 [arXiv:1807.11492]

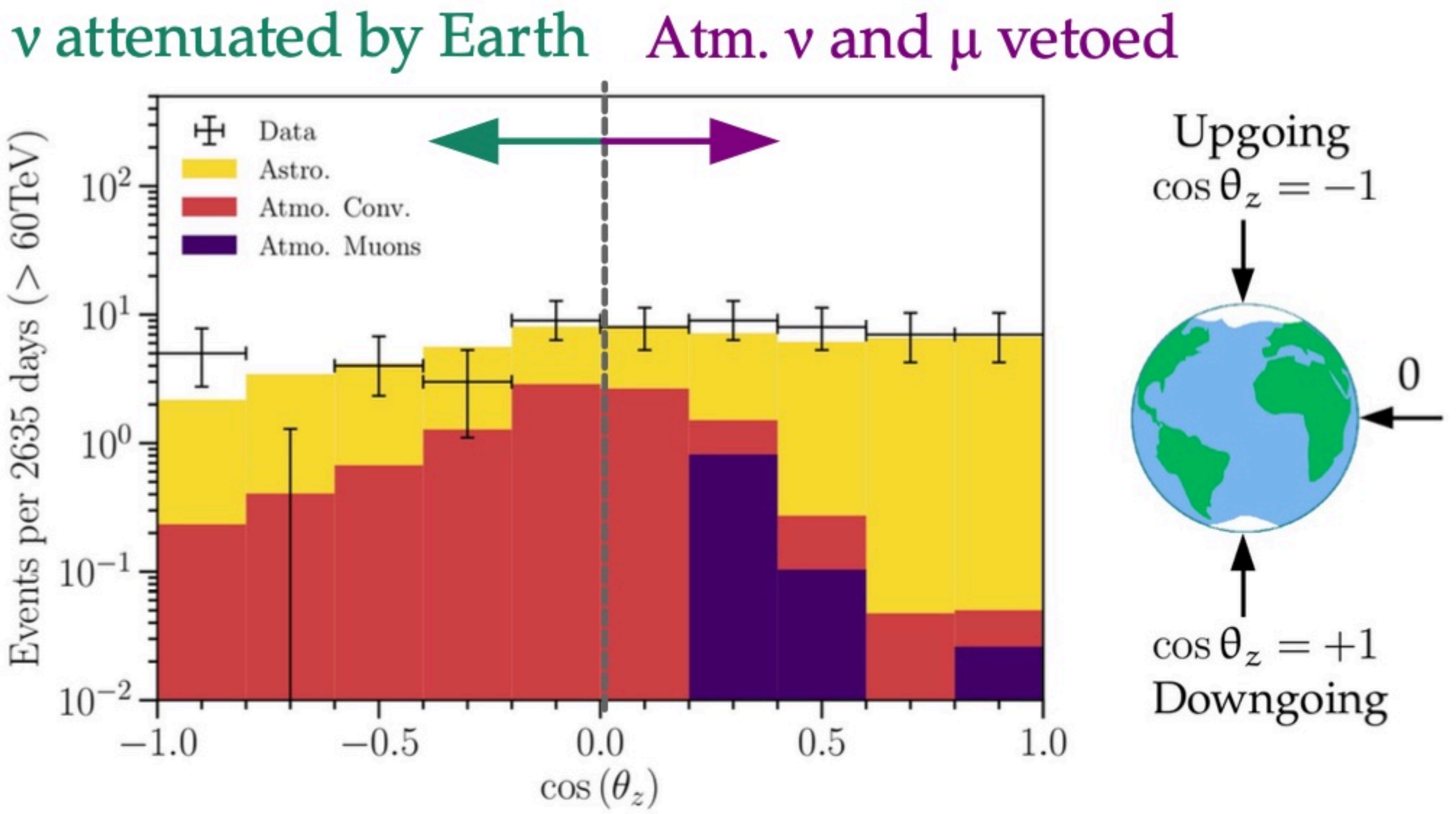

Abbasi et al [IceCube collaboration], arXiv:2011.03545], version taken from talk by Maurizio Bustamante

astrophysical and atmospheric neutrinos also have a different angular distribution: astrophysical roughly isotropic whereas atmospheric peaked at horizontal because least attenuation and largest pion decay probability

Discrete Extragalactic High Energy Neutrino Sources

IceCube neutrinos should be produced mostly within sources, not during propagation

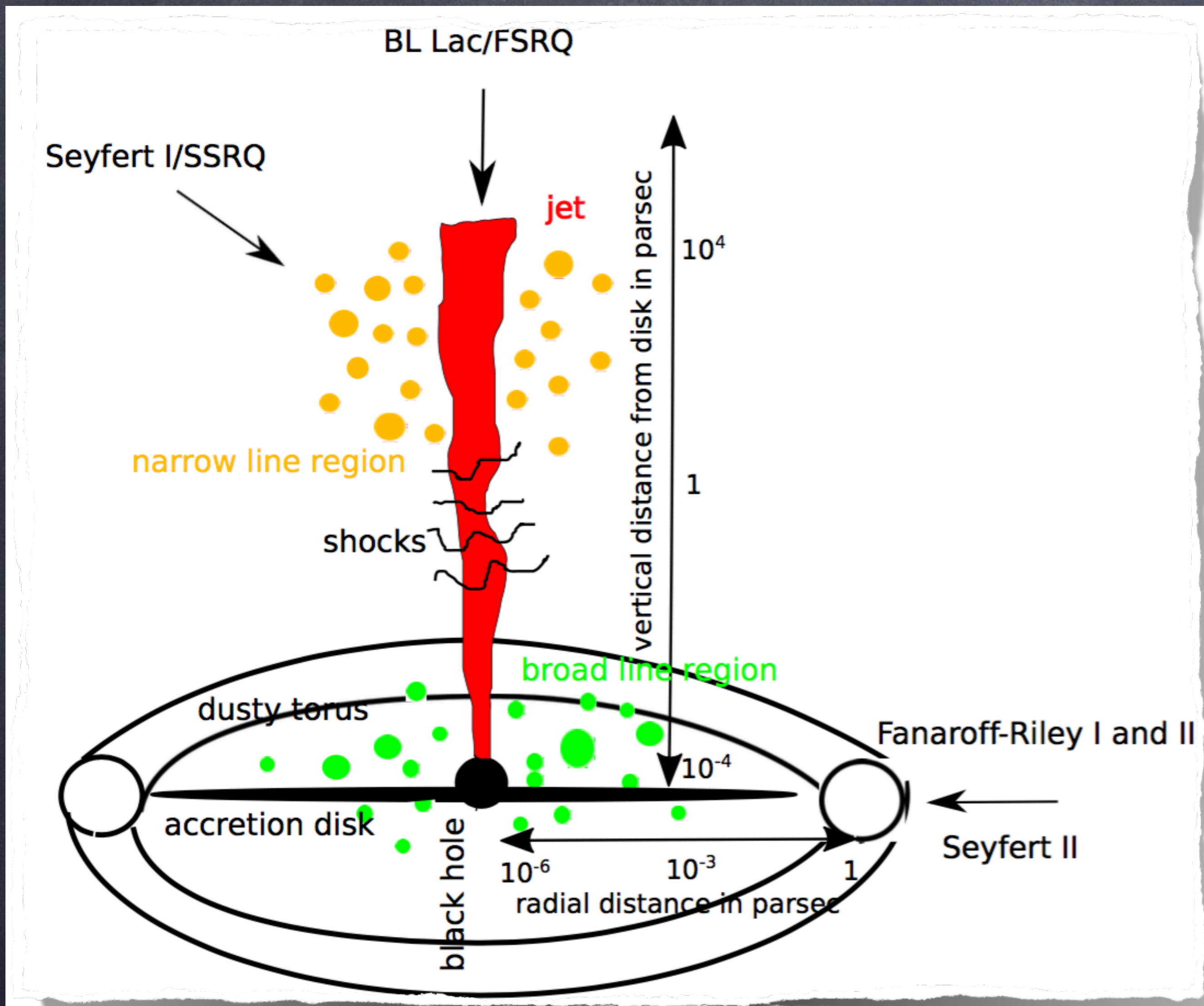

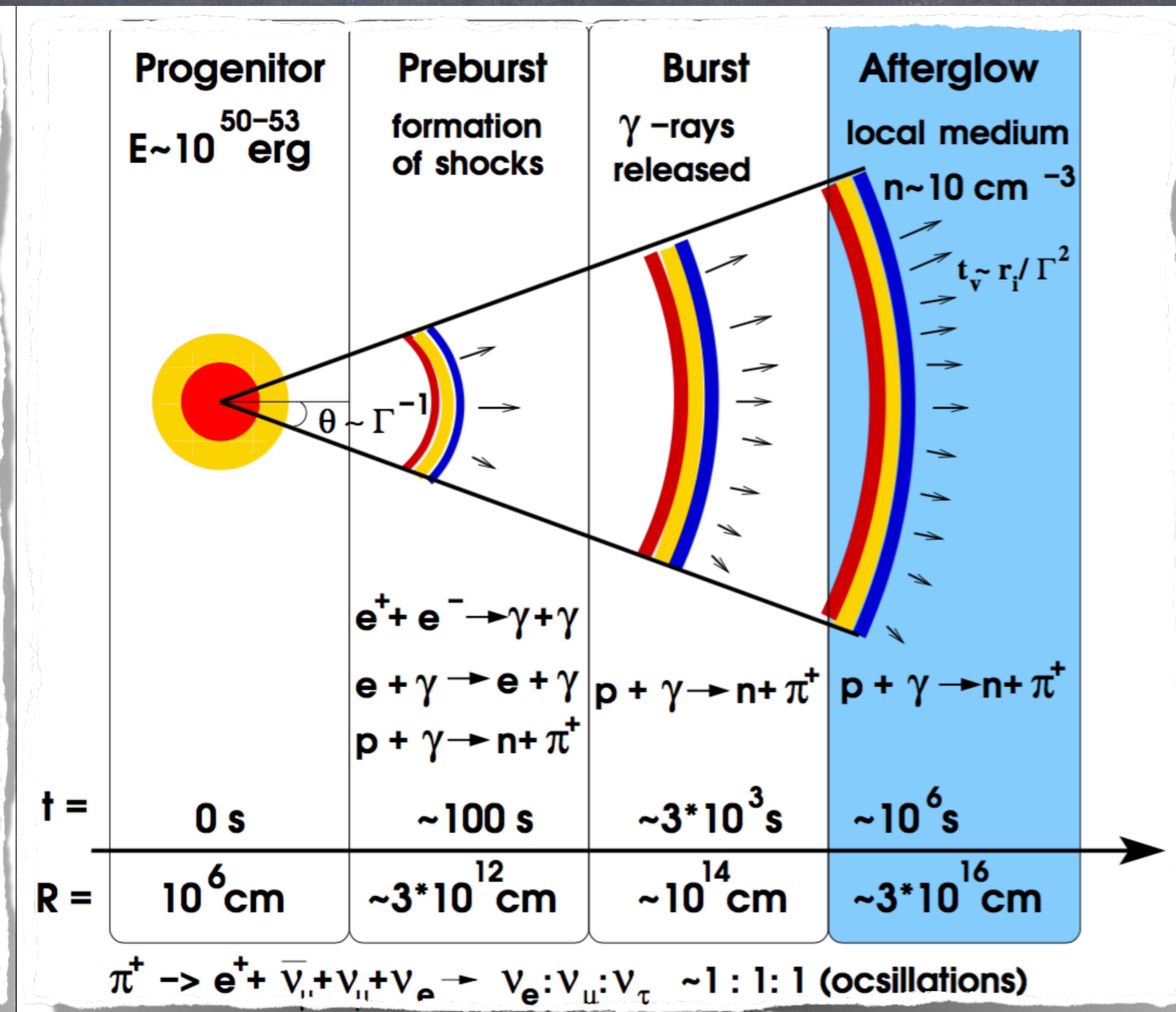

active galaxies **gamma ray bursts**

Figures adapted from J. Becker-Tjus, Phys.Rep. 458 (2008) 173

Neutrino Fluxes from Gamma-Ray Bursts

GRBs are optically thick to charged cosmic rays and nuclei are disintegrated => only neutrons escape and contribute to the UHECR flux by decaying back into protons

Diffuse neutrino flux from GRBs can thus be linked to UHECR flux (if it is dominantly produced by GRBs)

$$\Phi_\nu(E_\nu) \sim \frac{1}{\eta_\nu}\Phi_p\left(\frac{E}{\eta_\nu}\right) ,$$

where $\eta_\nu \simeq 0.1$ is average neutrino energy in units of the parent proton energy. Above ~ 10^{17} eV neutrino spectrum is steepened by one power of E_ν because pions/muons interact before decaying

Correlation studies with GRBs now constrain the GRB contribution to observed diffuse neutrino flux to < 1%, see IceCube collaboration ApJ 824 (2016) 115 [arXiv:1601.06484]; the relation above then also implies subdominant contribution of GRBs to ultra-high energy cosmic rays

A combination of the measured diffuse flux with upper limits on individual sources constrains neutrino source type

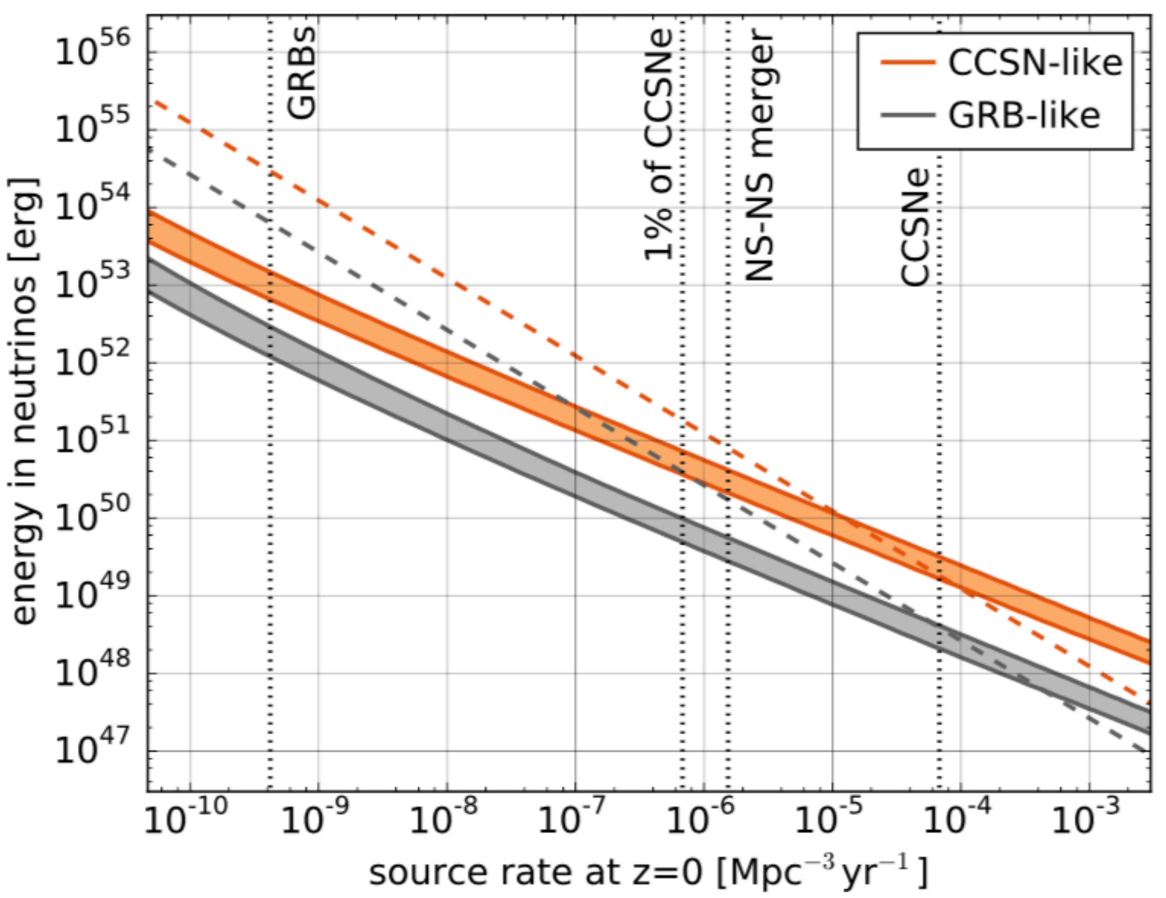

FIG. 2: Limits on the median source energy (90% c. l.) emitted in neutrinos between 100 GeV and 10 PeV within 100 s. The area above the bands is excluded for CCSN-like (orange) and GRB-like (gray) populations respectively. The upper edge of the limit corresponds to an $E^{-2.5}$ neutrino spectrum and the lower one to an $E^{-2.13}$ spectrum. The dashed lines show which source energy corresponds to 100% of the astrophysical flux for an $E^{-2.5}$ spectrum. The corresponding lines for an $E^{-2.13}$ spectrum would be lower by a factor of 13. The rate of long GRBs, NS-NS mergers and CCSNe is indicated. Beaming is included for long GRBs, but not for NS-NS mergers or CCSNe due to the unknown jet opening angles.

Aartsen et al [IceCube collaboration], PRL 122 (2019) 051102 [arXiv:1807.11492]

Sensitivity of existing and future experiments to ultra-high energy neutrinos

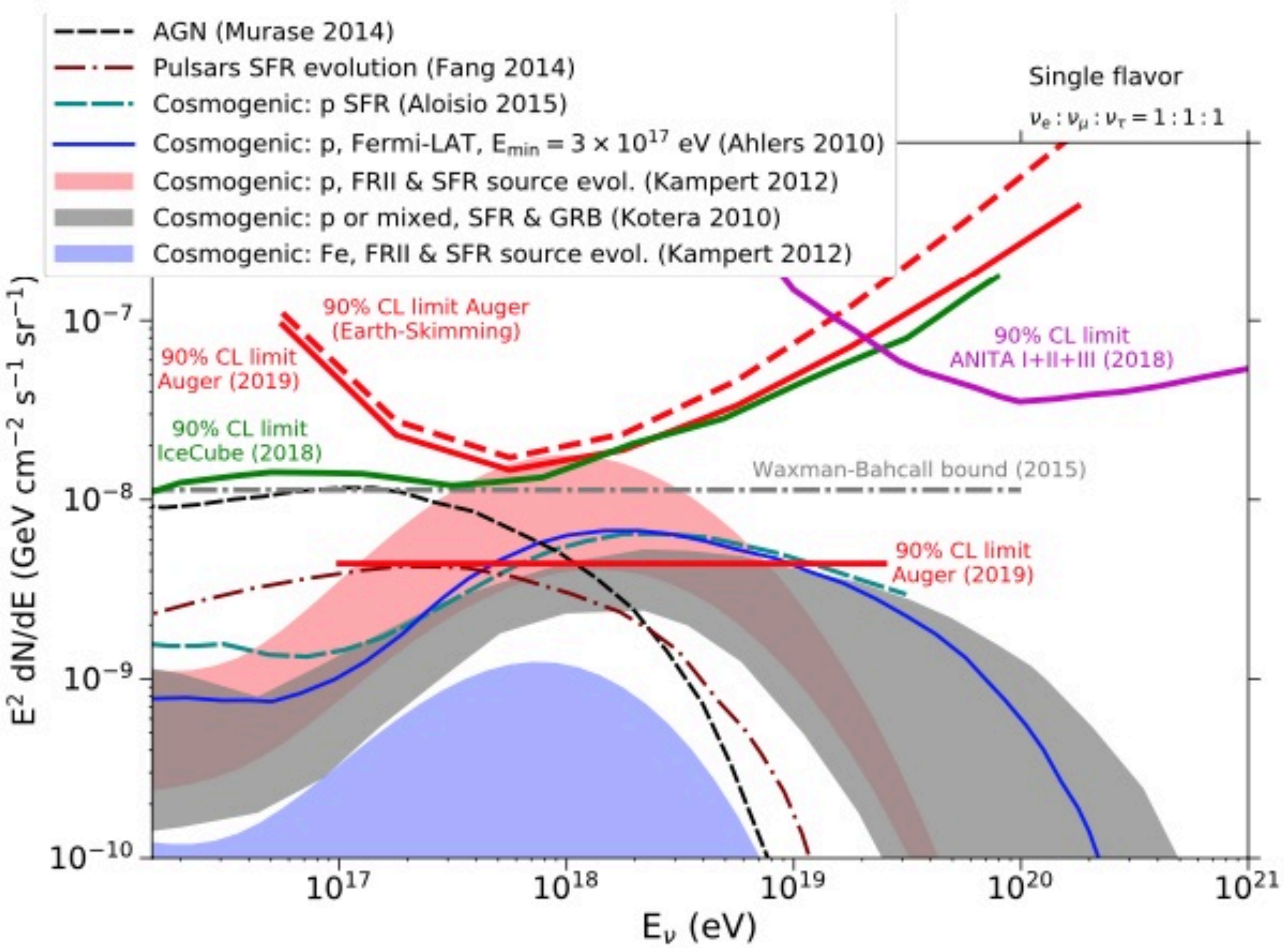

Figure 6. Pierre Auger Observatory upper limit (90% C.L.) to the normalization k of the diffuse flux of UHE neutrinos $\phi_\nu = k\, E_\nu^{-2}$ as given in eqs. (4.2) and (4.3) (solid straight red line). Also plotted are the upper limits to the normalization of the diffuse flux (differential limits) when integrating the denominator of eq. (4.2) in bins of width 0.5 in $\log_{10} E_\nu$ (solid red line — Auger all channels and flavours; dashed red line — Auger Earth-skimming ν_τ only). The differential limits obtained by IceCube [35] (solid green) and ANITA I+II+III [34] (solid dark magenta) are also shown. The expected neutrino fluxes for several cosmogenic [20, 60–62] and astrophysical models of neutrino production, as well as the Waxman-Bahcall bound [63, 64] are also plotted. All limits and fluxes are converted to single flavor.

Pierre Auger Collaboration, JCAP 10 (2019) 022

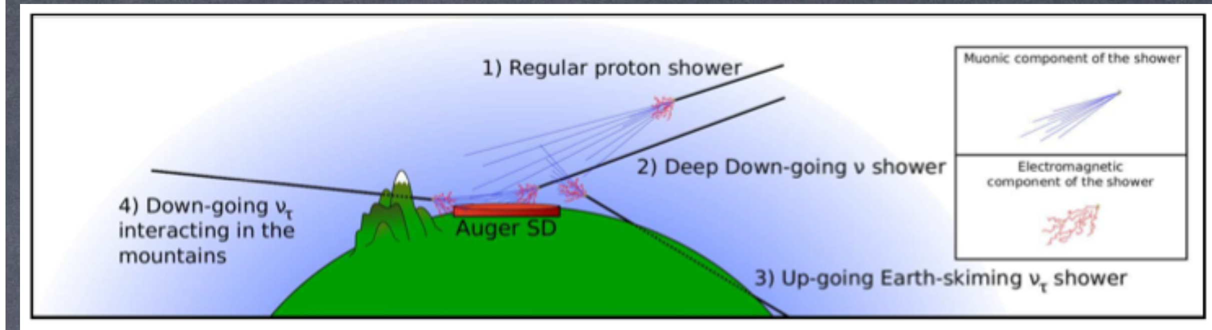

Vitagliano, Tamborra, Raffelt, Rev.Mod.Phys. 92 (2020) 045006

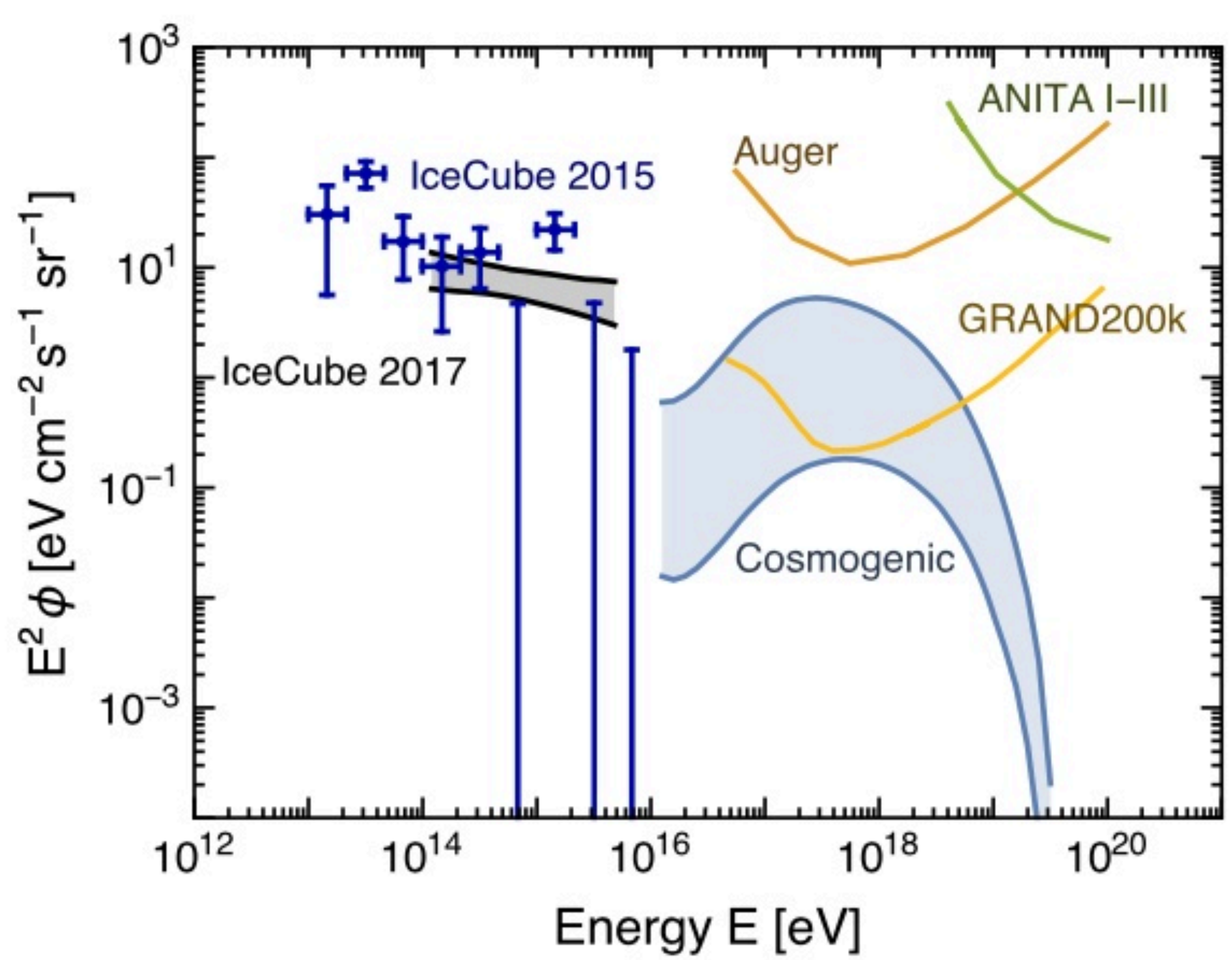

Multi-Messengers: The Big Picture

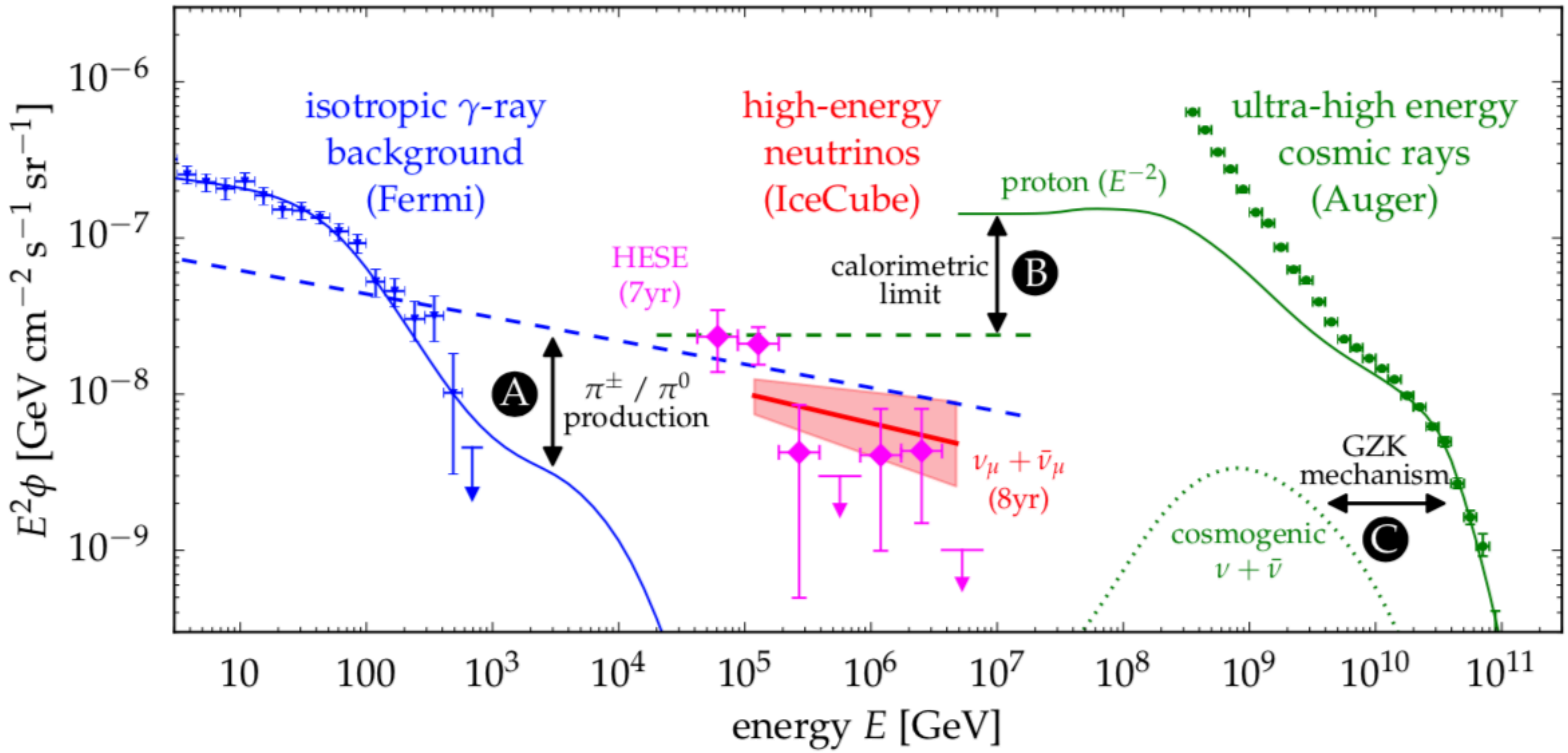

M. Ahlers, arXiv:1811.07633

Figure 1. The spectral flux (ϕ) of neutrinos inferred from the eight-year upgoing track analysis (red fit) and preliminary results of the seven-year HESE analysis [8] (magenta data) compared to the flux of unresolved extragalactic γ-ray sources [10] (blue data) and ultra-high-energy cosmic rays [11] (green data). The $\nu_\mu + \bar{\nu}_\mu$ spectrum is indicated by the best-fit power-law (solid line) and 1σ uncertainty range (shaded range). We highlight the various multimessenger relations: **A:** The joined production of charged pions ($\pi^\pm$) and neutral pions (π^0) in cosmic-ray interactions leads to the emission of neutrinos (dashed blue) and γ-rays (solid blue), respectively. **B:** Cosmic ray emission models (solid green) of the most energetic cosmic rays imply a maximal flux (calorimetric limit) of neutrinos from the same sources (green dashed). **C:** The same cosmic ray model predicts the emission of cosmogenic neutrinos from the collision with cosmic background photons (GZK mechanism).

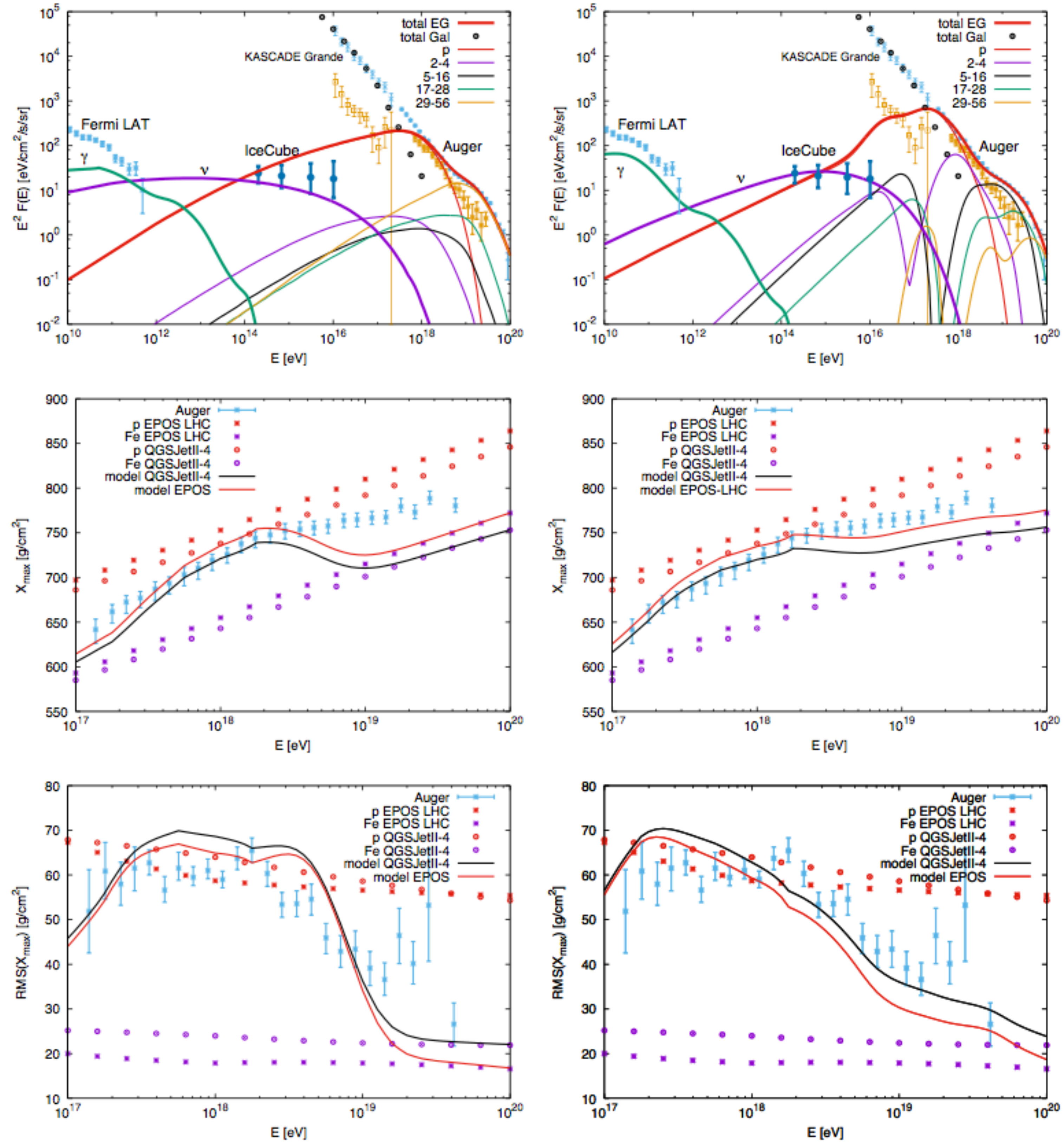

FIG. 1: Predictions for the diffuse flux (top) of five elemental groups together with the proton (orange errorbars) and total (blue errorbars) flux from KASCADE, KASCADE-Grande [9] and Auger (black errorbars) [8, 33], the EGRB from Fermi-LAT (red errorbars) [2], and the high-energy neutrino flux from IceCube (magenta errorbars) [3]; the middle and lower panels compare predictions for $X_{\rm max}$and RMS($X_{\rm max}$) using the EPOS-LHC [35] and QGSJET-II-04 [26] models to data from Auger [34]. Left panels for only hadronic interactions with $\alpha = 1.8$, $E_{\rm max} = 3 \times 10^{18}$ eV and BL Lac evolution. Right panels for both $A\gamma$ and Ap interactions with $\alpha = 1.5$, $E_{\rm max} = 6 \times 10^{18}$ eV, $\tau^{p\gamma} = 0.29$ and AGN evolution. The hadronic interaction depth is normalised as $\tau_0^{pp} = 0.035$.

a recent "minimal" model that explains diffuse spectra of primary cosmic rays, secondary gamma-rays and neutrinos in which primary cosmic rays interact hadronically and/or photo-hadronically around the sources

M. Kachelriess et al., PRD 96 (2017) 083006 [arXiv:1704.06893]

General Multi-Messenger Aspects

Blazars emitting significant neutrino sources should be loud in GeV γ-rays, but NOT in γ-rays above TeV.

This is because TeV γ-rays pair produce with “blue bump” photons of ~10 eV energy with a cross section $\sim\sigma_{Th} \sim 1$ b about a factor 10^4 larger than the pγ cross section that produces the neutrinos => If loud in > TeV γ-rays, optical depth for neutrino production would be very small.

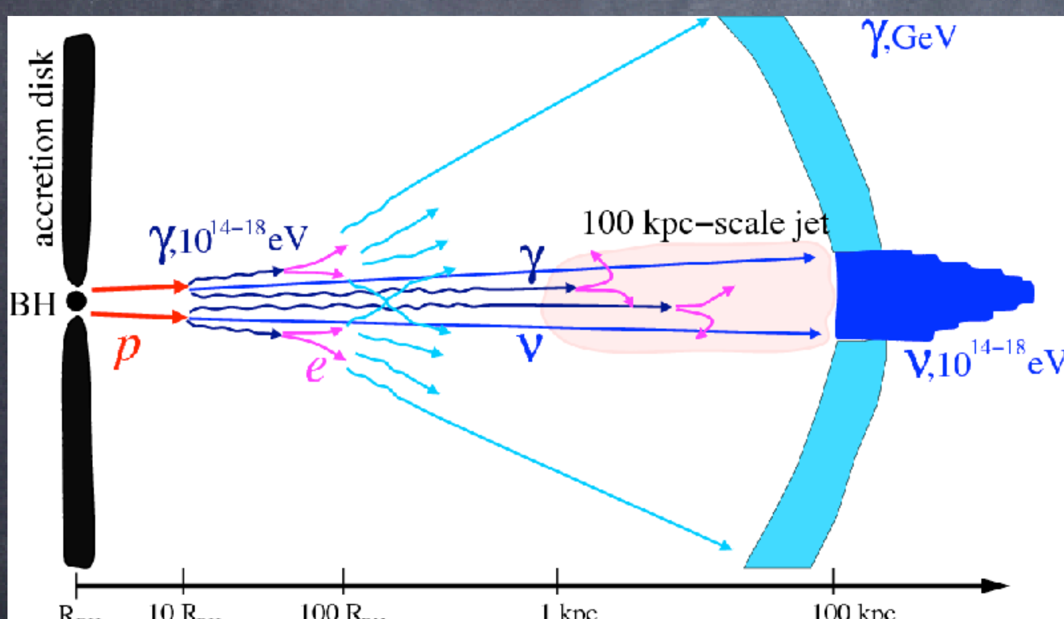

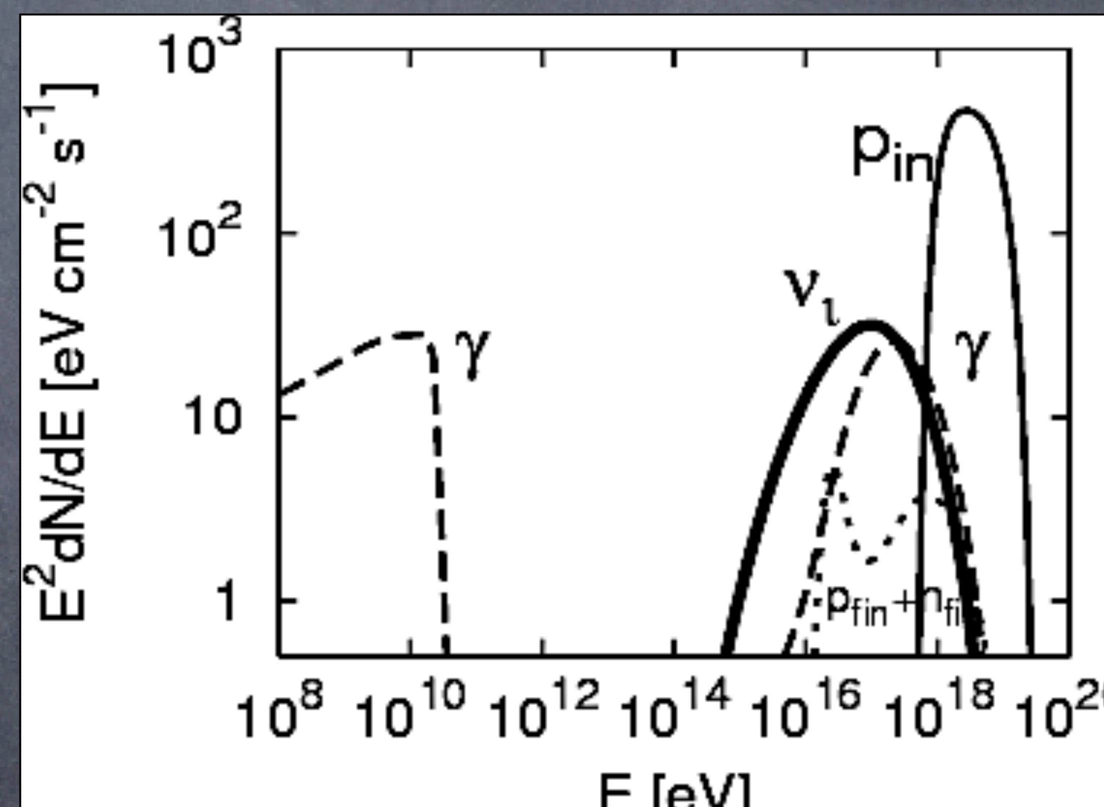

Neronov and Semikoz, Phys.Rev.D66 (2002) 123003

High Energy Neutrinos and Gravitational Waves

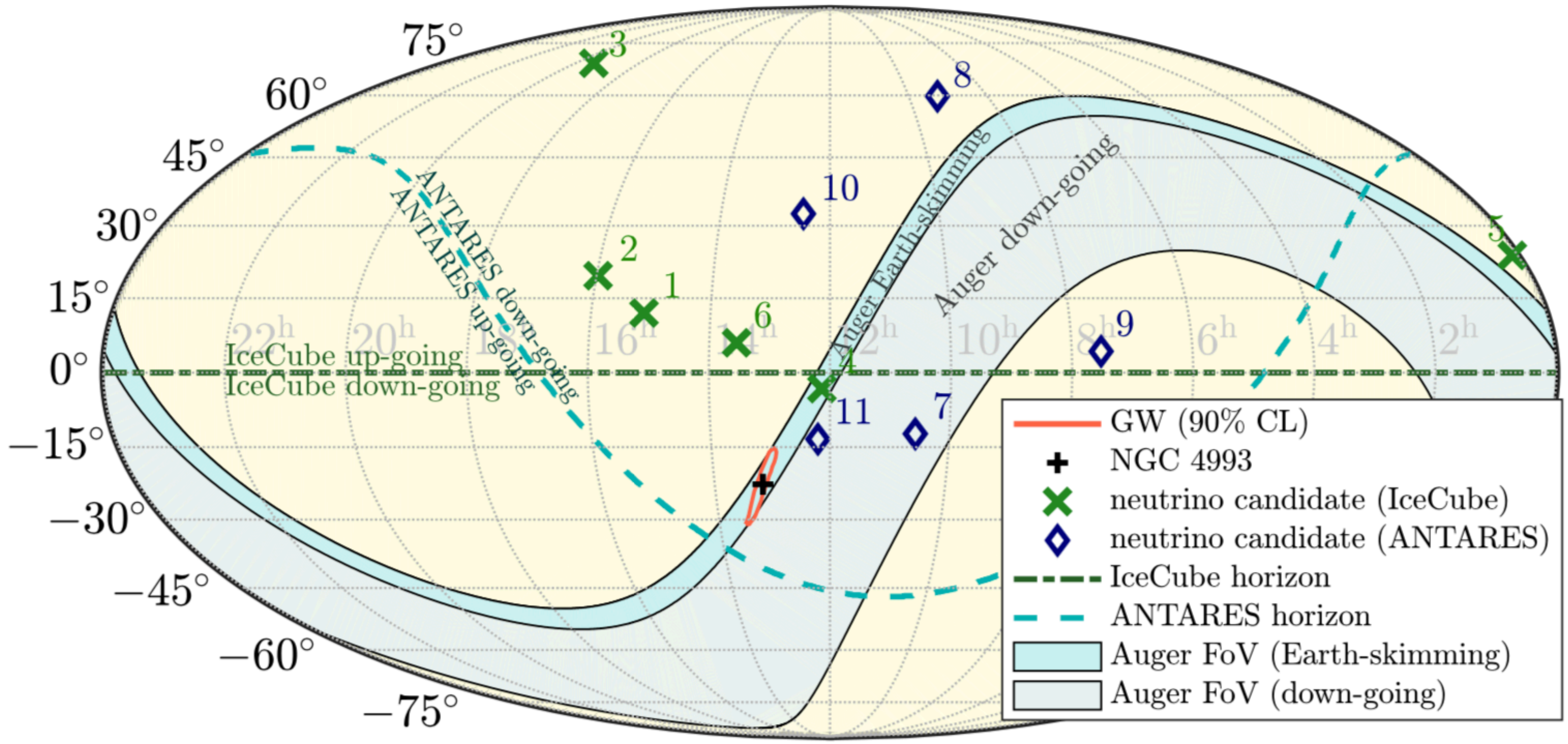

Antares, IceCube, Auger, LIGO, Virgo, ApJ Lett. 850 (2017) L35 [arXiv:1710.05839]

Figure 1. Localizations and sensitive sky areas at the time of the GW event in equatorial coordinates: GW 90% credible-level localization (red contour; Abbott et al. 2017c), direction of NGC 4993 (black plus symbol; Coulter et al. 2017a), directions of IceCube's and ANTARES's neutrino candidates within 500 s of the merger (green crosses and blue diamonds, respectively), ANTARES's horizon separating down-going (north of horizon) and up-going (south of horizon) neutrino directions (dashed blue line), and Auger's fields of view for Earth-skimming (darker blue) and down-going (lighter blue) directions. IceCube's up-going and down-going directions are on the northern and southern hemispheres, respectively. The zenith angle of the source at the detection time of the merger was 73.8° for ANTARES, 66.6° for IceCube, and 91.9° for Auger.

curiously, around the time of GW170817 Auger was in "Earth skimming mode" with maximal sensitivity, allowing relatively strong constraints

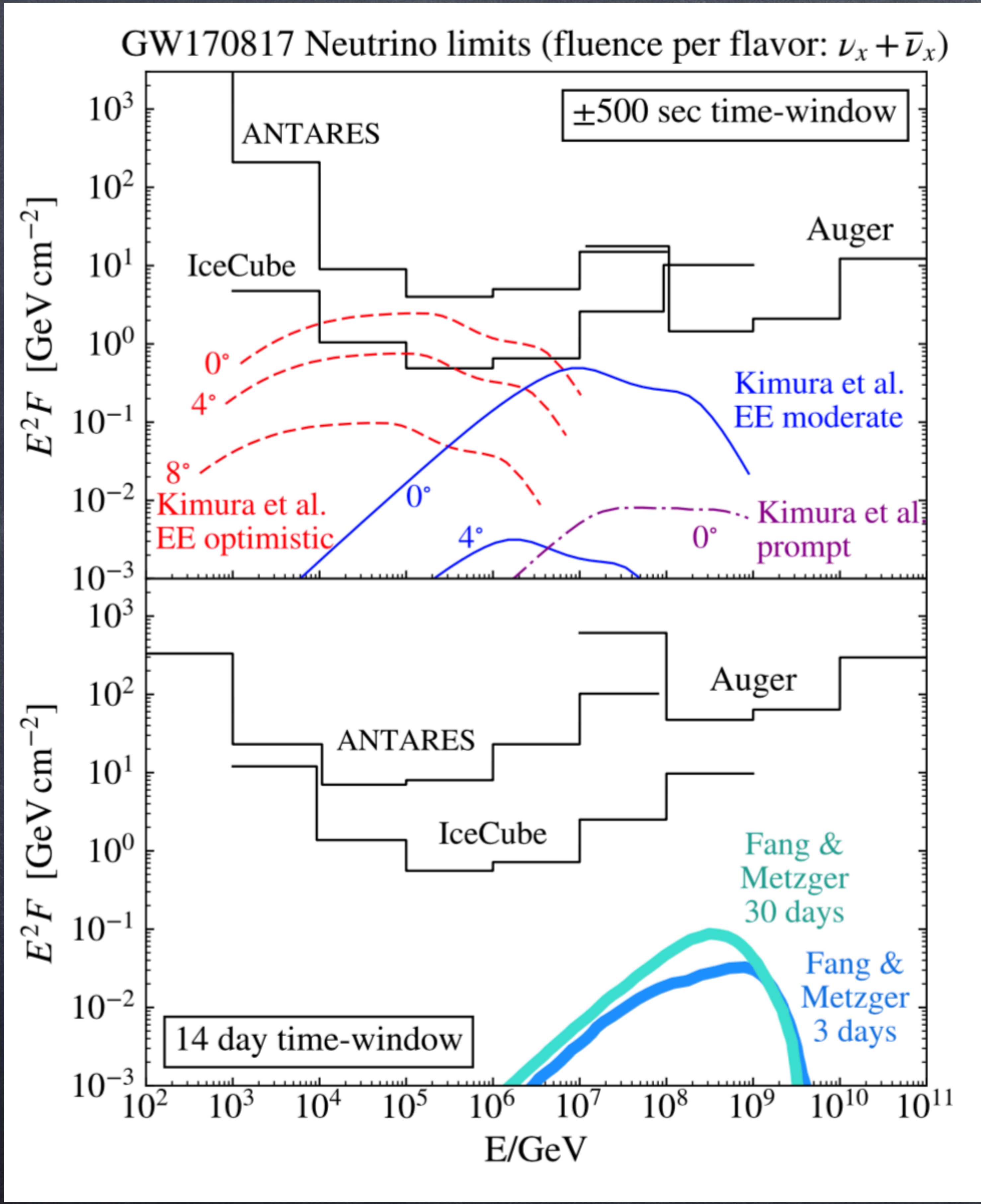

main message: most optimistic models start to be constrained

Antares, IceCube, Auger, LIGO, Virgo, ApJ Lett. 850 (2017) L35 [arXiv:1710.05839]

Dark Matter Candidates

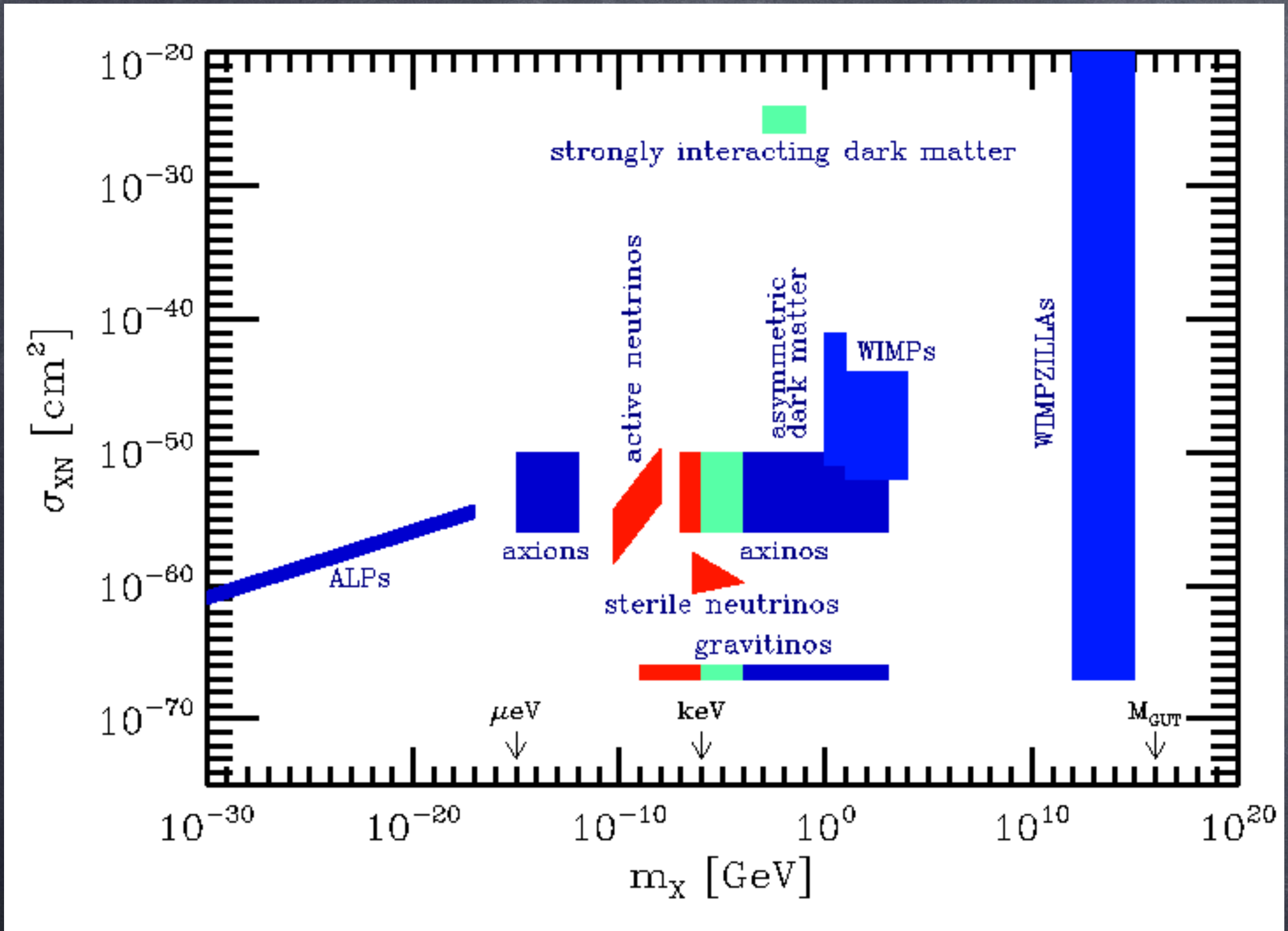

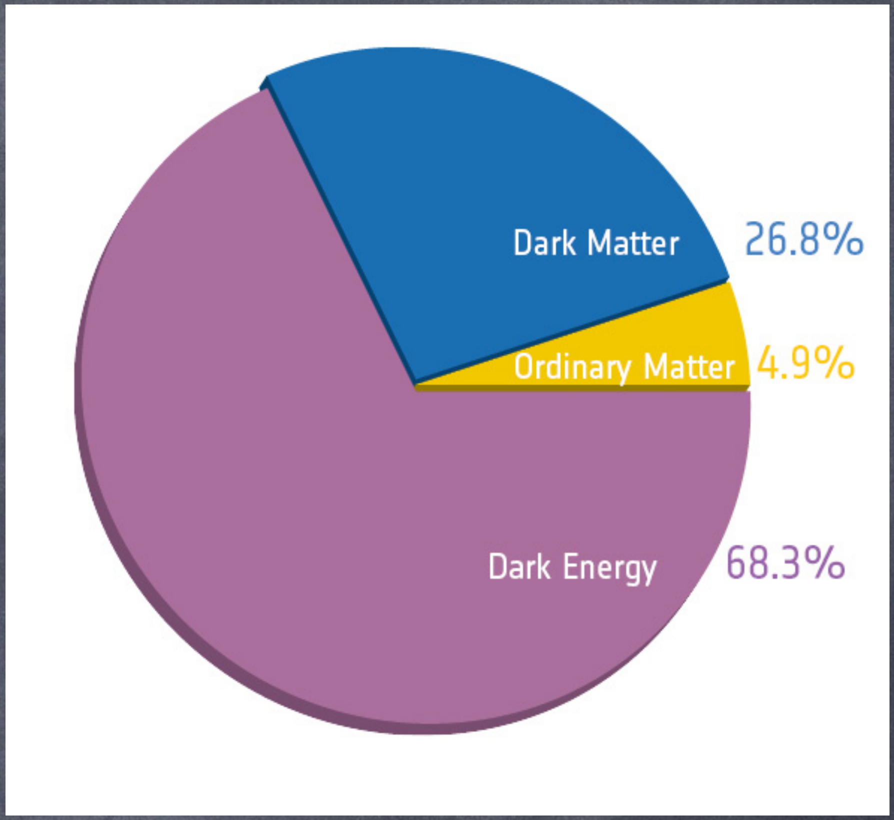

[PLANCK]

G. Sigl, book “Astroparticle Physics: Theory and Phenomenology”, Atlantis Press/Springer 2016

Axions, the strong CP problem and cosmology

In QCD an additional term of the form

$$\mathcal{L}_\theta = \frac{\alpha_s}{8\pi}\,\theta\, G^\alpha_{\mu\nu}\tilde{G}^{\mu\nu}_\alpha = \frac{\alpha_s}{8\pi}\,\theta\,\frac{1}{2}\epsilon^{\mu\nu\lambda\sigma}G^\alpha_{\mu\nu}G^\alpha_{\lambda\sigma}\,,$$

with α_s the strong coupling constant and θ a CP-odd constant, is not forbidden by any symmetry, but would give rise to electric dipole moment for the neutron

$$d_n = 3.6\times 10^{-16}\theta\, e\,\mathrm{cm}$$

which upon comparing with experimental upper limit gives $\theta < 10^{-10}$.
A solution would be to promote θ to a pseudo-scalar field with a Lagrangian

$$\mathcal{L}_a = \frac{1}{2}\partial_\mu a\partial^\mu a + \frac{\alpha_s}{8\pi f_a}\,a\,G^\alpha_{\mu\nu}\tilde{G}^{\mu\nu}_\alpha + \frac{s\alpha_{\rm em}}{8\pi f_a}\,a\,F_{\mu\nu}\tilde{F}^{\mu\nu} - V_a(a)\,,$$

Non-perturbative QCD instantons lead to mixing with pions and gives zero-temperature potential of the form

$$V_a(a) \simeq m_u\Lambda^3_{\rm QCD}\left(1-\cos\frac{a}{f_a}\right)\,,$$

expanding in a gives the vacuum axion mass

$$m_a \simeq 6 \times 10^{-6} \left(\frac{10^{12}\,\mathrm{GeV}}{f_a}\right) \mathrm{eV}\,.$$

at finite temperature the axion mass is given by the topological susceptibility,

$$m_a^2(T) = \frac{\chi(T)}{f_a^2}\,, \quad \chi(T) = \frac{\partial^2 V_\theta}{\partial\theta^2}(\theta = 0, T) = \frac{\langle Q_5^2\rangle(\theta = 0, T)}{\mathcal{V}}\,,$$

This is essentially given by the fluctuations of the topological quantum number

$$Q_5(t) \equiv \int d^3\mathbf{r} j_5^0(\mathbf{r}) = N_L^q - N_R^q$$

which can be calculated approximately within the dilute instant approximation or numerically on the lattice.

Axion-like particles (ALPs) in general have independent mass m_a and coupling f_a and often only coupling to photons is considered.

Axions, the strong CP problem and cosmology

a/f_a corresponds to an angular coordinate which for $T > f_a$ exhibits a chiral U(1) shift symmetry, known as Peccei-Quinn symmetry

spontaneous breaking of global Peccei-Quinn symmetry at temperature $T < f_a$: axion would be pseudo Nambu-Goldstone boson

axion acquires mass at QCD scale due to mixing with pions -> tilted Mexican hat, solves strong CP-problem because axion field is naturally driven to zero

axion field is frozen for $H > m_a$ with random values uncorrelated over causal distances

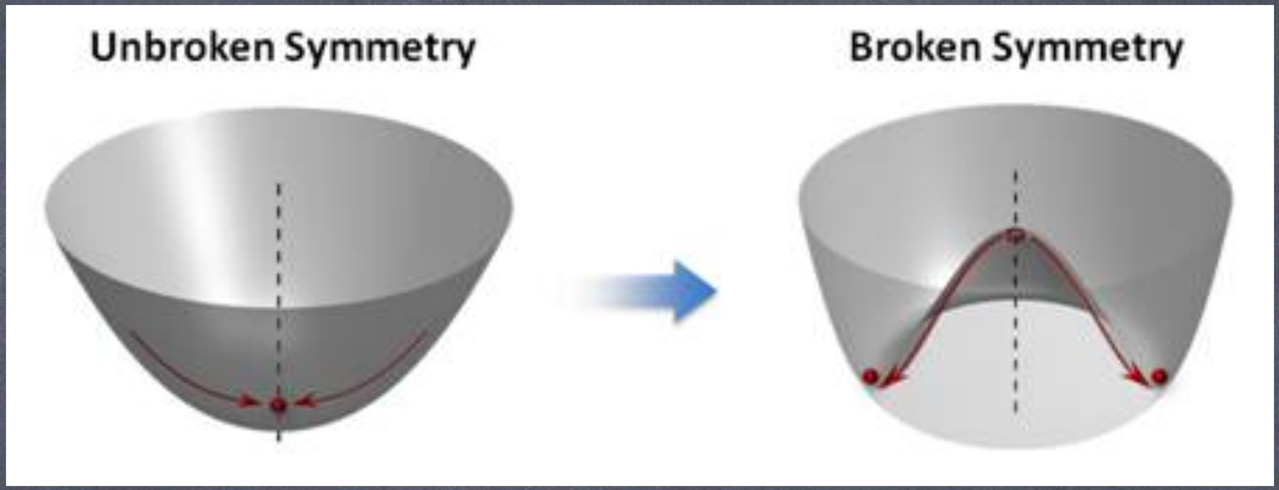

[Peking University]

$$\Phi(x) = \left[f_a + \rho(x)\right] e^{ia(x)/f_a}$$

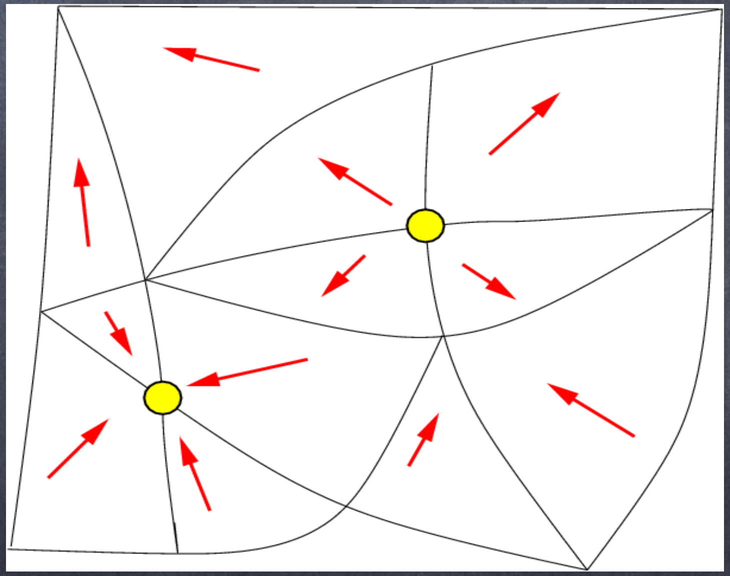

[Uhlmann et al. `10]

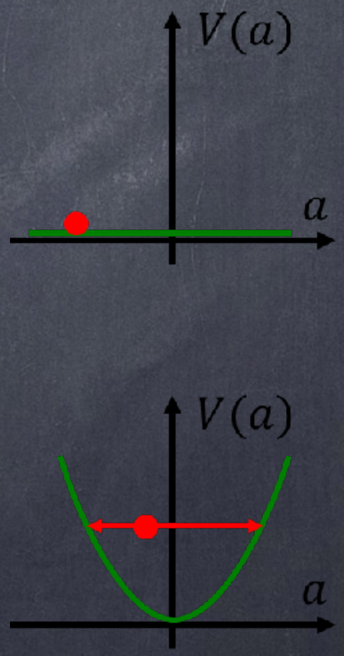

[Raffelt]

Once $H < m_a$ axion field starts to oscillate in its potential and behaves as pressure-less non-relativistic cold dark matter when averaged over oscillations:

$$\rho = \frac{\dot{\phi}^2}{2} + V_a(a)\,, \quad p = \frac{\dot{\phi}^2}{2} - V_a(a)$$

resulting relic density has contributions from inflationary quantum fluctuations, possible cosmic string decays and the misalignment mechanism. The latter contributes

$$\Omega_a h^2 \simeq 7.4 \times 10^{-4} \left(\frac{m_a}{\mu\mathrm{eV}}\right)^{1/2} \left(\frac{f_a}{10^{12}\,\mathrm{GeV}}\right)^2 \theta_{a,0}^2\,.$$

Details depend on the temperature dependence of the axion mass

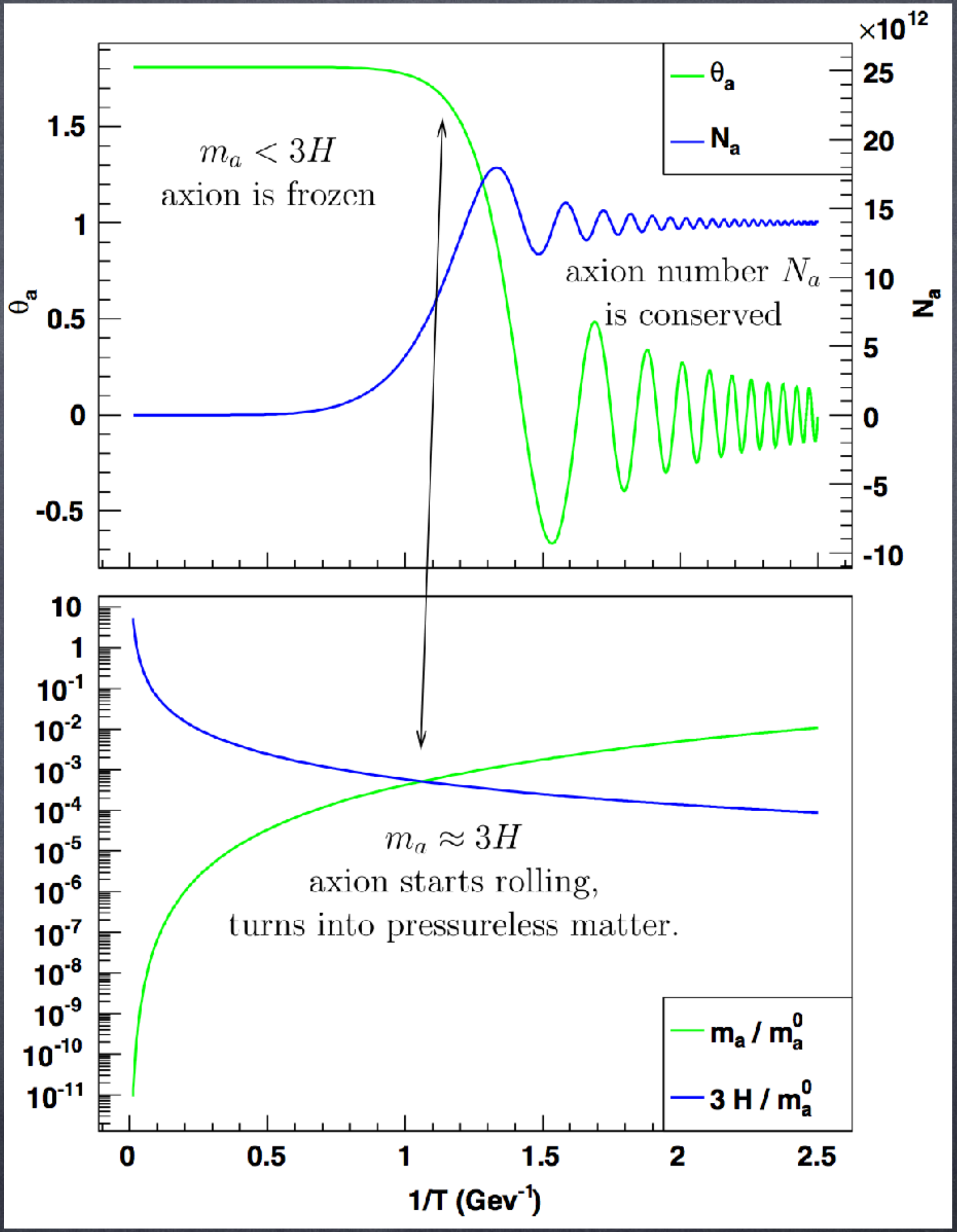

[Wantz,Shellard `09]

ALP-photon Coupling

fundamental coupling:

$$\frac{\alpha_{\rm em}}{8\pi}\frac{C_{a\gamma}}{f_a}\,a\,F_{\mu\nu}\tilde{F}^{\mu\nu} = \frac{e^2}{32\pi^2}\frac{C_{a\gamma}}{f_a}\,a\,F_{\mu\nu}\tilde{F}^{\mu\nu} = \frac{\alpha_{\rm em}}{8\pi}\frac{C_{a\gamma}}{f_a}\,a\,F_{\mu\nu}\tilde{F}^{\mu\nu} = \frac{g_{a\gamma}}{4}\,a\,F_{\mu\nu}\tilde{F}^{\mu\nu}\,, \tag{4}$$

where $\alpha_{\rm em} = e^2/(4\pi\epsilon_0)$ and

$$g_{a\gamma} \equiv \frac{\alpha_{\rm em}C_{a\gamma}}{2\pi f_a}\,. \tag{5}$$

can give rise to following effects:

- Primakoff conversions between ALPs and photons in background electromagnetic fields -> shining light through a wall, helioscopes, haloscopes
- modified photon refraction in ALP background -> Mathieu-type equations
- parametric amplification of photon amplitudes in ALP background -> Mathieu-type equations

Current Constraints and Future Sensitivities

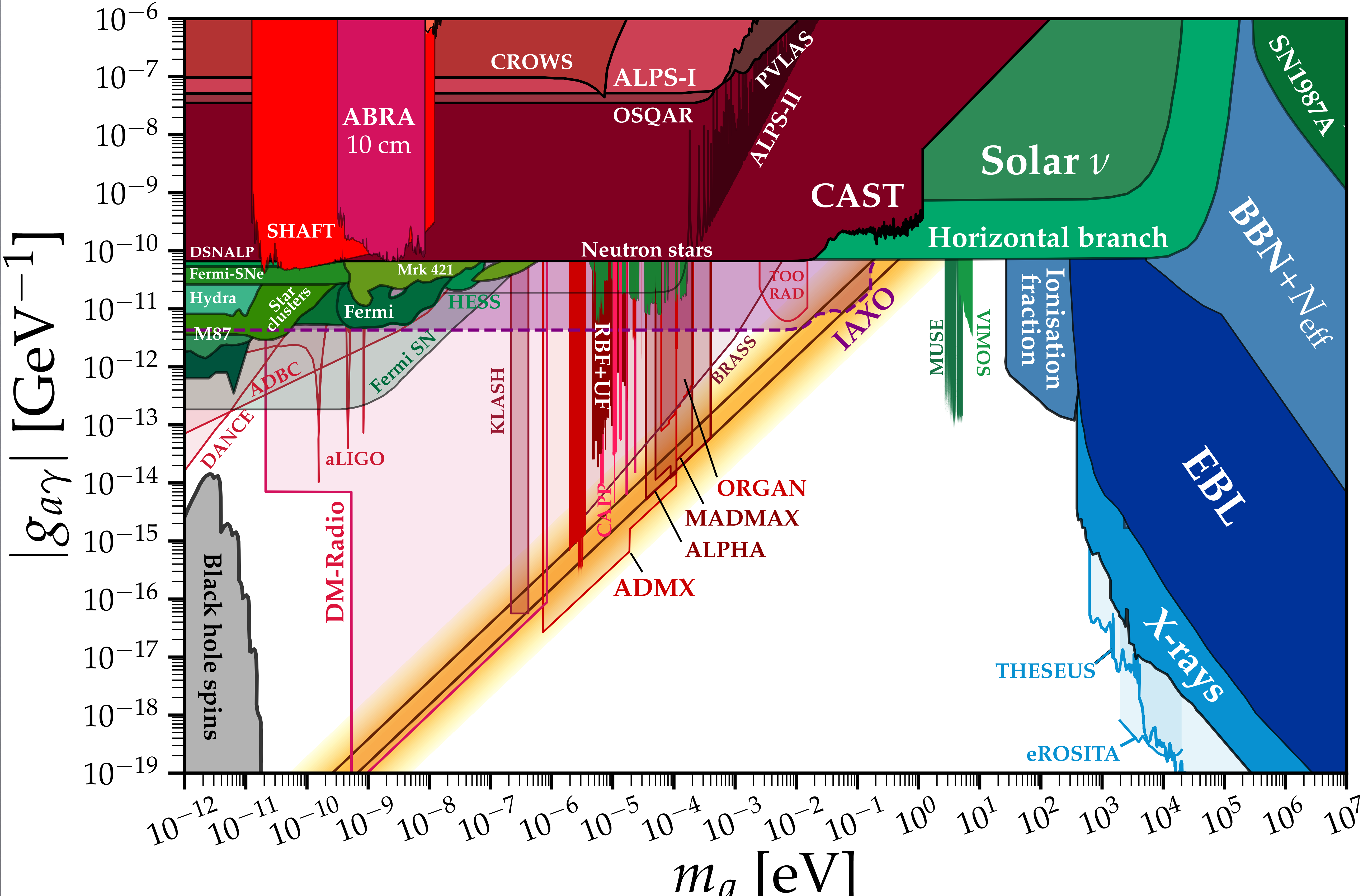

from git-hub repository https://cajohare.github.io/AxionLimits/ accessed on 25.8.2021

ALP-photon Conversion in Structured Magnetic Fields

The following is based on GS, Phys.Rev. D96 (2017) 103014 [arXiv:1708.08908]

Energy-momentum conservation: quantities for ALP, photon and magnetic field carry subscript a, γ, or none, respectively:

$$E_a = (m_a^2 + \mathbf{k}_a^2)^{1/2} = \omega_\gamma - \omega = (\omega_{\rm pl}^2 + \mathbf{k}_\gamma^2)^{1/2} - \omega\,, \quad \mathbf{k}_a = \mathbf{k}_\gamma - \mathbf{k}\,,$$

where the plasma frequency is given by:

$$\omega_{\rm pl} = \left(\frac{e^2 n_e}{\epsilon_0 m_e}\right)^{1/2} \simeq 5.6 \times 10^4 \left(\frac{n_e}{\rm cm^{-3}}\right)^{1/2} \,{\rm rad\,s^{-1}}\,.$$

propagation of converted photons requires $m_a \gg \omega_{pl}$. This will be the case for the objects considered here.
Also assume n_e ~ constant here (non-resonant conversion)

recently K. Kelley and P. J. Quinn, Astrophys. J. 845, 1 (2017) [arXiv:1708.01399] pointed out the possibility to search for ALP dark matter with radio telescopes; they used standard magnetic field estimates but assumed most of the power is on meter scales which is unlikely.

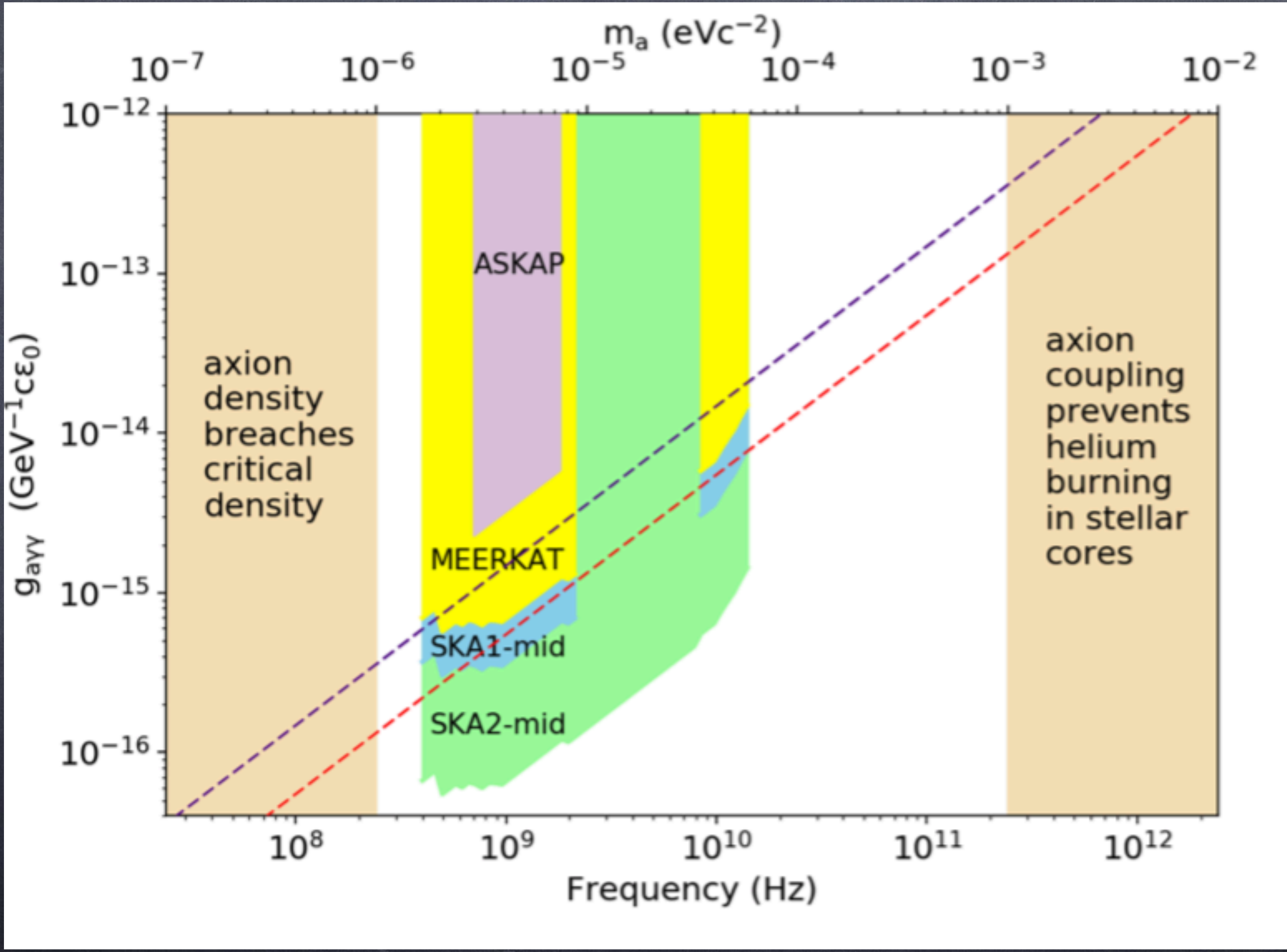

ALP-photon conversion rate can be written in terms of the magnetic field (static) power spectrum defined as

$$\rho_m = \frac{1}{2\mu_0 V}\int d^3\mathbf{r}|\mathbf{B}(\mathbf{r})|^2 = \frac{1}{2\mu_0 V}\int d^3\mathbf{k}|\mathbf{B}(\mathbf{k})|^2 = \int d\ln k\,\rho_m(k)\,,$$

Using $|\mathbf{k}_\gamma - \mathbf{k}_a| \sim k_\gamma \sim m_a$ and assuming a **homogeneous ALP distribution** with total mass $M_a = n_a m_a V$ this gives

$$R_{a\to\gamma} \simeq \pi g_{a\gamma}^2 \frac{M_a}{m_a^2}\rho_m(m_a)\,,$$

Integration over the line of sight dl this results in a **specific intensity per solid angle** [Jansky per steradian where 1 Jy = 10^{-26} W/(cm^2 Hz) = 10^{-23} erg/(cm^2 s Hz)]

$$I \simeq \pi \frac{g_{a\gamma}^2}{m_a^2}\frac{1}{\Delta}\int_{\mathrm{l.o.s.}} dl\,\rho_a(l)\rho_m(m_a, l)\,,$$

For example, for a supernova remnant at distance d for which $\rho_m(m_a)=f(m_a)\rho_m$ SKA would be sensitive to couplings

$$g_{a\gamma} \gtrsim 2\times 10^{-13}\,[m_a/\mu\mathrm{eV}][\Delta/10^{-3}]^{1/2}[d/(2\,\mathrm{kpc})]^{1/2}\,\mathrm{GeV}^{-1}/f(m_a)$$

Unfortunately f(k) is poorly known and might be <<1 [GS, PRD Phys.Rev. D96 (2017) 103014 [arXiv:1708.08908]]

Resonant Primakoff Conversion around Compact Objects

Full conversion (e.g. resonance between ALP mass and plasma frequency at distance r_s from neutron star center) gives

$$S_{\rm max} \simeq \frac{\rho_a}{m_a}\frac{v_a}{\Delta}\left(\frac{r_s}{d}\right)^2 \simeq 10^{-10}\left(\frac{m_a}{\mu{\rm eV}}\right)^{-1}\left(\frac{r_s}{10^6\,{\rm cm}}\right)^2\left(\frac{d}{\rm kpc}\right)^{-2}\,{\rm Jy}\,,$$

see also M.S.Pshirkov, J.Exp.Theor.Phys. 108 (2009) 384 [arXiv:0711.1264] who obtained higher fluxes, see also A. Hook et al., arXiv:1804.03145, F.P. Huang et al., arXiv:1803.08230

This would be detectable out to ~ pc distances, see also D. Marsh (Cambridge)

A. Hook et al., Phys.Rev.Lett 121 (2018) 241102 [arXiv:1804.03145] made a more detailed calculation of resonant conversion (when plasma frequency matches ALP mass) around neutron stars which results in

$$\frac{d\mathcal{P}(\theta=\frac{\pi}{2},\theta_m=0)}{d\Omega} \approx 4.5\times 10^8\ \mathrm{W}\left(\frac{g_{a\gamma\gamma}}{10^{-12}\ \mathrm{GeV}^{-1}}\right)^2 \left(\frac{r_0}{10\ \mathrm{km}}\right)^2 \left(\frac{m_a}{1\ \mathrm{GHz}}\right)^{5/3} \left(\frac{B_0}{10^{14}\ \mathrm{G}}\right)^{2/3} \left(\frac{P}{1\ \mathrm{sec}}\right)^{4/3} \left(\frac{\rho_\infty}{0.3\ \mathrm{GeV/cm^3}}\right) \left(\frac{M_{\mathrm{NS}}}{1\ M_\odot}\right) \left(\frac{200\ \mathrm{km/s}}{v_0}\right),$$

$$S = 6.7\times 10^{-5}\ \mathrm{Jy}\left(\frac{100\ \mathrm{pc}}{d}\right)^2 \left(\frac{1\ \mathrm{GHz}}{m_a}\right)\times \left(\frac{200\ \mathrm{km/s}}{v_0}\right)^2 \left[\frac{d\mathcal{P}/d\Omega}{4.5\times 10^8\ \mathrm{W}}\right].$$

Advantage: Depends on plasma and magnetic field structure only through adiabaticity of conversion (plasma scale height, mixing through magnetic field at resonance)

Line width from one source is order v_a^2 (ALP energy spread, energy conservation, all coming from one direction), whereas order v_a from ensemble of sources (Doppler effect)

A. Hook et al., Phys.Rev.Lett 121 (2018) 241102 [arXiv:1804.03145]

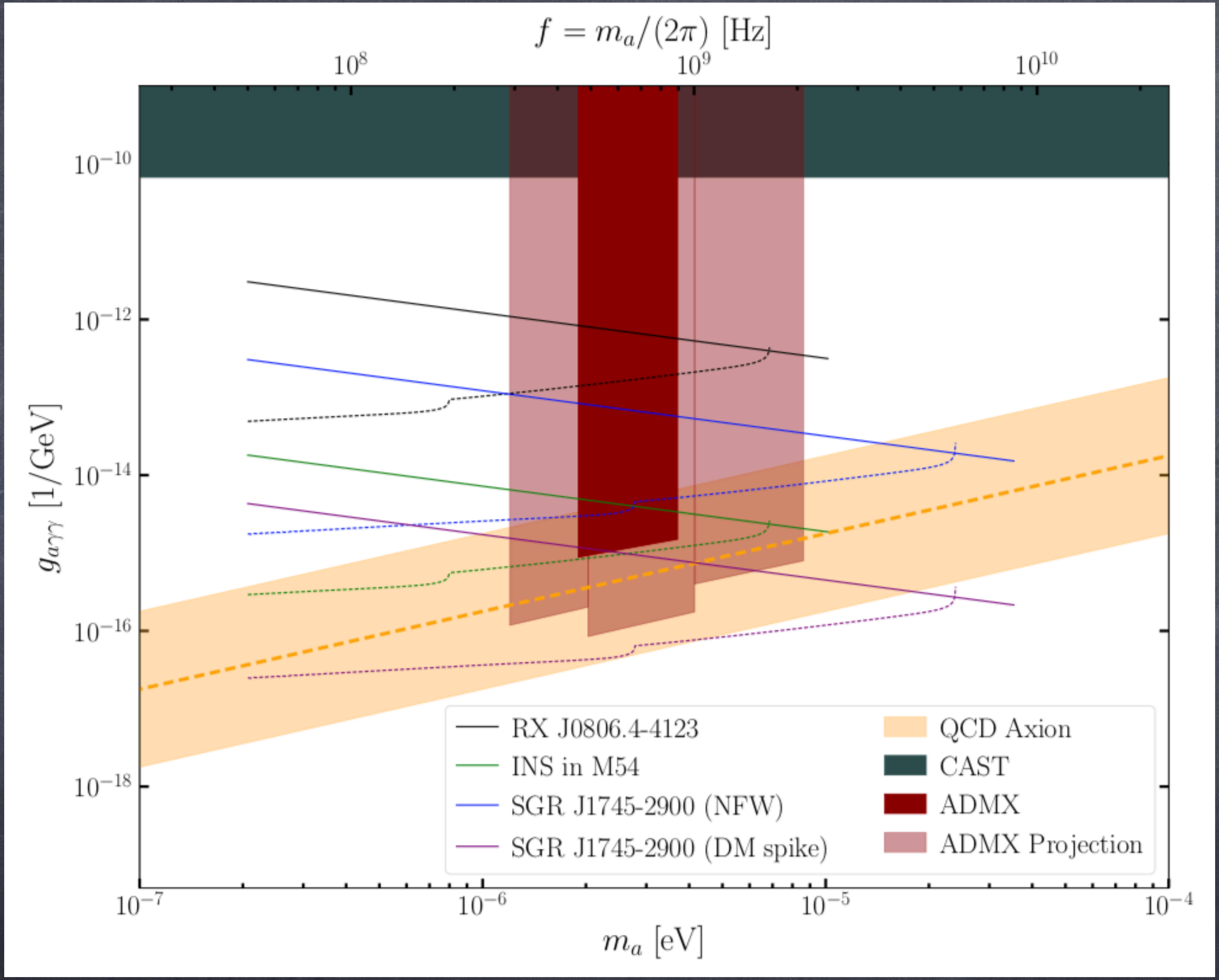

takes into account ALP density enhancement around galactic center (but spike may not be realistic)

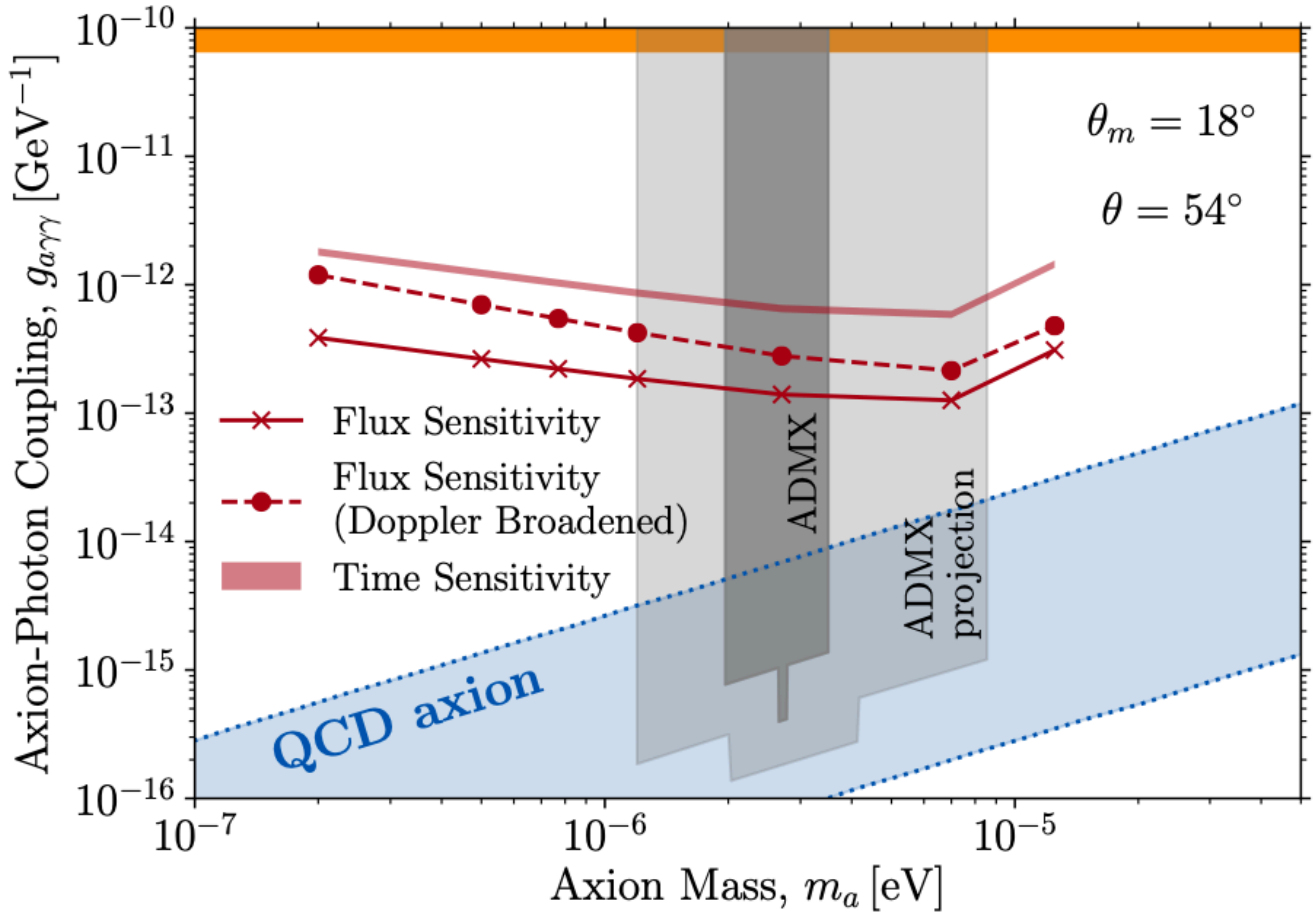

M. Leroy et al., arXiv:1912.08815

FIG. 6. **Projected sensitivity to the axion-photon coupling from radio observations.** We consider the isolated NS J0806.4-412 and assume $\tau_{\rm obs} = 100$ hrs. The two red lines correspond to the sensitivity limit for two line broadening scenarios as described in the text. The red solid line only accounts for the DM velocity distribution far from the NS where as the red dashed line also accounts for Doppler broadening from the rotation of the NS magnetosphere. The red band shows the minimum coupling required to detect the time variation of the signal (here we neglect Doppler broadening).

resonant axion-photon conversion from ray tracing simulations: line width depends on (complicated) source details

Many more recent works:
R.A. Battye et al, arXiv:2104.08290, arXiv:2107.01225

S.J. Witte et al., arXiv:2104.07670

A.J. Millar et al, arXiv:2107.07399

Recent proposal to consider cumulative fluxes

e.g. from all neutron stars and magnetic white dwarfs in globular clusters such as Omega Centauri, Wang, Bi, Yin, arXiv:2109.00877

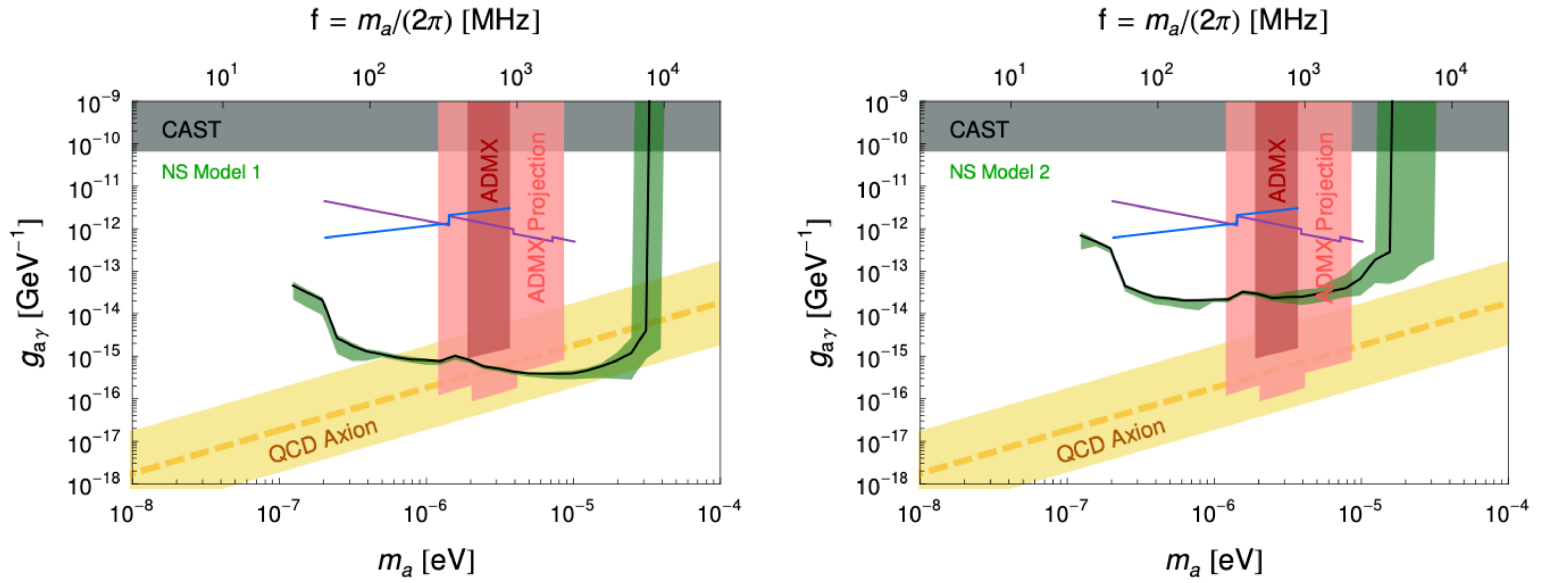

FIG. 6. *The combined projected sensitivity (pure NSs case) to $g_{a\gamma}$ as a function of the axion mass m_a for SKA1 and LOFAR with 100 hours observations of the ω Cen is shown in the green band. The green band contains ten separate sets of NS samples, and its upper and lower boundaries represent the maximum and minimum values, and the black solid line represent the median value. The left panel assumes NS model 1, wile the right panel takes NS model 2. For comparison, the results of the isolated NS RX J0806.4-4123 and MWD WD 2010+310 are shown with purple and blue solid lines. The QCD axion is predicted to lie within the yellow band. The limits set by CAST and ADMX (current and projected) are indicated by the gray and red regions, respectively.*

Spontaneous and Stimulated Decays

compare Primakoff conversion rate

$$\frac{1}{\tau_a} \simeq \frac{\pi g_{a\gamma}^2}{m_a} \rho_m(m_a) \simeq 9.7 \times 10^{-38} \left(g_{a\gamma} 10^{14}\,\mathrm{GeV}\right)^2 \left(\frac{m_a}{\mathrm{meV}}\right)^{-1} \left(\frac{B}{\mathrm{mG}}\right)^2 f(m_a)\,\mathrm{s}^{-1}\,,$$

with spontaneous decay rate

$$\frac{1}{\tau_a} = \frac{g_{a\gamma}^2 m_a^3}{64\pi} \simeq 1.5 \times 10^{-38} \left(g_{a\gamma}\, 10^{14}\,\mathrm{GeV}\right)^2 \left(\frac{m_a}{\mathrm{meV}}\right)^3 \mathrm{s}^{-1}\,.$$

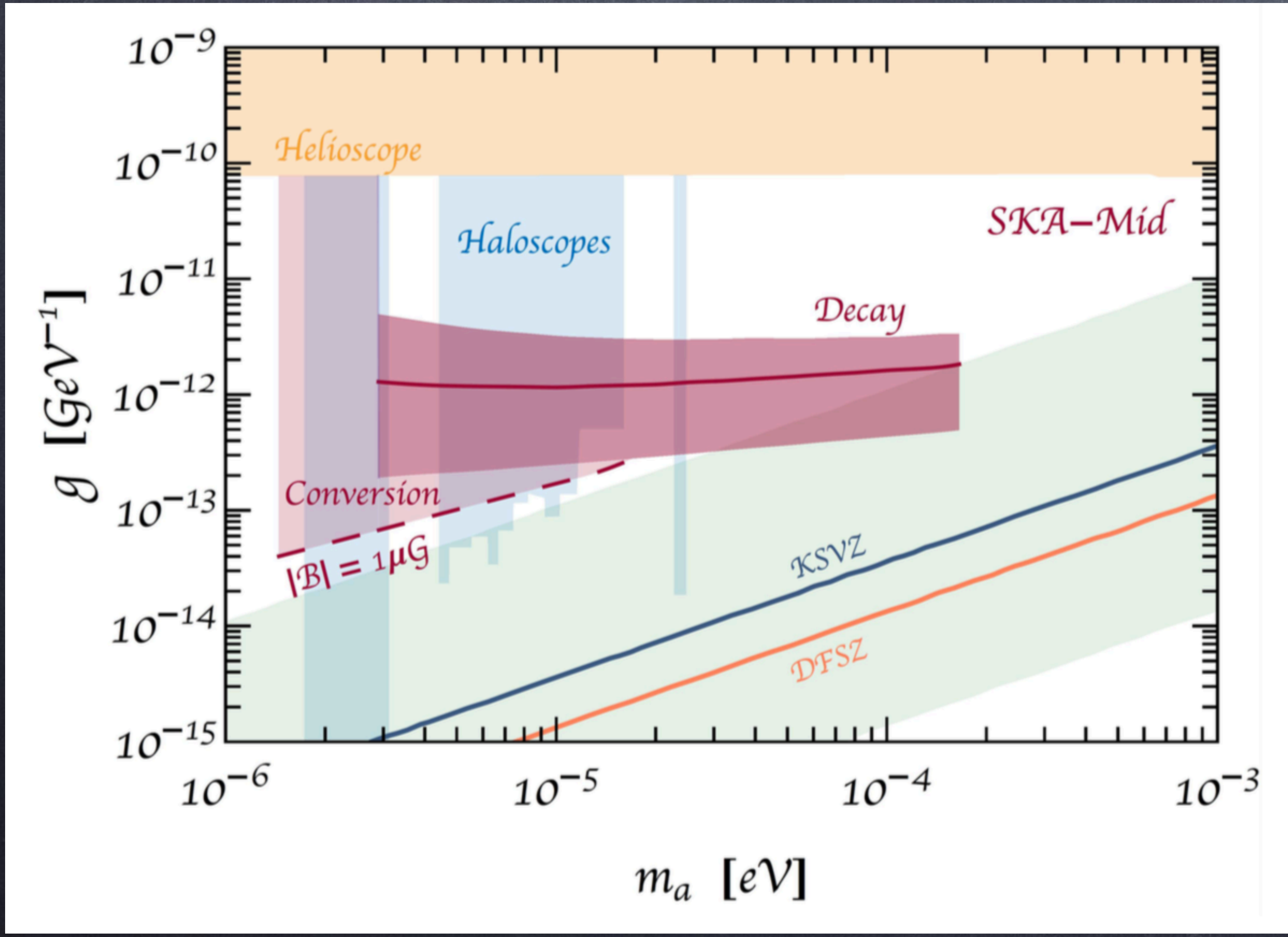

A. Caputo et al., PRD 98, 083024(2018) [arXiv:1805.08780], see also I.Tkachev, PLB 191 (1987) 41;
T.W. Kephart and T.J. Weiler, PRD 52, 3226 (1995)

Spontaneous decay can get enhanced by factor $1 + 2f_\gamma(m_a)$ in stimulated decay where $f_\gamma(m_a)$ is the photon occupation number at the ALP mass (related to parametric resonance, see below)

A. Caputo et al., JCAP 1903 (2019) 027 [arXiv:1811.08436]

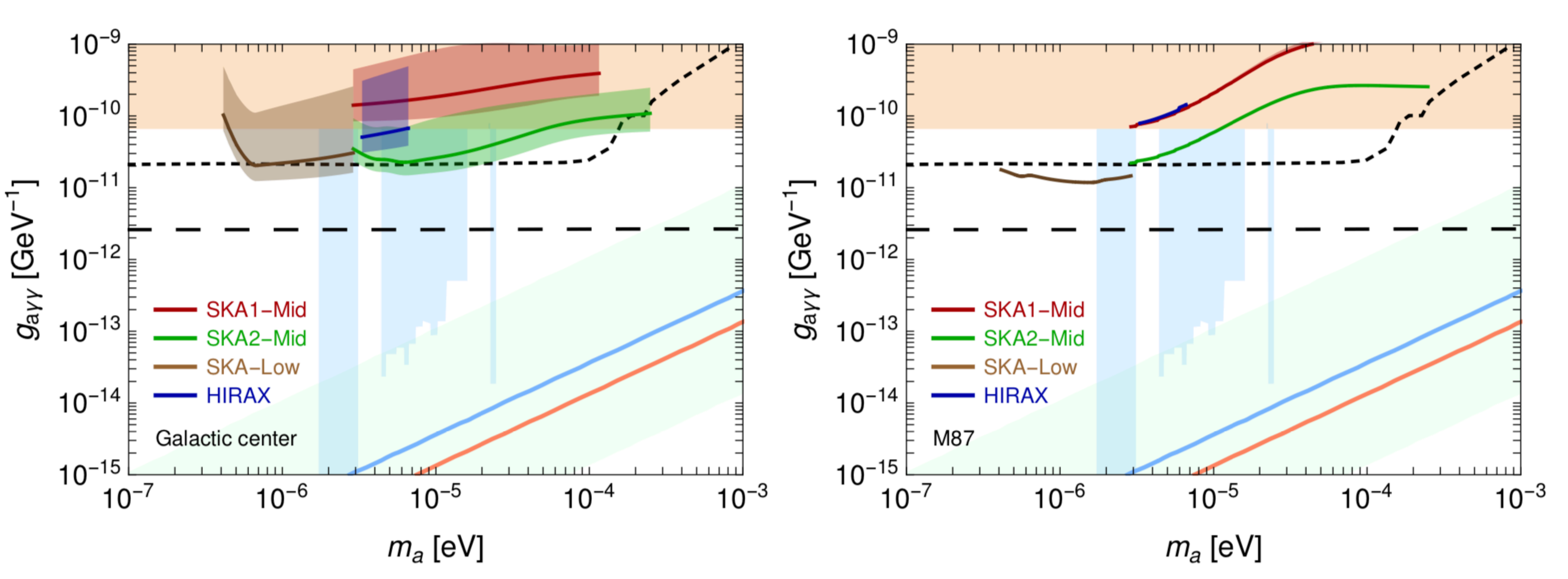

projected sensitivities from Galactic center observations

Modified Electrodynamics

Modified Maxwell equations in presence of photon-ALP coupling

$$\nabla \cdot \mathbf{E} = \frac{\rho_{\rm em}}{\epsilon_0} + \frac{\mathbf{B}\cdot\nabla a}{\epsilon_0 M_a}\,, \qquad \nabla\times\mathbf{B} = \frac{\partial \mathbf{E}}{\partial t} + \mu_0\,\mathbf{j}_{\rm em} + \frac{\mathbf{E}\times\nabla a - \mathbf{B}\partial_t a}{\epsilon_0 M_a}$$

Often one uses the coupling $g_{a\gamma} = 1/M_a$. In Lorentz gauge for a wave propagating in the z-direction with circular polarisation this yields

$$\left(\partial_t^2 - \partial_z^2\right) A_\pm = \pm\, i g_{a\gamma} \left[(\partial_z a)(\partial_t A_\pm) - (\partial_t a)(\partial_z A_\pm)\right]$$

In the absence of resonances this can be solved with the ansatz

$$A_\pm(t,z) = F_\pm(t,z)\exp\left[-i\omega t + ikz + iG_\pm(t,z)\right]$$

To first order in m_a/ω and $g_{a\gamma}$ this is solved by

$$\omega = k\,, \quad F = \text{const}\,, \quad G_\pm(t,z) = \mp\frac{g_{a\gamma}}{2}a(t,z) + f(z-t)$$

for an arbitrary function f(x).

M.A. Fedderke, P.W. Graham, S. Rajendran, Phys.Rev. D100 (2019) 015040 [arXiv:1903.02666]

ALP-Photon Conversion through Parametric Resonance

Tkachev Sov.Astron.Lett. 12 (1986) 305, Pisma Astron.Zh. 12 (1986) 726,
see also M.P. Hertzberg and E.D. Schiappacasse, JCAP 1811 (2018) 004 [arXiv:1805.00430]

From the modified Maxwell equations for a homogeneous ALP field $a(t)=a_0 \sin m_a t$ for a photon momentum mode k one obtains a Mathieu-type equation of the form

$$\left[\frac{d^2}{dx^2} + A - 2q\cos(2x)\right] A_\pm = 0$$

for the two circularly polarised photon fields $A_\pm$ with $x=m_a t/2$ and

$$A = \frac{4k^2}{m_a^2}, \quad q = \pm \frac{2k}{\epsilon_0 M_a}\frac{a_0}{m_a}$$

For $q<1$ (narrow resonance) there are resonances at $A = 1 \pm q$ growing with a rate in x of ~ q/2. The resulting band width is $k = m_a(1 \pm q)/2$

This corresponds to the crossed spontaneous decay into $k=m_a/2$ photons.

For $q>1$ other resonances are at $A\sim 2q$ growing with a rate in x of ~1 (probably not relevant here)

Case 1: Diffuse galactic dark matter

$$\rho_a \simeq \frac{1}{2} m_a^2 a_0^2 \longrightarrow a_0 \simeq 2.2 \left(\frac{\mu\mathrm{eV}}{m_a}\right) \mathrm{keV}$$

which implies a narrow resonance with

$$q \sim 2.3 \times 10^{-19} \left(g_a \cdot 10^{14}\,\mathrm{GeV}\right) \left(\frac{\mu\mathrm{eV}}{m_a}\right)$$

could give a few e-folds in Galaxy, but extremely narrow line

Case 2: ALP stars

estimates based on Visinelli et al., Phys Lett. B 777 64 (2018) [arXiv:1710.08910]

$a_0 \sim f_a^2/M_{pl}$ -> narrow resonance parameter

$$q \simeq C_{a\gamma} \frac{\alpha_{\mathrm{em}}}{2\pi} \frac{f_a}{M_{\mathrm{Pl}}} \sim 10^{-9} \left(\frac{f_a}{10^{12}\,\mathrm{GeV}}\right)$$

The radius of an axion star is $R \sim 1/(q m_a)$ and the kinetic energy of axions in an axion star is $\sim q m_a$. Therefore, impinging radio photon beams could be enhanced by $m_a\, q/(m_a q)$ thus potentially by several e-folds. But detailed numbers suggest no significant constraints. See also A. Arza, Eur.Phys.J. C79 (2019) 250 [arXiv:1810.03722] Details depend on ALP star structure.

Also axion stars probably cover too small a fraction of the sky to give observable effects. On the other hand, if a large fraction of the axion star could be converted to radio photons [Hertzberg and Schiappacasse, JCAP 1811 (2018) 004 [arXiv:1805.00430], Tkachev, PLB 191, 41]. Note that spontaneous ALP decay probably not crucial to seed this because radio photons are always around.

Interesting conceptual questions when back reaction becomes important

$$\Box a + \frac{\partial V_a}{\partial a}(a) = \frac{\mathbf{E}\cdot\mathbf{B}}{M_a}\,.$$

For example, parametric enhancement is consistent with momentum conservation, no recoil when photon beam is enhanced;
See axion dark matter echo effect, A. Arza, P.Sikivie, Phys.Rev.Lett. 123 (2019) 131804 [arXiv:1902.00114]
parametric enhancement is same process as stimulated ALP decay that leads to exponential growth, see Carenza, Mirizzi, GS, PRD 101 (2020) 103016 [arXiv:1911.07838]

Carenza, Mirizzi, GS, PRD 101 (2020) 103016 [arXiv:1911.07838] performed a more detailed calculation of axion condensate decay into photons:

Number of produced photons in mode **k**:

$$N_{\mathbf{k}}(t) = N_{\mathbf{k}}(0)e^{2\mu t} + 2(\cosh(2\mu t) - 1)$$

Number of converted axions depends on number of photon modes:

$$\Delta N_a \sim N_d N_t [N_{m_a/2}(T) - N_{m_a/2}(0)]$$

where in a clump of size L, $N_d \simeq (Lm_a)^2/(4\pi)$ and $N_t \simeq \mu L/\pi$, see also R.F. Sawyer, arXiv:809.01183 and arXiv:1908.04298. To avoid overproduction of radio background one requires

$$\frac{\Delta N_a}{N_a} f_{\rm dm} \lesssim \frac{\Omega_\gamma(m_a/2)}{\Omega_{\rm dm}} \frac{\Delta\nu}{\nu}$$

which requires

$$\mu L \lesssim \frac{1}{2} \ln\left[\frac{\Omega_\gamma(m_a/2)}{f_{\rm dm}\Omega_{\rm dm}} \frac{N_a}{N_d N_t (N_{m_a/2}(0) + 1)} \frac{\Delta\nu}{\nu}\right] \lesssim 30\,.$$

For example, for the axion clumps discussed in Schiappacasse and Hertzberg, Astropart. Phys. 01 (2018) 037; 03 (2018) E01 one has

$$\mu = \frac{1}{\sqrt{8}} g_{a\gamma} \rho_{\rm max}^{1/2} = 1.7 \times 10^{-9} \left(\frac{m_a}{10^{-5}\,{\rm eV}} \right) \left(\frac{g_{a\gamma}}{10^{-11}\,{\rm GeV}^{-1}} \right)^{-1} {\rm km}^{-1}$$

Photon Propagation on a structured ALP background field (modified wave equations)

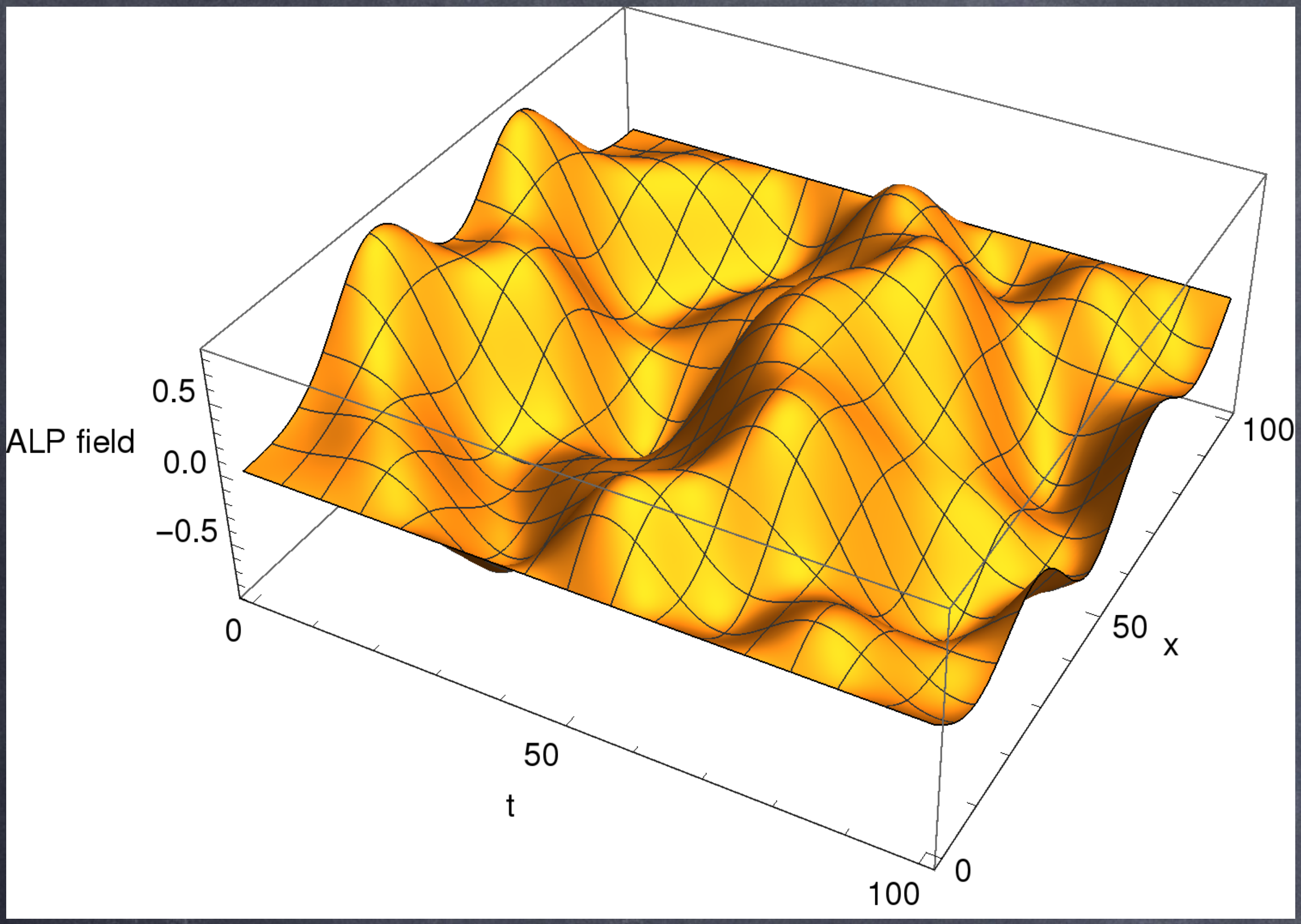

example for a localised ALP over density profile

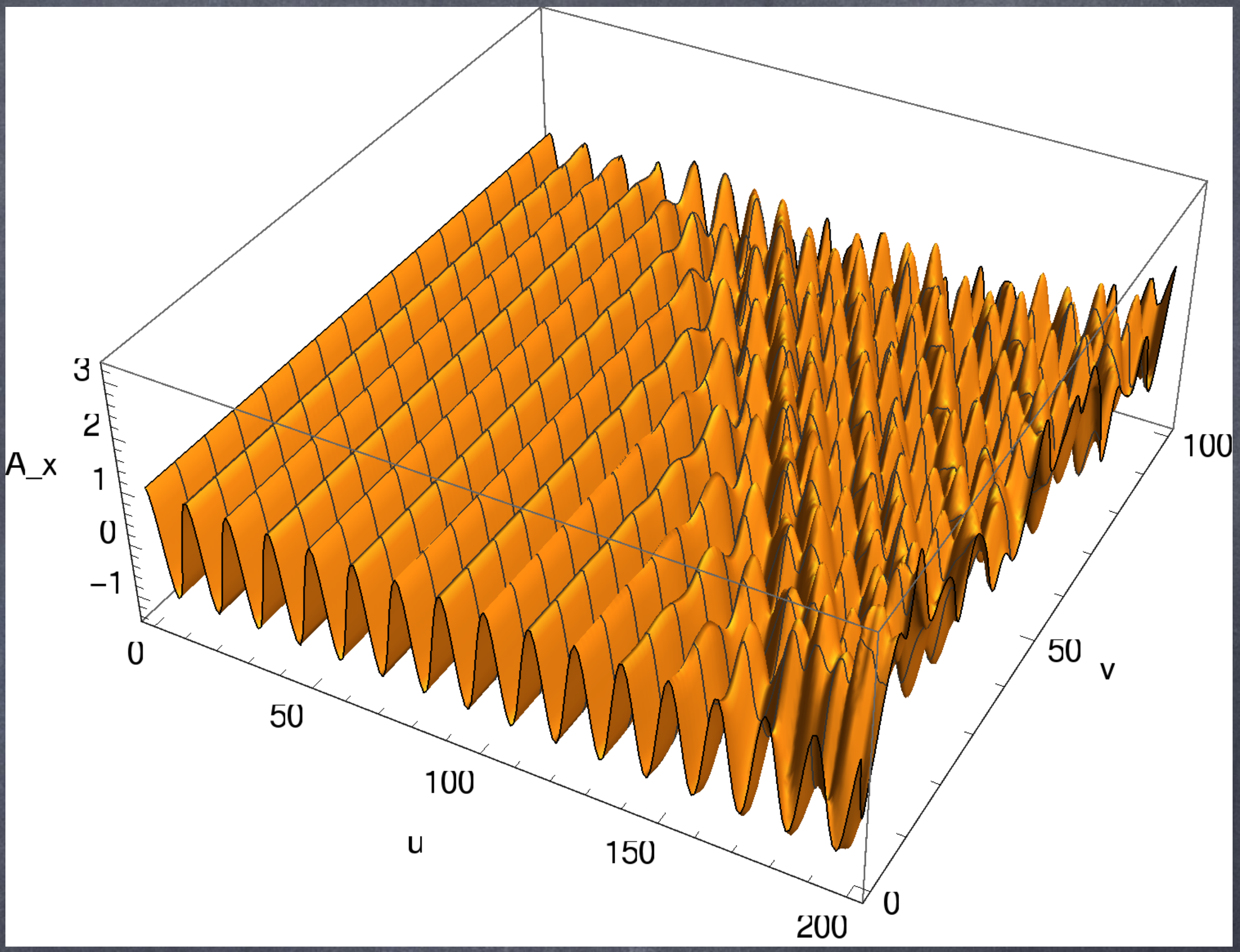

evolution of x-component of photon vector potential impinging on ALP distribution, $u=x-t$, $v=x+t$

preliminary simulations by G. Sigl

Numerical Simulations of modified wave equation in an inhomogeneous ALP background in $x \pm c_0 t$ coordinates: Example for $m_a = 1., k = 0.5, g_{a\gamma} = 1.$ (resonance)

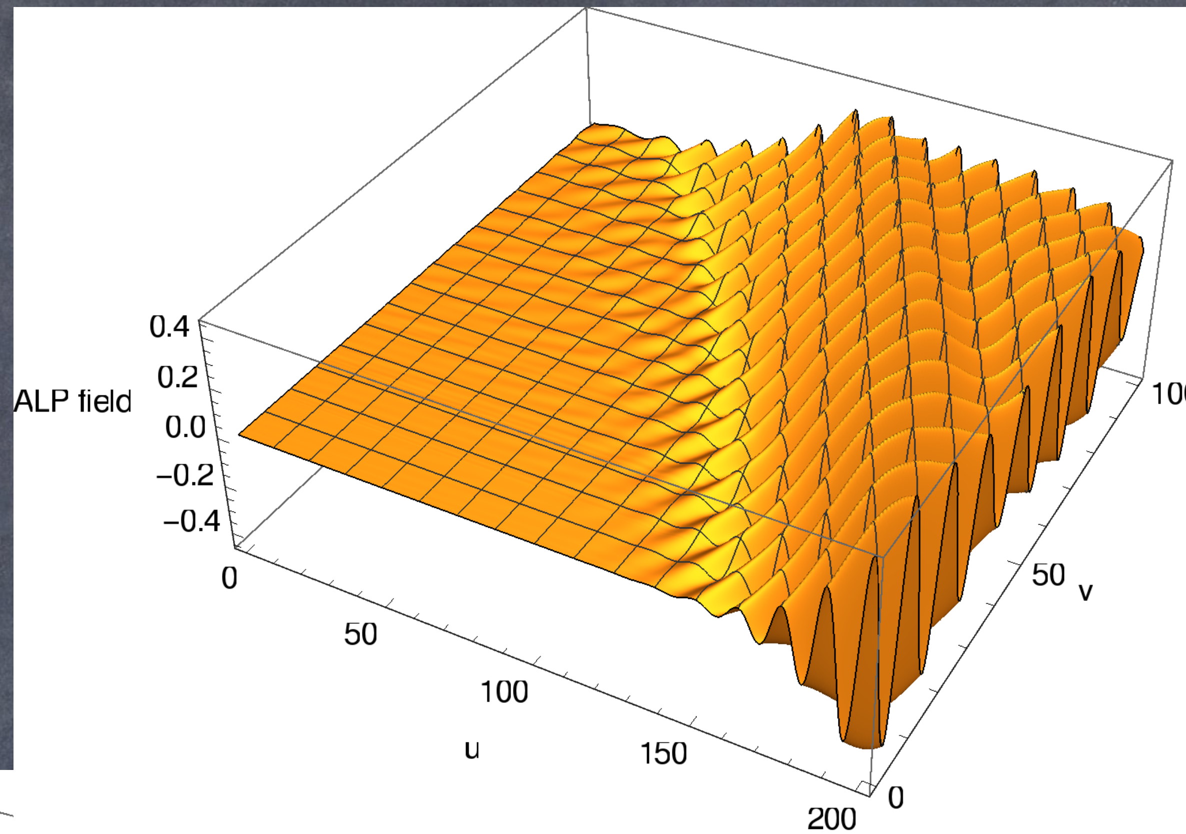

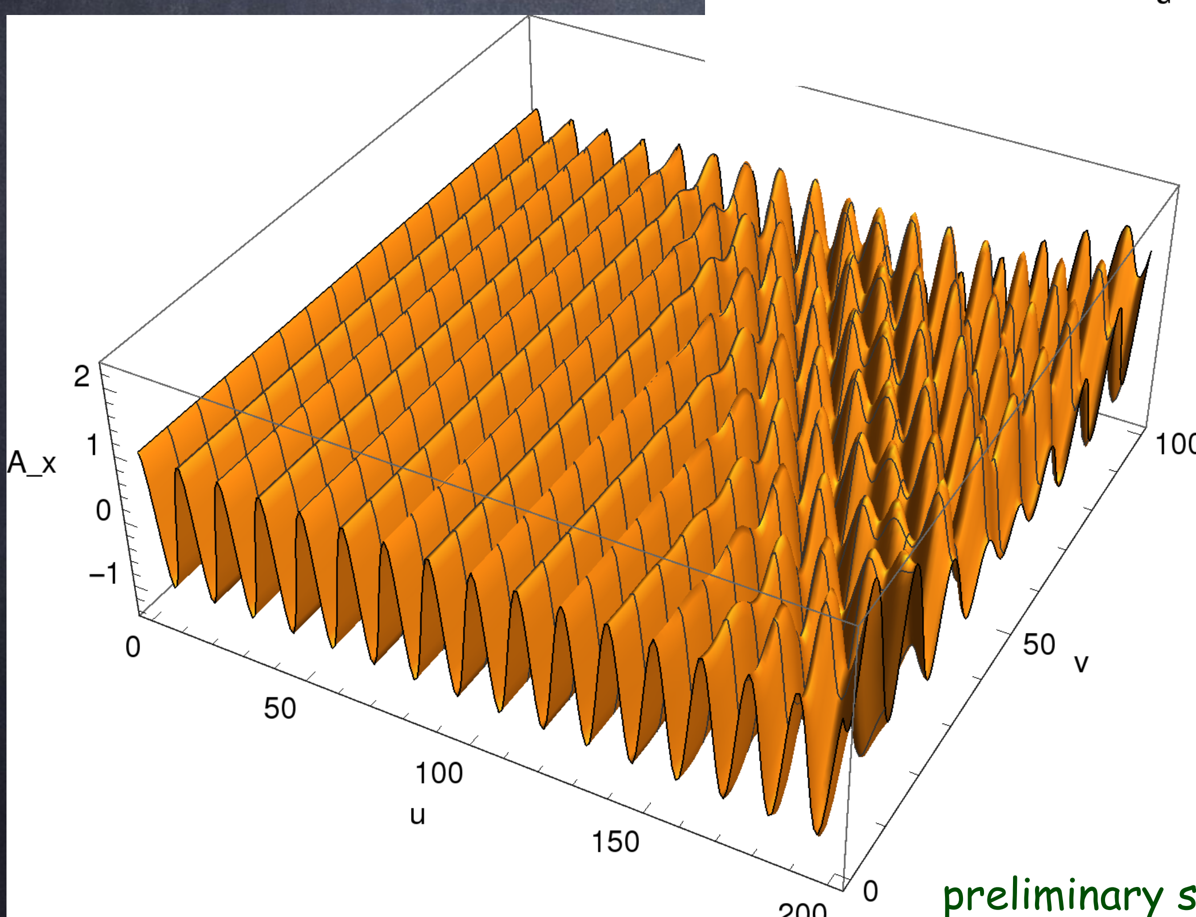

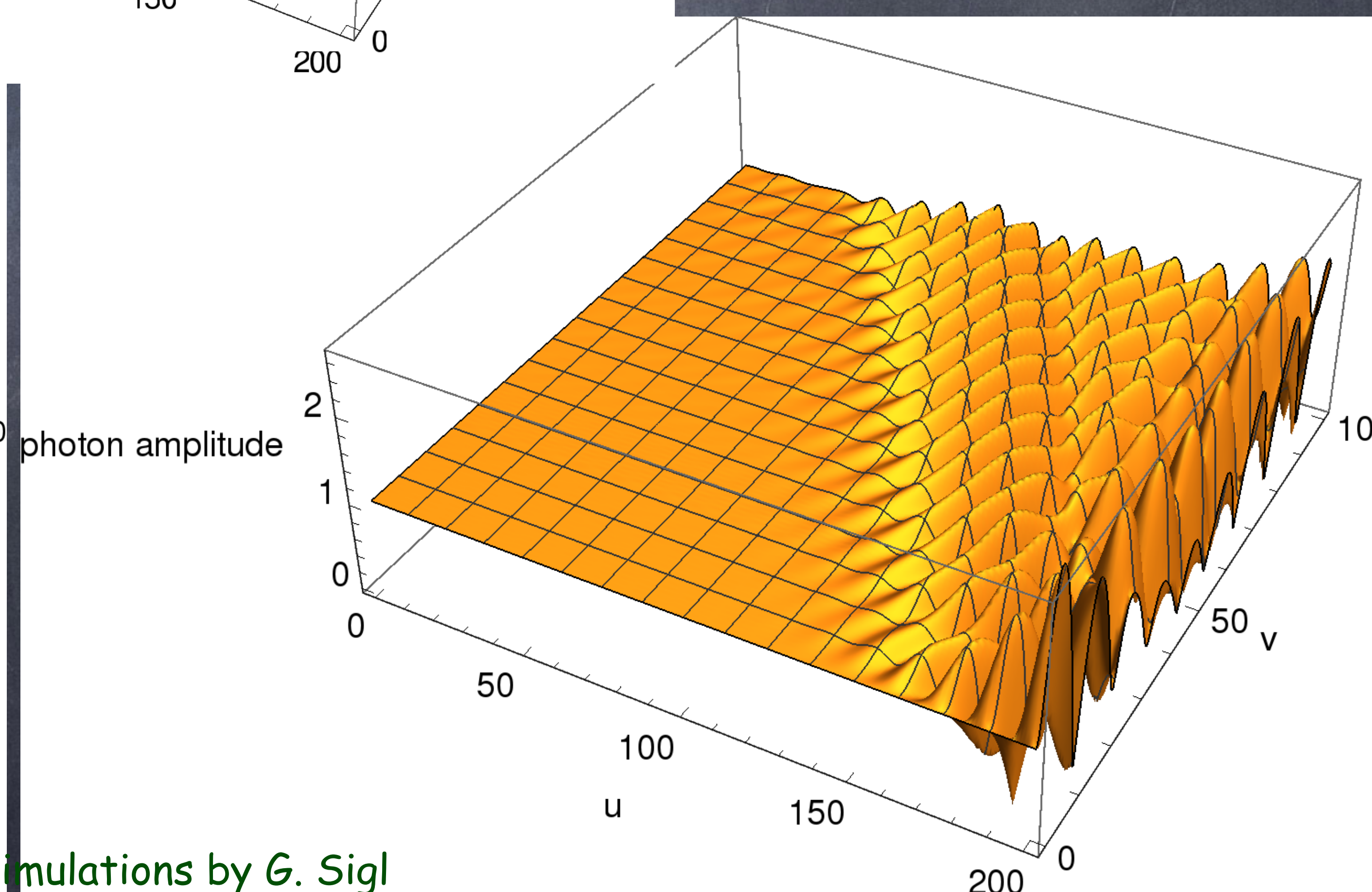

preliminary simulations by G. Sigl

Study of solutions of modified wave equation under study by several groups, see e.g. L. Chen and T.Kephart, arXiv:2002.07885 (Photon directional profile from stimulated decay of axion clouds with arbitrary momentum distributions) and Z. Wang et al., arXiv:2002.09144 (Resonant instability of axionic dark matter clumps)

Birefringence in an ALP Background

on small length scales the Mathieu equation leads to the dispersion relation

$$\omega = k \mp \frac{m_a g_{a\gamma}}{2\epsilon_0} a_0 \cos(m_a t + \delta)\,,$$

which leads to birefringence with a phase shift

$$\Delta\phi_1 \simeq \frac{g_{a\gamma}}{\epsilon_0} a_0 \simeq 10^{-20} \left(g_{a\gamma} 10^{14}\,\mathrm{GeV}\right) \left(\frac{\mu\mathrm{eV}}{m_a}\right)\,.$$

Note that this does not depend on photon wavenumber and thus any waveband can be applied. Adding in quadrature phase shifts from domains $l_c > 1/m_a$ in which the axion field is coherent (i.e. phase δ ~ constant) yields

$$g_{a\gamma} \lesssim 3 \times 10^{-13}\, \Delta\phi\, v_a^{-1/2} \left(\frac{m_a}{10^{-22}\,\mathrm{eV}}\right)^{1/2} \left(\frac{10\,\mathrm{kpc}}{d}\right)^{1/2} \mathrm{GeV}^{-1}\,,$$

where $\Delta\phi$ is an upper limit on the observed phase shift.

Same effect also used in experimental approaches, e.g. birefringent cavities, arXiv:1809.01656

Effect of inhomogeneous ALP backgrounds: stochastic versus coherent polarisation rotation

The above solution to first order in m_a/ω and $g_{a\gamma}$

$$A_\pm(t,z) = F_\pm \exp\left[-i\omega(t-z) + ig_{a\gamma}a(t,z)/2 + f(t-z)\right]$$

would imply for the rotation angle

$$\Delta\theta = \frac{g_{a\gamma}}{2}\int_{\mathscr{C}} ds n^\mu \partial_\mu a = \frac{g_{a\gamma}}{2}\left[a(t_f, z_f) - a(t_i, z_i)\right]$$

Thus, rotation angle would not depend on path, but only on values of ALP field at the endpoints.

M.A. Fedderke, P.W. Graham, S. Rajendran, Phys.Rev. D100 (2019) 015040 [arXiv:1903.02666]

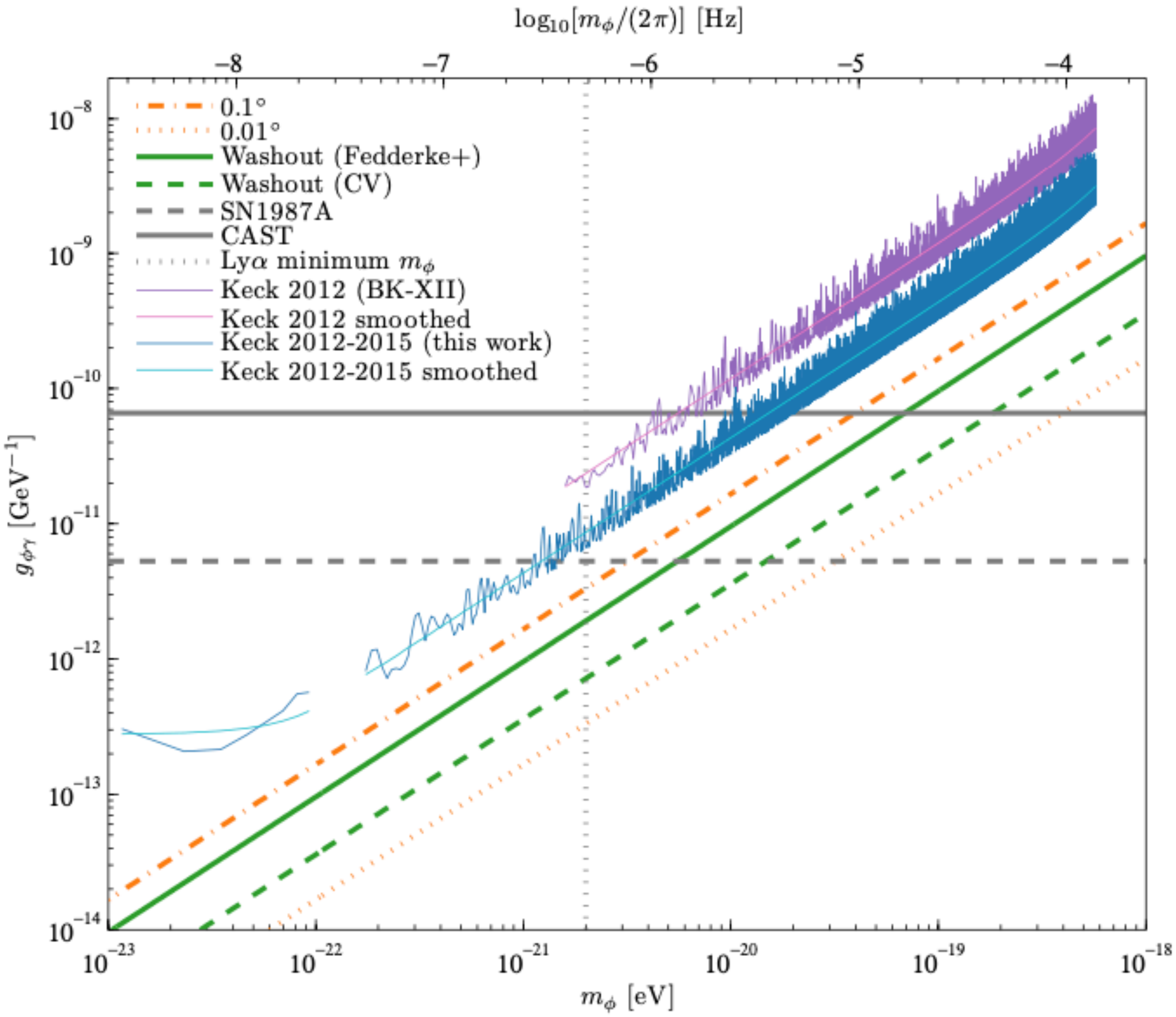

FIG. 3. Excluded regions in the mass-coupling parameter space for axion-like dark matter (cf. BK-XII Fig. 6 [1]). All constraints push the allowed regions to larger masses and smaller coupling constants, i.e., toward the bottom right of the figure. If the dark matter is assumed to consist entirely axionlike particles, i.e., if $\kappa = 1$, then our constraints (blue) are immediately implied by Eq. 4 of BK-XII and the results of Fig. 2. A smoothed approximation is shown in cyan (Eq. 15). The analogous limits and smoothed approximation from BK-XII are shown in purple and magenta. The orange dot-dashed and dotted lines show the constraints that would be achieved if the rotation amplitude were constrained to 0.1° and 0.01°, respectively. The green solid line shows the constraint set by Fedderke et al. [9] from the washout effect (BK-XII Sec. I) in *Planck* power spectra. The dashed green line shows the cosmic-variance limit for the washout effect. The dashed grey horizontal line shows the limit from the lack of a gamma-ray from SN1987A [17]. The solid grey horizontal line is the limit set by the CAST experiment [24]. The dotted grey vertical line is a constraint on the minimum axion mass from observations of small-scale structure in the Lyman-α forest [26], and we note that several similar bounds have also been set by other considerations of small-scale structure [27–30].

P.A.R. Ade et al,
BICEP/Keck collaboration
arXiv:2108.03316

Other studies used polarisation data from other objects

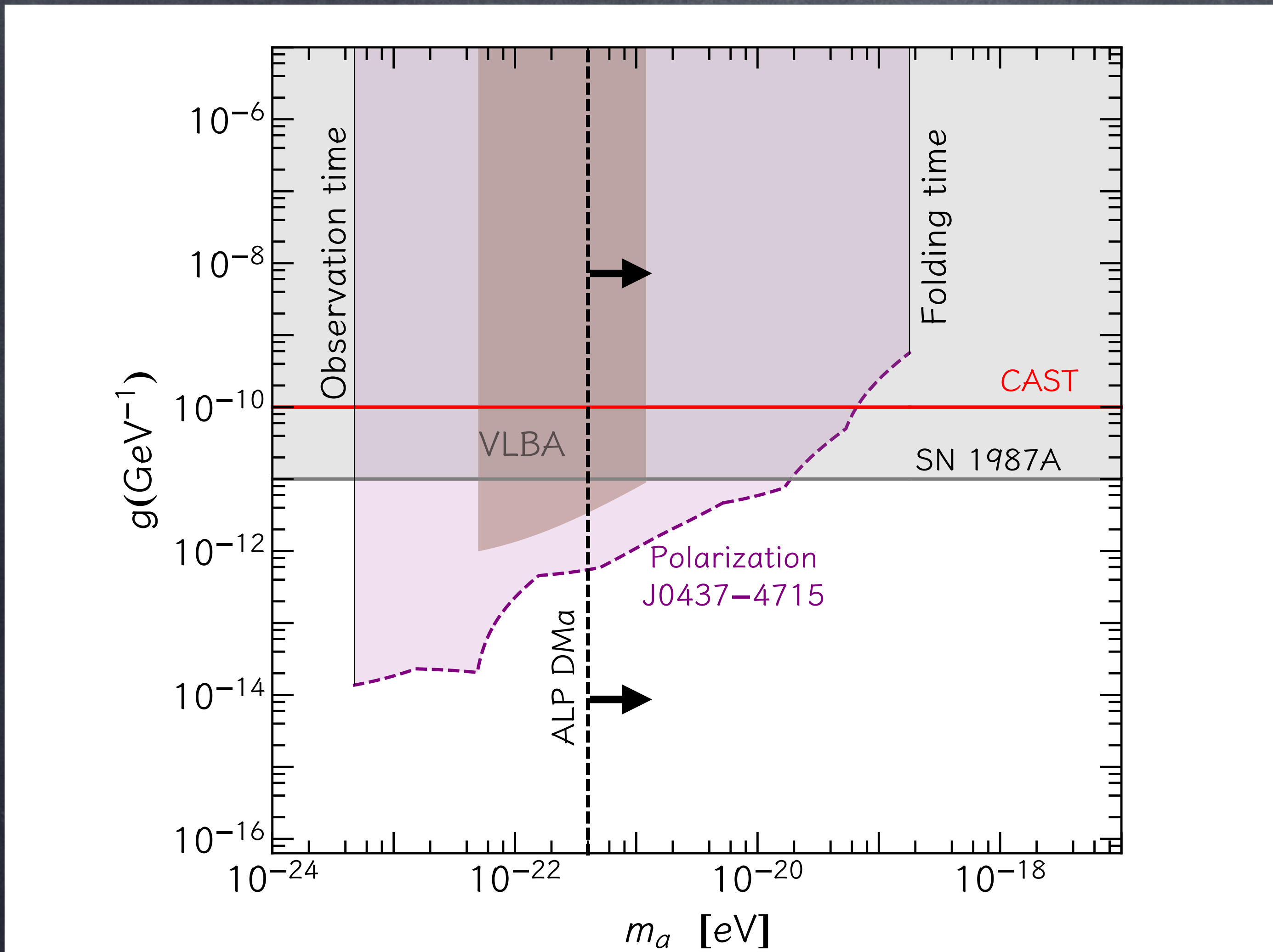

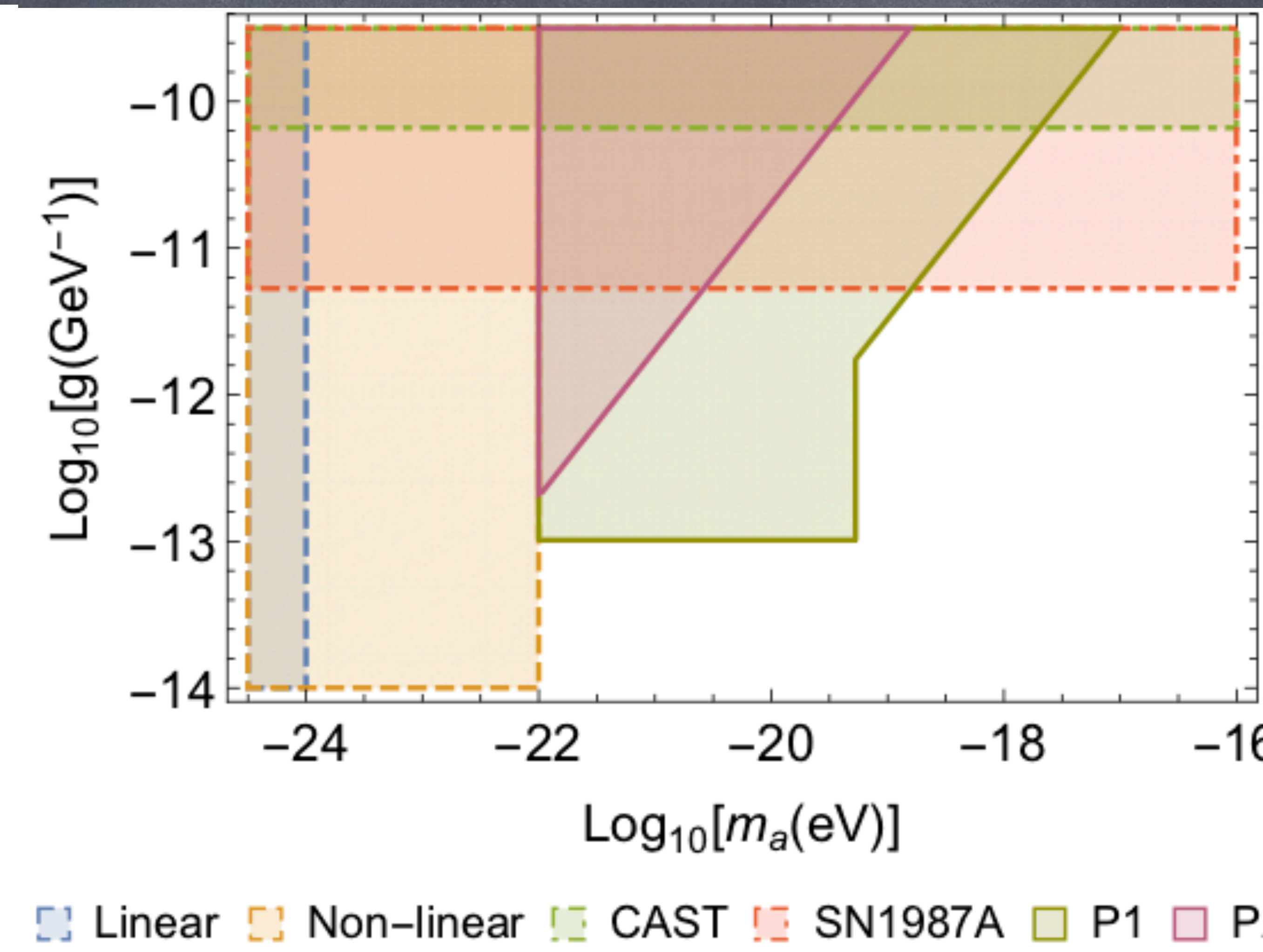

pulsar timing:
Caputo et al., Phys.Rev. D 100 (2019) 063515 [arXiv:1902.02695]

linearly polarised pulsar light:
T. Liu, G. Smoot, Y. Zhao, arXiv:1901.10981

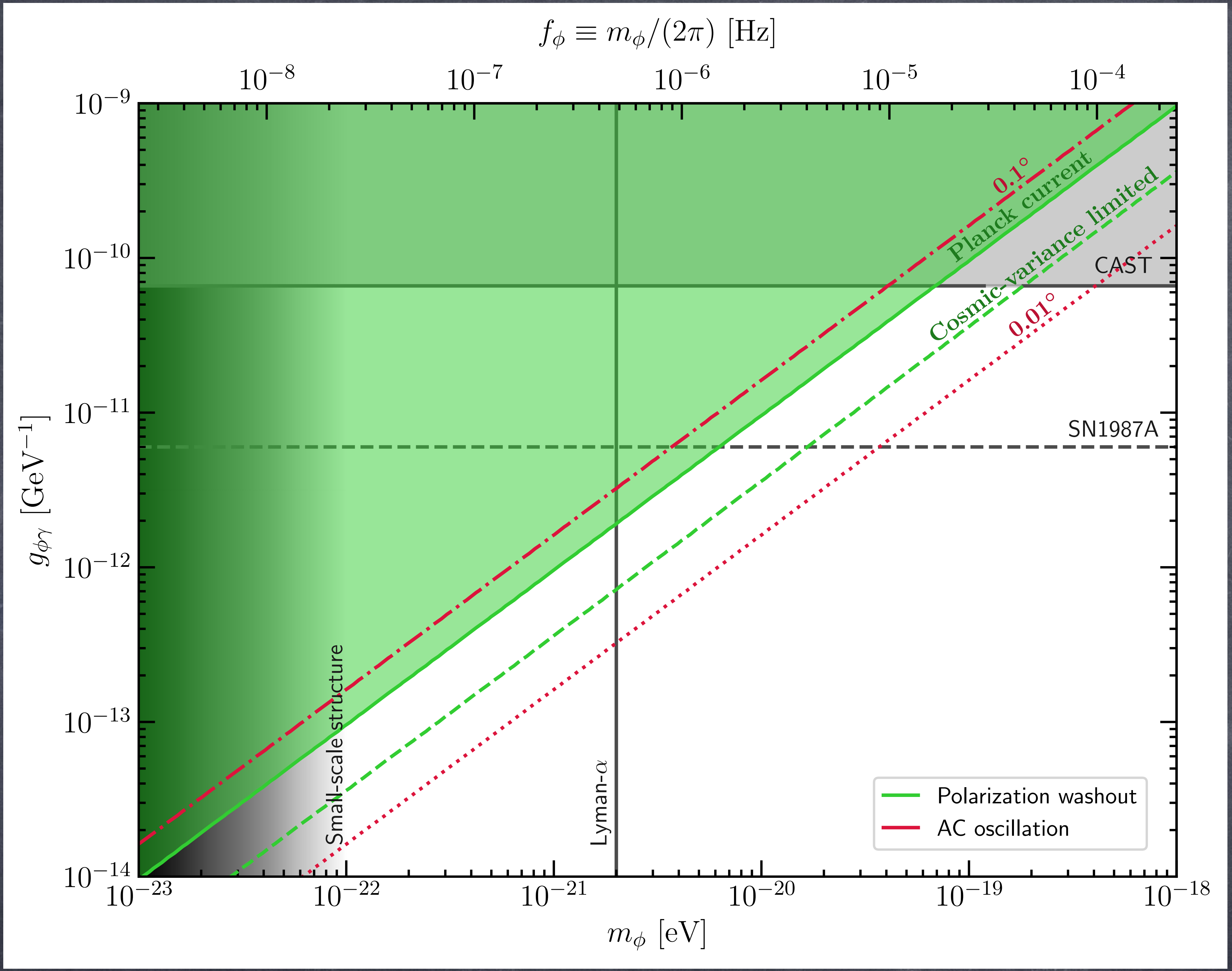

CMB polarization: M.A. Fedderke, P.W. Graham, S. Rajendran, Phys.Rev. D100 (2019)015040 [arXiv:1903.02666]
polarisation of AGN jets: M.M. Ivanov et al., JCAP 02 (2019) 059 [arXiv:1811.10997]
polarisation of protoplanetary disk emission: T. Fujita, R. Tazaki, K. Toma, Phys.Rev.Lett. 122 (2019) 191101 [arXiv:1811.03525]

Another curiosity of birefringence: Chiral light bending

D. Blas et al., Phys.Dark Univ. 27 (2020) 100428 [arXiv:1910.11907] claim that there is no light bending, separation of different circular polarisations, to any order of $g_{a\gamma}$, as long as the photon frequency $\omega \gg m_a$.

In contrast, J.I. McDonald and L.B. Ventura arXiv:1911.10221 claim this is only true to linear order in $g_{a\gamma}$, and in the presence of background plasma, there is refraction even in linear order in $g_{a\gamma}$.

Applications ?

Conclusions 1

1.) The sources of ultra-high energy cosmic rays are still not identified due to rather small anisotropies; composition seems to become heavier at the highest energies which appears economic in terms of shock acceleration power

2.) The observed X_{max} distribution of air showers provides potential constraints on hadronic interaction models: Some models are in tension even when "optimizing" unknown mass composition; however, systematic uncertainties are still significant.

3.) IceCube neutrinos already constrain their sources which should be sufficiently numerous: Gamma-ray bursts are unlikely as main sources

4.) Multi-messenger modeling sources including gamma-rays and neutrinos start to constrain the source and acceleration mechanisms

Conclusions 2

1.) Linelike radio emissions from dark matter-ALP conversion into photons in magnetic fields may be detectable with current and future radio telescopes such as LOFAR and SKA

2.) However, the most crucial (and least known) parameter is the magnetic field power on the ALP mass scale which is in the meter regime for μeV ALP masses. MHD modes in the presence of coherent magnetic fields would play an important role but their intensity is currently unclear.

3.) Spontaneous decay (interesting above ~10^{-5} eV) and parametric amplification in ALP stars are independent of magnetic fields, but the latter depends a lot on ALP star structure and their formation (not well understood yet but many opportunities for collaboration !)

4.) Resonant conversion around compact stellar objects may give interesting signals less dependent on magnetic field structure

5.) Birefringence induced in photons propagating in an oscillating axion background should be wavelength independent (thus also relevant e.g. for X-rays) and could lead to further constraints.